Acceleration and Spatial Diffusion of Galactic Cosmic Rays

DISSERTATION
zur Erlangung des Grades eines
Doktors der Naturwissenschaften

in der
Fakultät für Physik und Astronomie
der Ruhr-Universität Bochum

von
RALF WEYER
Institut für Theoretische Physik IV
Ruhr-Universität Bochum

Bochum 2005

1. Gutachter: Prof. Dr. Reinhard Schlickeiser

2. Gutachter: PD Dr. Horst Fichtner

Tag der mündlichen Prüfung: 12.07.2005

Für meine Eltern und meine Schwester

The effort to understand the universe is one of the very few things that lifts human life a little above the level of farce, and gives it some of the grace of tragedy.

Steven Weinberg, The First Three Minutes:
A Modern View of the Origin of the Universe

Das Bestreben, das Universum zu verstehen, hebt das menschliche Leben ein wenig über eine Farce hinaus und verleiht ihm einen Hauch von tragischer Würde.

Steven Weinberg, Die ersten drei Minuten,
Der Ursprung des Universums

Contents

4

Chapter 1

Introduction

The field of astroparticle physics is a symbiosis of elementary particle physics, astrophysics, astronomy and plasma physics. Large astrophysical objects like supernovae, galaxies, radiation fields and the interstellar medium are linked with the propagation, acceleration and interaction of elementary particles like photons, neutrinos, electrons and positrons, neutrons, protons and antiprotons and higher Z nuclei in different isotopic forms. The energies of these observed cosmic rays span a wide range up to energies exceeding the values at terrestrial laboratories by orders of magnitude.

The main topic of this work are the hadronic cosmic rays of energies from a few GeV up to $10^{15} - 10^{17}$ eV, which are supposed to be of galactic origin. The astrophysical sources of these nuclei are still experimentally not confirmed, although it is assumed, that they run through the same pre-acceleration processes as cosmic ray electrons, which have been detected indirectly by synchrotron radiation and high energy gamma-rays from supernova remnants. After injection into the interstellar medium the particles interact with plasma waves and the interstellar gas. One main question in cosmic ray physics is the transformation of macroscopic energy stemming, for example, from supernova explosions and from plasma waves in the interstellar medium into particle energy and, thus, explaining the spectra and chemical composition measured at the location of the sun.

The theory of acceleration by shock waves, like the shock fronts of supernova remnants, can explain injection spectra of charged hadronic cosmic rays, which have to first order the form of power laws. These spectra are now processed by the interaction of the cosmic ray particles with plasma waves existing in the interstellar medium. An unsolved problem in astroparticle physics is the influence of the stochastic reacceleration by these plasma waves. In this work we investigate the diffusive spatial and stochastic momentum transport of cosmic rays by the turbulence

of the interstellar medium to explain the spectra measured by satellites, balloon-borne and airshower experiments at the earth. The importance of the theoretical considerations follows from the lack of in situ measurements of the processes in the interstellar medium.

A mathematical description of the propagation processes is provided by the transport equation, a second-order linear partial differential equation in time, space and momentum. For the first time we use analytical solutions of the stationary transport equation to calculate the final energy spectra of hadronic cosmic rays. This has the advantage of a better mathematical control of the results in contrast to a purely numerical solution of the differential equation. We have to accept, however, some approximations and simplifications using this method. We neglect the terms of spatial and momentum convection and also continuous loss processes, which have been shown to be not important for nuclei. The calculations are first performed for protons. Later we discuss the consideration of catastrophic losses, like spallation in the interstellar gas for nuclei with $Z > 1$. We assume a cylindrical symmetry and a homogeneous spatial source distribution and insert well-established spatial and momentum injection functions. The final integrals can only be calculated numerically, but analytical approximations and consistency checks are made.

In the end, we fit the data for different parameter sets and some best-fit astrophysical parameters are yielded. The importance of stochastic reacceleration of galactic cosmic rays in the galactic plasma is evaluated.

This work is structured as follows:

In **Chapter 2** we first give an overview of three populations of cosmic rays, solar, galactic and extragalactic. In the galactic cosmic ray section we deal especially with conclusions from galactic gamma rays, possible sources of hadronic cosmic rays, their acceleration, transport and propagation and their loss processes. Then we describe the measurements of solar cosmic rays and the direct and indirect detection techniques of higher energetic cosmic rays. For completeness we shortly mention neutrino detectors. Some properties of the galactic plasma and the superimposed plasma waves are presented.

In **Chapter 3** the mathematical way to the transport equation is sketched, which is central for this work. In the following, we consider only the stationary transport equation.

Analytical solutions with and without catastrophic losses of this transport equation are presented in **Chapter 4**. The solutions, provided by the scattering time method

separating the equation in a spatial and a momentum part, are infinite eigenfunction double sums consisting of spatial and momentum functions. The calculations of the momentum integrals are more sophisticated than those of the spatial integrals, because the Green's functions of the momentum part enter, including modified Bessel functions for the case with catastropic losses and confluent hypergeometric functions for the case without catastrophic losses.

The momentum parts of the solutions are studied in **Chapter 5**. We carry out theoretical and numerical consistency checks and approximate the solutions for different momentum regimes by inserting a power law momentum injection function. We also consider a momentum source spectrum with a dispersive index, which could be more realistic.

In **Chapter 6** we calculate the spatial part of the solution for different source functions.

Now, in **Chapter 7**, we can calculate the spectra of galactic cosmic ray protons. First, we introduce the diffusion coefficients for a mixture of slab Alfvén waves and fast magnetosonic waves as the assumed turbulence in the galactic plasma and calculate some typical eigenvalues. After taking into account the solar modulation of the galactic cosmic rays, the calculated spectra are compared with experimental data for different astrophysical parameter sets.

In **Chapter 8** we deal with the momentum solution integral including catastrophic losses for nuclei above hydrogen. The confluent hypergeometric functions enter in the respective Green's functions. Their analytical properties and numerical treatment are investigated.

In the end a summary is given and the results are discussed.

8

Chapter 2

Basics

In this introductory chapter we first give an overview of the different species of cosmic rays, depending on particle nature, energy and origin, followed by a section describing the main measurement techniques for cosmic rays.

Focusing on the topic of this work, especially informations on the galactic cosmic rays, like their potential sources and their propagation are presented.

Connected to the mechanisms of propagation and to the cosmic rays themselves is the theory of plasmas and plasma waves.

2.1   Overview Cosmic Rays

Cosmic rays in general are high energetic particles or photons stemming from outer space. The following particles can be measured: photons, neutrinos, electrons and positrons, neutrons, protons and antiprotons and higher Z nuclei in different isotopic forms.

The energies of the cosmic rays span a wide range of many of orders of magnitudes up to about 10^{21} eV (see Fig. 2.1). The hadronic spectrum can be described by a power law

$$\frac{dN}{dE} \sim E^{-\gamma} \tag{2.1}$$

over a wide range with a spectral index of $\gamma \simeq 2.7$ up to the order of 10^{15} eV. Then the spectrum steepens to an index of $\gamma \simeq 3$, the transition region is called the "knee" (cf. Fig. 2.2). At about 10^{18} eV the spectrum flattens again (the so called "ankle").

Wether the knee feature is due to a change of chemical composition, of acceleration mechanisms or different sources is still an important open question. In this work we try to model the energy regime from about 10^9 eV to about 10^{17} eV.
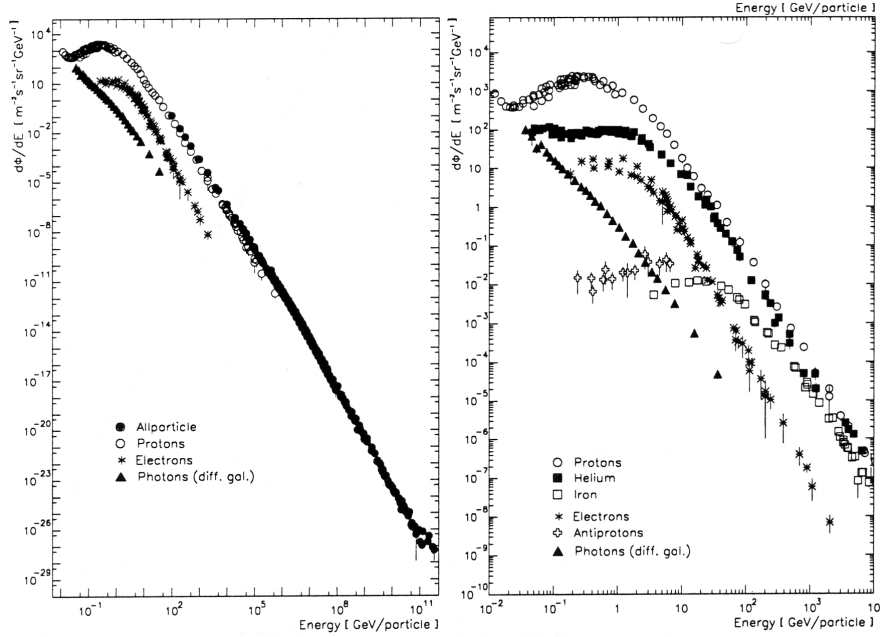
Figure 2.1: Energy spectrum of the hadronic cosmic rays, antiprotons, electrons and photons. Taken from [Wiebel-Sooth 1998].

The cosmic ray photon energies extend the electromagnetic spectrum above the MeV gamma-rays. Photons have the advantage of a straight propagation from their sources to the detectors at the position of earth, while charged particles are bent by magnetic fields.

The measured electron spectra are also shown in Fig. 2.1. The higher energetic electron component of the cosmic rays has to be purely of galactic origin, in contrast to the hadronic part, due to the inverse Compton losses of high energy electrons in the 3K thermal microwave background radiation.

The theoretically expected neutrino-spectra are sketched in Fig. 2.3.

Like photons, neutrinos point directly to their sources but they have the advantage not to suffer from electromagnetic loss processes. If they will be detected at TeV energies, they would be a signature for hadronic cosmic ray accelerators, because high energy neutrinos can only result form hadrons hitting material and producing
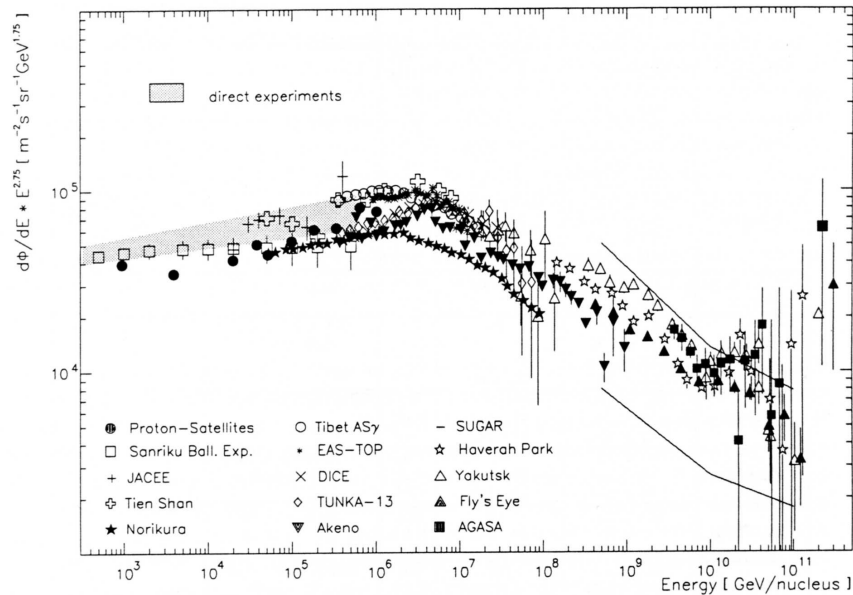
Figure 2.2: The allparticle energy spectrum as measured by different ground-based experiments and three direct ones (see Section 2.2). For comparison the allparticle flux obtained by adding up the single spectra of individual nuclei as measured by the bulk of direct experiments is also given. To emphasize the changes in the spectral slope, the differential flux is multiplied by $E^{2.75}$. Taken from [Wiebel-Sooth 1998].

mesons through the cascade

$$
\begin{aligned}
p + p/\gamma & \longrightarrow & \pi^{\pm}/K^{\pm} + \pi^0 + ... \\
K^{\pm}/\pi^{\pm} & \longrightarrow & \mu^{\pm} + \nu_{\mu}/\bar{\nu}_{\mu} \\
\mu^{\pm} & \longrightarrow & e^{\pm} + \nu_e\bar{\nu}_{\mu}/\bar{\nu}_e\nu_{\mu}
\end{aligned}
$$

in contrast to photons that can - besides the π^0-decay - also be provided by synchrotron radiation and inverse Compton scattering by electrons. More about neutrino astrophysics can be found for example in [Klapdor & Grotz 1989].

The main tasks of astroparticle physics are to find the astrophysical sources of the cosmic rays, to understand their acceleration, propagation and interaction processes, and to explain the energy spectra and the chemical composition of the hadronic cosmic rays measured at the location of earth.

Additionally, we can learn something about high energy particle interaction processes beyond the standard model, because the highest energies of the cosmic rays
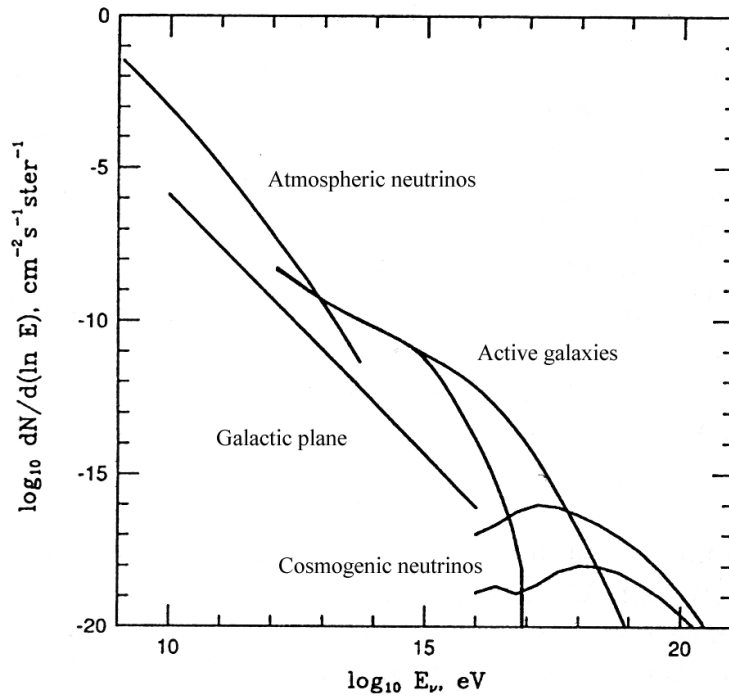
Figure 2.3: Theoretical energy spectrum of cosmic neutrinos ([Klapdor-Kleingrothaus & Zuber 1997]). Atmospheric neutrinos are produced by hadronic interactions of the incident cosmic ray nucleons with the molecules of the atmosphere (cf. Fig. 2.23). Neutrinos of the galactic plane stem from supernovae and from interactions of the cosmic rays with the interstellar medium. Neutrinos from active galaxies are generated in the proton cascades of the jets (cf. Subsection 2.1.3) and cosmogenic neutrinos are relics of the big bang.

lie some orders of magnitude above the energies which can be achieved by the modern particle accelerators, like CERN, DESY, FERMILAB etc.

On the one hand the cosmological evolution of our world is directly connected to the standard model of elementary particle physics and its extension, the Grand Unified Theories (GUTs), on the other hand some predictions of the GUTs can be tested by cosmic ray physics (see for example Subsection 2.1.3).

The cosmic rays also probe cosmic background photon fields, like the 3K microwave background, the IR and optical background fields (cf. Fig. 2.4).
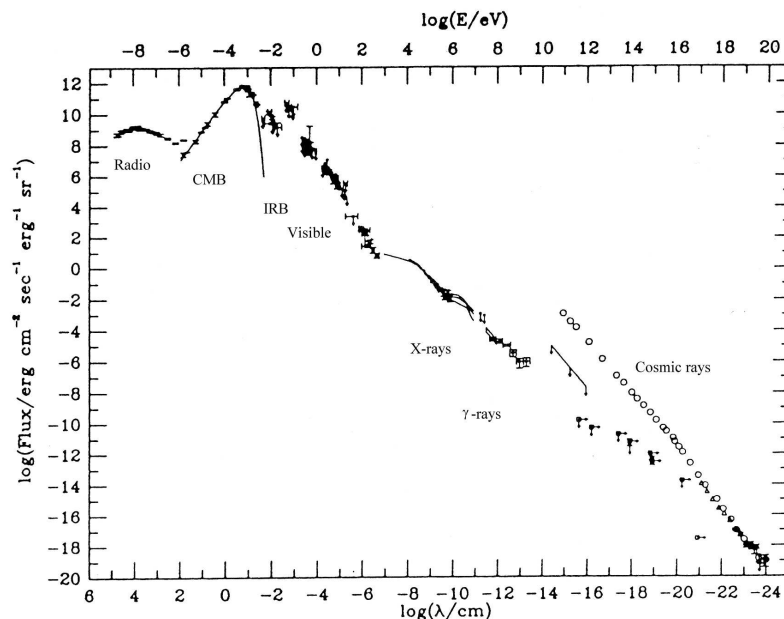
Figure 2.4: The measured photon background spectrum. (CMB = Cosmic microwave background, IRB = Infrared background). Adapted from [Ressell & Turner 1990].

Because the charged cosmic rays are influenced by magnetic fields and plasma waves in the sources and on their way through the space, information about the properties of the magnetic fields and the plasma waves is also provided indirectly by modelling the acceleration and propagation processes. In this work we will also test some assumptions about plasma wave turbulence in the interstellar medium.

The observed antiproton and positron fluxes can be explained as secondaries resulting from baryon-baryon-collisions and still there is no hint that today there exists a considerable amount of antimatter as a relic from the early phase of the universe. Anti-nuclei with $Z \geq 2$ cannot be produced by hadronic interactions in the interstellar and intergalactic medium, so if they exist, they have to be cosmological, but no detection has been reported so far.

In the following subsections we deal with the different categories of cosmic rays. In the low energy region up to a few GeV experimental evidence confirmed their origin from the solar wind, which we will discuss in Subsection 2.1.1. For the cosmic rays of higher energies there is still a debate of their sort of sources in the galaxy (cf. Subsection 2.1.2), the ultrahigh energy cosmic rays have to be extragalactic (cf. Subsection 2.1.3) because of their large gyroradii in the galactic magnetic field,

14

which exclude a trapping in the galaxy.

What can be inferred from the chemical composition of cosmic rays being similar to the solar system elemental composition (Fig. 2.5) is that they seem to stem from stellar-like sources.
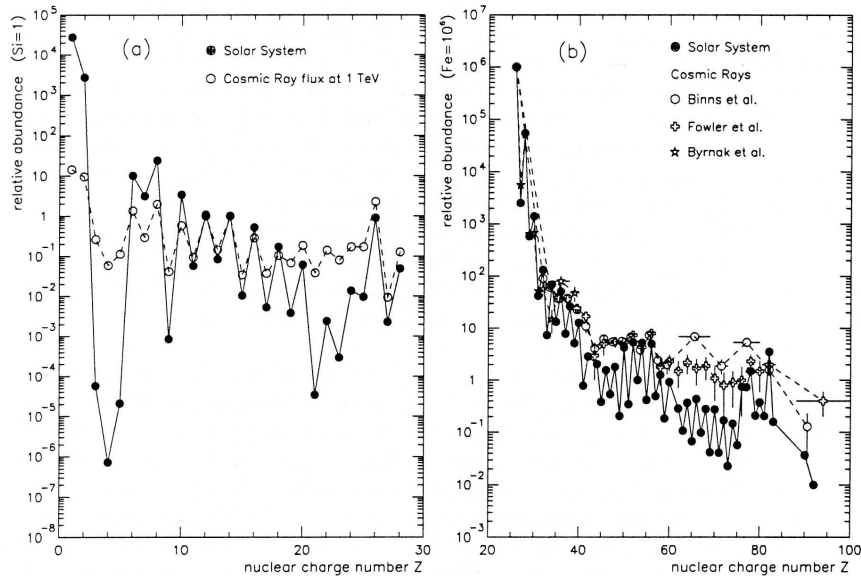
Figure 2.5: Abundances of the cosmic rays in comparison to those in the solar system. (a) The elements H - Ni, normalized to Si = 1, cosmic ray flux at 1 TeV/nucleus. (b) The elements Fe - Fm, normalized to Fe = 10^6, cosmic ray flux > 1.5 GeV/nucleon. The overabundance of Lithium, Beryllium and Boron and also the sub-iron group in the cosmic rays is a result of the spallation of Carbon, Nitrogen and Iron. Graph taken from [Wiebel-Sooth 1998].

The interactions of nuclei in the interstellar medium give rise to second-order features of this distribution, like the overabundance of Lithium, Beryllium and Boron and also the sub-iron group in the cosmic rays, the spallation products of Carbon and Nitrogen, respectively Iron.

For a survey of the field of cosmic ray physics consult, e. g., the books of [Schlickeiser 2001], [Pohl 2002] or [Berezinskii et al. 1990]. An introduction of particle physics can be found, e. g., in [Berger 1992] and [Griffiths 1996]. [Harwit 1988], [Voigt 1991] and [Unsöld & Baschek 1999] deal with astrophysics and astronomy.

2.1.1 The Heliosphere

Although galactic cosmic rays are the main topic of this work, the advantage of heliospheric physics is the possibility of in situ measurements and the study of plasma waves, shock acceleration of particles, particle transport and so on. Moreover, the modulation of galactic cosmic rays by the heliosphere is relevant for fitting the data in Chapter 7.

The solar corona, photographed in Figs. 2.6, 2.7 and 2.8, is a hot plasma with a temperature of a few million degrees and represents the outer solar atmosphere, which turns into a continuous plasma stream of coupled particles and magnetic fields, the solar wind.
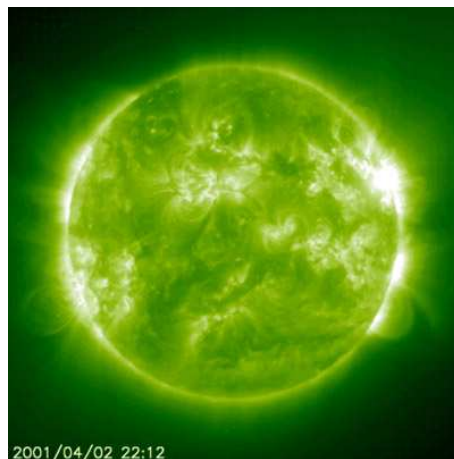
Figure 2.6: The solar corona in the extreme UV, observed by the EIT (Extreme ultraviolet Imaging Telescope) onboard SOHO (The Solar and Heliospheric Observatory, a project of ESA and NASA).

This plasma flow encounters the interstellar medium and forms the heliospheric bubble, separated by the heliopause from the interstellar plasma (Fig. 2.9).

Because of the relative motion of the sun with respect to the local interstellar medium, an asymmetry with a bow shock and a heliotail develops. An adaption of the solar wind plasma to the surrounding medium takes place at the heliospheric shock. The magnetic field lines emerging from the sun wind up by the rotation of the sun, forming the Parker spiral. The heliosphere is an example of an astrosphere, which may be found around every star.
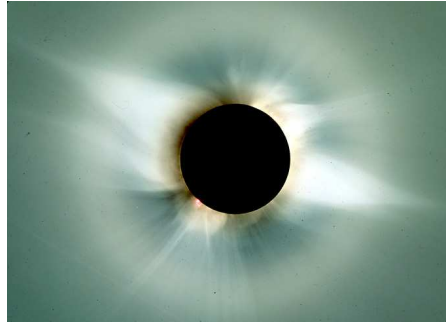
Figure 2.7: The solar corona, photographed by the Evans Solar Facility (National Solar Observatory, Sacramento Peak). The solar disk itself is hidden by an artificial eclipse.
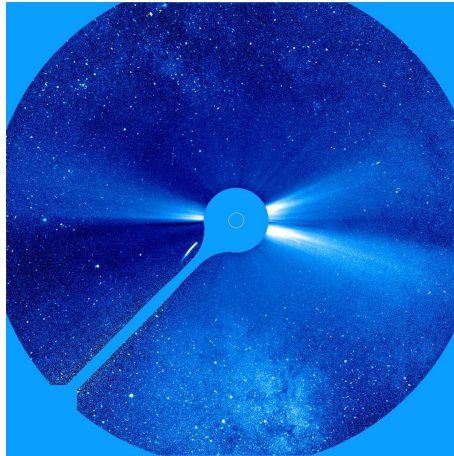
Figure 2.8: The outer solar corona in UV, photographed by LASCO (Large Angle and Spectrometric Coronagraph) onboard SOHO. The solar corona passes into the solar wind.

Several production processes for energetic particles can be found in the solar system:

- solar flares in the corona can accelerate ions up to energies of several GeV and electrons up to energies of 100 MeV (see Fig. 2.10);

- shock waves occur at coronal mass ejections (CMEs), which are fed by the energy stored in the coronal magnetic field and released in violent reconnection processes;

- corotating interaction regions (CIRs) in the solar wind plasma, forming when slow solar wind streams are overtaken by fast ones and, as a consequence, the resulting shocks can accelerate particles to higher energies;
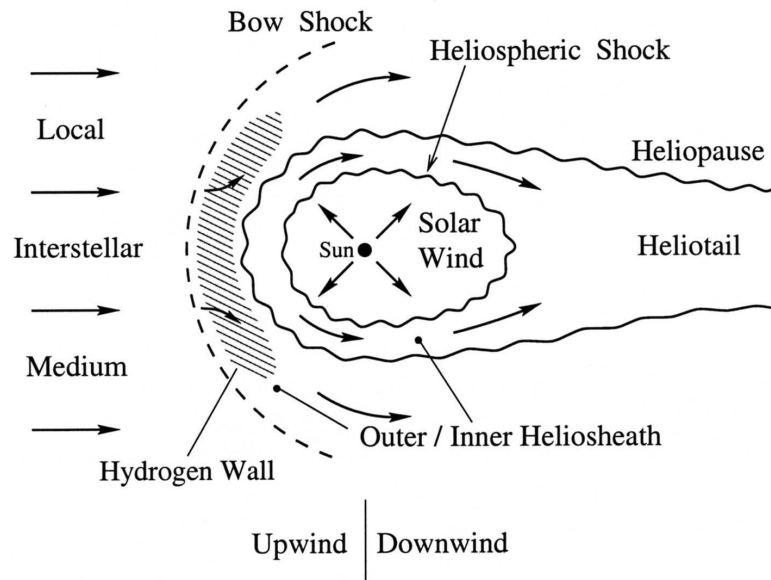
Figure 2.9: A sketch of the heliosphere, taken from [Scherer et al. 2000]. In the rest frame of the sun, the plasma flow of the local interstellar medium is probably compressed to form a bow shock.

- shock waves at planetary magnetospheres interacting with the solar wind plasma;

- the heliospheric termination shock (cf. Fig. 2.9);

- the energetic anomalous cosmic rays (ACR) begin their life as neutral atoms of the local interstellar medium that penetrate the heliosphere and are ionized by the solar wind or solar UV radiation, then called pick-up-ions (PUI), which are pre-accelerated while convecting with the solar wind to the heliospheric shock. Then a fraction of them is shock-accelerated at the termination shock, representing the ACR. For a review of this topic read e. g. [Fichtner 2000].

- planetary magnetospheres, like the Jupiter magnetosphere, can emit energetic electrons.

The reversal of the magnetic dipole field of the sun in a cycle of about 22 years is the cause of a higher solar activity, indicated by more sun spots and a stronger, more turbulent and differently structured solar wind.

The solar activity influences the low energetic galactic cosmic rays up to energies of
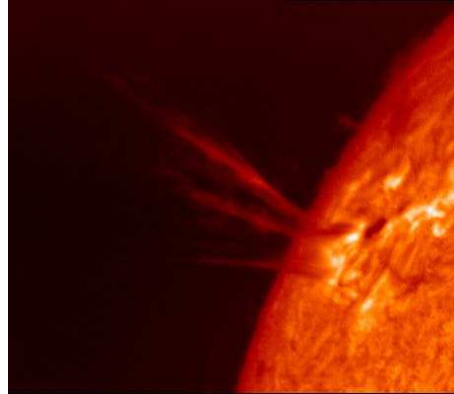
Figure 2.10: A solar flare on the photosphere of the sun. Photographed by the SOON
Telescope on Hawaii (National Solar Observatory/Sacramento Peak).

about 5 GeV. For a high activity state the galactic cosmic rays are shielded stronger
by the small-scale plasma wave turbulence superimposed on the solar wind. Fig.
2.11 shows the anticorrelation of the sun spot numbers, as indicators of solar activ-
ity, and the flux of the galactic cosmic rays measured indirectly on earth by neutron
monitors, which count the hadronic component of the induced airshowers (refer to
Subsection 2.2.3).
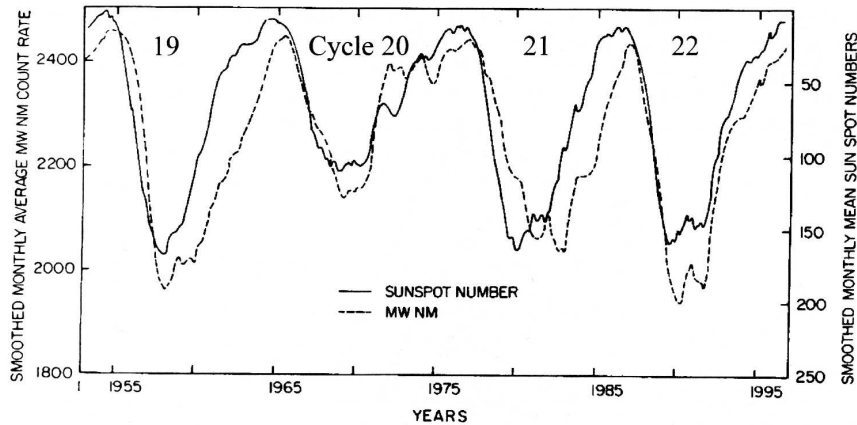
Figure 2.11: Yearly running averages of galactic cosmic ray intensities measured with
the Mount Washington neutron monitor (dashed line), compared to the
monthly mean sunspot numbers (solid line) from 1954 to 1996 (from
[Lockwood & Webber 1997]). Sunspot numbers and the flux of galactic cos-
mic rays are anticorrelated. Typical galactic cosmic ray energies detected by
neutron monitors range from about 500 MeV to 20 GeV.

The resulting energy spectra of cosmic rays are modulated in the low energy regime with the solar activity (Fig. 2.12). In Chapter 7 we will use a simple model to take into account this solar modulation.
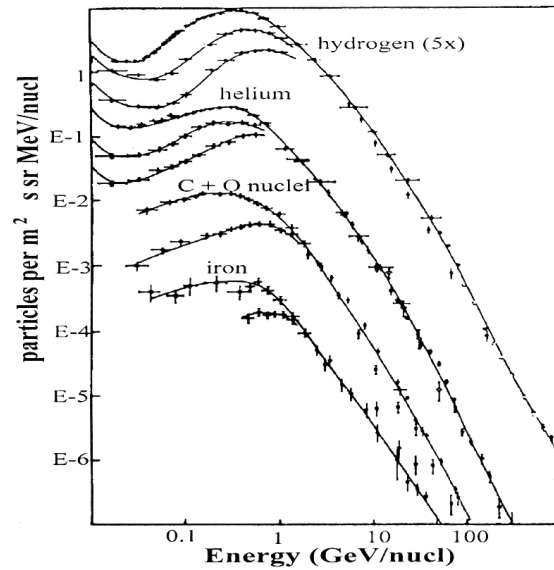
Figure 2.12: Spectra of galactic cosmic rays for different nuclei. At the low energy regime the influence of solar modulation changes the fluxes depending on the solar activity. Taken from [Meyer et al. 1974].

Low energetic cosmic rays up to energies of about several tens of GeV (geomagnetic cutoff) are shielded additionally from the earth by its magnetosphere (Fig. 2.13).

For more information about the heliosphere and the earth's magnetosphere consult e. g. the books of [Scherer et al. 2000], [Kallenrode 1998], [Glassmeier & Scholer 1991] and [Prölss 2001].
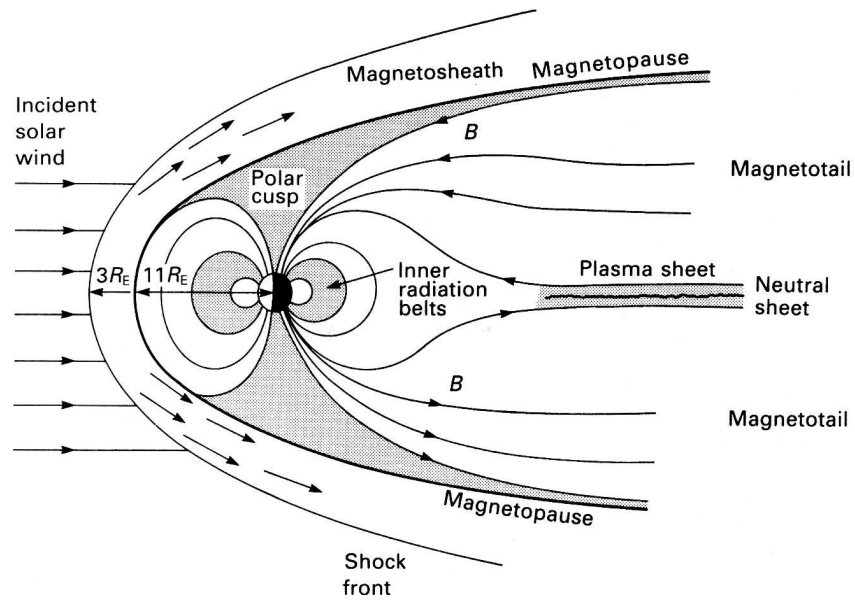
Figure 2.13: Structure of the earth's magnetosphere, taken from [Longair 1992]. Analogously to the relative motion of the heliosphere in the interstellar medium, a bow shock emerges as the solar wind encounters the magnetosphere.

2.1.2 Galactic Cosmic Rays

This work is mainly dealing with hadronic galactic cosmic rays. But cosmic hadrons, leptons and gamma-rays are strongly connected, so the first part is devoted to the gamma-rays. Then, we introduce possible sources for cosmic ray particles and describe their acceleration. The transport equation, a central theme of this work, is introduced and two of its special cases are presented. After that, some features of galactic cosmic ray propagation and loss processes during this propagation are discussed.

Galactic Gamma-rays

A complete gamma-ray sky survey was given by the EGRET (Energetic Gamma Ray Experiment Telescope) onboard the CGRO (Compton-Gamma-Ray-Observatory) satellite (Fig. 2.14).
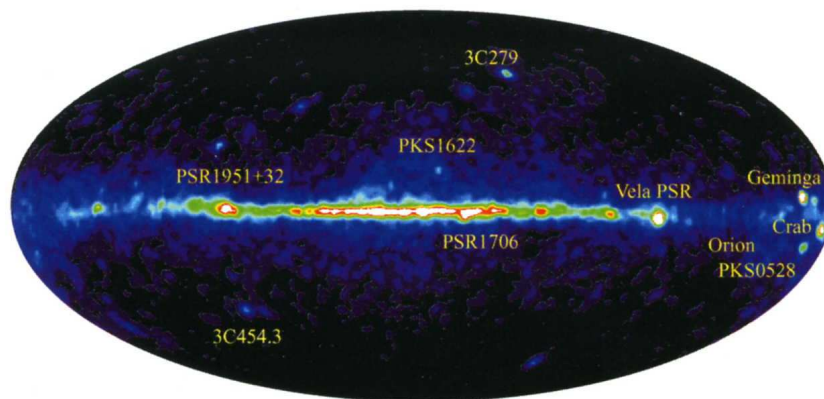
Figure 2.14: All-sky map from EGRET with energies of gamma-rays > 100 MeV. The picture has a galactic coordinate system with the origin in the center of the map. Taken from [Schönfelder 2001].

The bright gamma-ray band of our galaxy is mainly caused by the interaction of cosmic rays with the interstellar gas, like bremsstrahlung and π_0-decay, supplemented by inverse Compton boosted starlight by cosmic rays. The local spectrum of hadronic cosmic rays may not be representative for the galaxy, hence gamma-ray observations are important to sample a much larger region. Also some point sources, like pulsars, have been identified.

For photon energies in the TeV regime, Cherenkov telescopes detecting the induced airshowers have to be used (cf. Subsection 2.2.3). [Bojahr 2002] compiles a list of

sources above an energy of 250 GeV: Crab M1 (plerion, see Fig. 2.15), AE Aqr (cataclysmic variable), PSR 1706-44 (plerion), Vela (plerion), SN 1006 (supernova remnant shell), RX J1713.7-3946 (supernova remnant shell), Cassiopeia A (supernova remnant shell, see Fig. 2.17), Centaurus X-3 (X-ray-binary), PSR B1509-58 (plerion), TeV J2032+4131 (unknown object type). Recently the H.E.S.S. (High Energy Stereoscopic System) group [Aharonian et al. 2005] reported about eight new unknown very high energy gamma-ray sources in the galaxy; three of them are associated with supernova remnants.
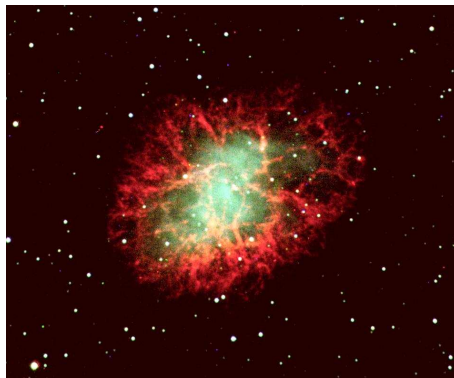
Figure 2.15: The Crab Nebula, a remnant of a supernova that exploded in 1054. In the center lies a pulsar with a frequency of 30 Hz. The red color indicates the recombination of electrons with protons to form neutral hydrogen. The green color traces the ultrarelativistic electrons gyrating around the strong magnetic field of the inner nebula. Such a supernova remnant with a pulsar supplying energetic electrons emitting sychrotron radiation is called a plerion.

The TeV gamma-ray spectra of shell-type supernovae can be explained by electron acceleration models with shock waves (in Fig. 2.16 a shell-type supernova remnant is shown), but still there is no experimental evidence of photons induced by hadrons. Nevertheless, one assumes similar acceleration mechanisms for hadrons and expects hadronic cosmic rays from supernova remnants also producing high energy gamma-rays from neutral pion decay, with a luminosity too low in most supernova remnants to be detected by EGRET, but airshower experiments may be sensitive to high energy photons (cf. [Drury et al. 1994]). The contribution of secondary electrons and positrons from charged pion decay to bremsstrahlung, inverse-Compton and synchrotron emission of supernova remnants is negligible (cf. [Schönfelder 2001]).

For reviews of galactic gamma-ray astronomy we refer, e. g. to [Völk 2001] and [Pohl 2001].
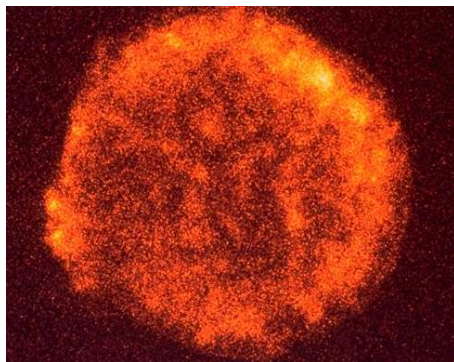
Figure 2.16: Tycho's supernova remnant shock wave detected in X-rays. The interstellar material encountered by the shock wave becomes heated and stirred up. Tycho is a shell-type supernova remnant. Although for some remnants of this type gamma-rays of TeV energies have been measured, indicating high energetic charged particles accelerated at the shock wave, this is not the case for Tycho as yet.

Tycho's supernova emerged 1572. Taken by the X-ray satellite ROSAT (Röntgen Satellite).

Possible Sources of Hadronic Galactic Cosmic Rays

For the requirements of cosmic ray source power, in the following a crude estimate of cosmic ray energetics is given. From radioactive cosmic ray nuclei a lifetime of hadronic cosmic rays of approximately $t_{c.r.} \approx 10^8$ yr $\approx 3 \cdot 10^{15}$ s is obtained. The energy density of hadronic cosmic rays is in the order of

$$w_{c.r.} \approx 0.5 \text{ eV/cm}^3 \approx 10^{-12} \text{ erg/cm}^3 . \qquad (2.2)$$

With a typical volume of the halo (see subsequent subsections) with a radius $L \approx 15$ kpc $\approx 5 \cdot 10^{22}$ cm and a half-height of $H \approx 10$ kpc $\approx 3 \cdot 10^{22}$ cm

$$V = 2\pi L^2 H \approx 5 \cdot 10^{68} \text{ cm}^3 \qquad (2.3)$$

we get a total cosmic ray energy of

$$W_{c.r.} \sim w_{c.r.} V \approx 10^{56} \text{ erg} \qquad (2.4)$$

and, thus, a luminosity of

$$L_{c.r.} \sim \frac{W_{c.r.}}{t_{c.r.}} \approx 10^{40} \text{ erg/s} . \qquad (2.5)$$

Another way is to consider the average path length of the relativistic cosmic rays traversing the interstellar matter:

$$\lambda = c\,\bar{\rho}\,t_{c.r.} \approx 5 \text{ g/cm}^{-2} \tag{2.6}$$

where $\bar{\rho}$ is the average gas density of the cosmic ray volume. Then again we obtain a cosmic ray power of the same order of magnitude:

$$L_{c.r.} = \frac{W_{c.r.}}{t_{c.r.}} = \frac{cw_{c.r.}\bar{\rho}V}{\lambda} = \frac{cw_{c.r.}M_g}{\lambda} \approx 6 \cdot 10^{40} \text{ erg/s} \tag{2.7}$$

where we have inserted a galactic gas mass of $M_g \approx 10^{43}$ g.

Analogous considerations lead us to the total energy and the luminosity of the electron component, if we assume $w_e \approx 10^{-2}w_{c.r.}$ and $t_e \approx 10^{15}$ s:

$$W_e \sim w_e V \approx 10^{54} \text{ erg} \tag{2.8}$$

and

$$L_e \sim \frac{W_e}{t_e} \approx 10^{39} \text{ erg/s} \tag{2.9}$$

which is only one order of magnitude lower than the total power of the hadronic cosmic ray component.

If we now compare the results with the average cosmic ray luminosity of the sun $L_{c.r.,\odot} \approx 10^{25}$ erg multiplied with the factor 10^{11}, because the mass of the galaxy is $M_G \approx 10^{11}M_\odot$, we get a crudely estimated cosmic ray luminosity of 10^{36} erg/s for the whole galaxy, if only normal stars would contribute.

In contrast, supernovae deliver sufficient energy to sustain the flux of cosmic rays, because if on average every 30 years a supernova explodes in our galaxy with an energy of $10^{49} - 10^{51}$ erg - without the energy of the neutrinos - their contribution in power is roughly $10^{40} - 10^{42}$ erg/s, which is in the claimed order of magnitude. From analyzing cosmogenic nuclei on meteorites one has derived that the flux of cosmic rays has been nearly constant for the past 10^9 years. Because the particles leak out of the galaxy much faster, the sources have to support the flux continuously.

Other possible sources, which could deliver power within the same orders of magnitude, are stellar winds of hot OB-stars and pulsars, but there are some theoretical arguments why pulsars cannot produce power law energy spectra reaching to high energies (cf. [Pohl 2002]).

In supernova remnants synchrotron emission from electrons in the radio regime can be detected, as it is shown in Fig. 2.17. But one also expects continuum non-thermal synchrotron emission up to photon energies in the X-ray region in some supernova remnants, as reported for Cas A (cf. [Allen et al. 1997]) and for some other remnants. This X-ray emission is a clue to electrons with energies up to several tens of TeV.
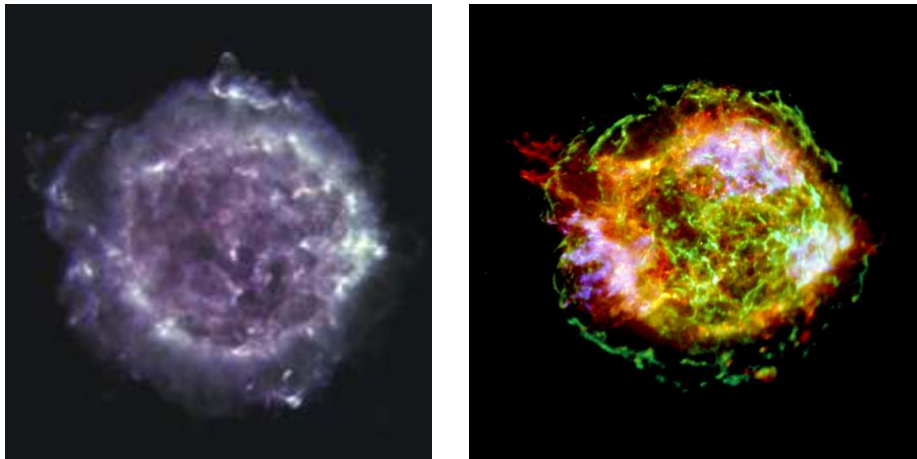
Figure 2.17: Supernova remnant Cas A in radio (left) and in X-ray (right) frequency range.

Cassiopeia A is the remnant of a supernova explosion that occured over 300 years ago in our galaxy.

The radio emission is synchrotron radiation of shock-accelerated electrons detected with the VLA (Very Large Array) telescope in New Mexico.

The X-ray picture from the CHANDRA observatory is a composite of three X-ray bands: low energy (red), medium energy (green) and high energy (blue). The bright outer ring marks the location of a shock wave generated by the supernova explosion.

Cas A is also a TeV gamma-ray emitter, due to high energy electrons.

The detected radio synchrotron emission has the form of a power law. In the text book of [Schlickeiser 2001] it is calculated that a power law electron energy spectrum with a spectral index s leads to a synchrotron radiation power law with a spectral index of $\frac{1}{2}(s-1)$. We can conclude that there have to be energetic electrons with a power law energy spectrum in supernova remnants. The average spectral index of the measured radio synchrotron radiation of supernova remnants in our galaxy

is approximately 0.5, according to [Green 2000], consequently $s \approx 2$ for electrons. This is in agreement with the investigations in [Pohl & Esposito 1998].

We have the opportunity to observe other galaxies to consolidate the idea, that supernova remnants are the sources of galactic cosmic rays. For example, from radio synchrotron measurements of the galaxy M33 [Duric et al. 1995] imply that the supernova remnants account for the bulk of the relativistic particles in that galaxy.

For some supernova remnants also TeV gamma-rays have been measured, as stated in the previous subsection. These gamma-rays could be microwave background photons boosted by high energy electrons (cf. [Pohl 2002]) or products of neutral pion decays.

Reviews of supernovae being possible sources of galactic cosmic rays can be found, e. g. in [Drury et al. 2001] and [Berezhko 2001].

Supernova remnants are located mainly in the galactic disk. Some fits for their distribution are used in Chapter 6.

Figure 2.18: Filaments of shocked interstellar gas, part of the expanding blast wave from the supernova remnant Cygnus Loop. Cygnus Loop is thought to have been expanding for 5.000 - 10.000 years. Observed by the Hubble Space Telescope.

Acceleration

The acceleration process for cosmic ray electrons and nucleons in supernova remnants and strong stellar winds is supposed to be a diffusive shock acceleration, if the wind of the star or the supernova shell hits material of the interstellar medium (cf. Fig. 2.18).

Shock acceleration in the first order leads to power law energy spectra. The particles are scattered by self-generated plasma waves in the shock front and in this process, some of the macroscopic kinetic energy of the shock front is transfered to the particles. For an exact mathematical solution of this problem, a non-linear treatment is required, which, however, is difficult to solve because the shocks are neither steady nor planar. In detail the spectra could deviate from pure power laws, as it is shown, for example, in a Monte Carlo approach in [Baring et al. 1999]. A review of shock acceleration can be found in [Kirk & Dendy 2001].

Though the clear experimental evidence for hadronic cosmic rays to be stemming from supernovae is unfortunately still missing (cf. e. g. [Reimer & Pohl 2002]) - except for the supernova remnant SN 1006, for which interpretations for a hadronic origin exist according to [Berezhko et al. 2002] -, one assumes the same acceleration mechanism for nucleons as for the electrons. This is reasonable, because the age of a supernova is much shorter than the radiative loss times of the accelerated nucleons and electrons.

The particles can reach only a certain maximum energy E_{max} being equal for electrons and protons after acceleration, depending on the astrophysical parameters of the supernova. For example, the supernova remnant Cas A should be able to accelerate protons to energies well above 10^6 GeV (cf. [Allen et al. 1997]), because of its extremely strong magnetic field in the order of 10^{-3} G. The maximum possible theoretical energies for supernova remnants can also be deduced from the Hillas plot in Fig. 2.20 discussed subsequently.

After the injection into the interstellar medium, the particles are reaccelerated by scattering on plasma waves existing in the medium. This stochastic acceleration is subject of investigation in the following chapters.

In this work, we assume a power law behaviour (cf. e. g. [Drury et al. 2001]) $\sim E^{-\beta}$ of the initial source spectra with a maximum energy E_{max}. In models without reacceleration an exponent of $\beta \simeq 2.1$ is favoured, and if taking into account reacceleration, values of $\beta \simeq 2.4$ are yielded, according to the discussion of [Drury et al. 2001]. The spectral indices β could be varying for different supernova remnants, which is called dispersion. We will discuss the consequences for measured spectra in Chapter 5.

In the following we present a short basic treatment of particle acceleration leading to a power law behaviour, according to [Gaisser 1990]. In shock fronts or in collisions with plasma waves we assume that a particle gains a fraction of energy

$\Delta E = \xi E$ with every collision, so that after n collisions the resulting energy is

$$E_n = E_0(1 + \xi)^n .\tag{2.10}$$

The initial injection energy of the particle is E_0. The number of collisions needed to reach a certain energy E then follows as

$$n = \frac{\ln\left(\frac{E}{E_0}\right)}{\ln(1 + \xi)} .\tag{2.11}$$

With an escape probability P_{esc} for every collision we get a probability of $(1 - P_{esc})^n$ that the particle is still in the acceleration mechanism after n collisions. The amount of particles, that are accelerated up to energies above an energy E is

$$N(> E) \sim \sum_{m=n}^{\infty} (1 - P_{esc})^m = \frac{(1 - P_{esc})^n}{P_{esc}} .\tag{2.12}$$

With the above calculated n:

$$N(> E) \sim \frac{1}{P_{esc}}(1 - P_{esc})^{\frac{\ln E/E_0}{\ln(1+\xi)}} = \frac{1}{P_{esc}}\left(\frac{E}{E_0}\right)^{\frac{\ln(1-P_{esc})}{\ln(1+\xi)}} .\tag{2.13}$$

Thus, we get a power law behaviour in such an acceleration process:

$$\boxed{N(> E) \sim \frac{1}{P_{esc}}\left(\frac{E}{E_0}\right)^{-\gamma}}\tag{2.14}$$

with a spectral index of

$$\gamma = -\frac{\ln(1 - P_{esc})}{\ln(1 + \xi)} ,\tag{2.15}$$

which is for $P_{esc} \ll 1$ and $\xi \ll 1$:

$$\gamma \approx \frac{P_{esc}}{\xi} .\tag{2.16}$$

P_{esc} is the ratio of a characteristic time scale T_{cycle} for one acceleration cycle and a characteristic time scale T_{esc} for the escape from the acceleration region.

For a finite acceleration time t with $n_{max} = t/T_{cycle}$ a maximum energy of

$$E_{max} = E_0(1 + \xi)^{\frac{t}{T_{cycle}}}\tag{2.17}$$

is reached.

Now it depends on the fraction of energy gain ξ how efficient the process can be. We call it a first-order Fermi acceleration process, when $\xi \sim v/c$, and a second-order Fermi process if $\xi \sim (v/c)^2$. In shock fronts we encounter the first-order Fermi acceleration, and in the interstellar medium we deal with second-order Fermi acceleration, the so called stochastic momentum diffusion, which is a main theme of the present work.

If we assume Alfvén waves as scattering centers for the particles, their magnetic component is much stronger than their electric component, so that the particles can gain nearly no energy in an interaction with such a wave. The increase in energy is a result of the different velocities of the scattering centers in front and behind the shock front. If the waves itself have a velocity v_A, the particles can gain or loose energy, when they are scattered by the waves, but on average there is no change in the momentum. There remains a stochastic diffusion in momentum space with a typical momentum diffusion equation for the phase space distribution function $\tilde{f}$:

$$\frac{\partial \tilde{f}}{\partial t} - \frac{1}{p^2}\frac{\partial}{\partial p}\left(A_2 p^4 \frac{\partial \tilde{f}}{\partial p}\right) = Q(p) \ . \tag{2.18}$$

This diffusion term is part of the full transport equation for the galactic cosmic rays.

Transport of Galactic Cosmic Rays

A derivation of the complete transport equation can be found in the text book of [Schlickeiser 2001]. We will sketch this in Chapter 3. Here we only present and discuss the terms of the equation:

$$\begin{aligned}
\frac{\partial f}{\partial t} - S(\vec{x}, p, t) \ = \ & \frac{\partial}{\partial z}\left[\kappa_{zz}\frac{\partial f}{\partial z} - Vf\right] \\
& + \frac{1}{p^2}\frac{\partial}{\partial p}\left(p^2 A_2 \frac{\partial f}{\partial p} + \frac{p^3}{3}\frac{\partial V}{\partial z}f - p^2\dot{p}f\right) \\
& - \frac{f}{T_c}
\end{aligned} \tag{2.19}$$

Here, we used the isotropic phase space distribution function f. The transport equation is a linear partial differential equation of second-order in time, space and momentum with non-constant coefficients. The first term on the right hand side decribes spatial diffusion with a diffusion coefficient κ_{zz}, as will be shown subsequently. The next term represents spatial convection with a cosmic ray bulk speed of V. The next two terms are responsible for the acceleration and deceleration in momentum, namely the momentum diffusion (Fermi acceleration of second-order)

with a diffusion coefficient A_2 and momentum convection (Fermi acceleration of first-order). The fifth term takes into account continuous loss processes, like synchrotron radiation or bremsstrahlung while the last term represents catastrophic losses, that means spallation of the cosmic ray nuclei with $Z > 1$, characterized by a typical time scale T_c.

In this work, we assume no galactic wind and neglect the two convection terms. This holds exactly, if we suppose equal amounts of forward and backward moving Alfvén waves in the interstellar medium, because then the diffusion coefficient A_1 in

$$V := \frac{1}{4p^2} \frac{\partial(p^2 v A_1)}{\partial p} \tag{2.20}$$

vanishes to zero, as it is shown in [Stawicki 2003], and hence V, too.

In this work, we deal only with the stationary transport equation, that means $\frac{\partial f}{\partial t} = 0$. This is justified because, as mentioned above, the cosmic ray flux can be considered as constant for our purposes during the past 10^9 years. For time-dependent calculations refer to, e. g., the work of [Büsching et al. 2005].

A Simple Diffusion Model

Now, as a simple example for a purely spatial diffusion, we neglect momentum diffusion and convection of the particles. Spatial diffusion is described by the relation of the flux of particles to the spatial gradient of the particle density:

$$\vec{j}(\vec{x}, t) = -\kappa \nabla n(\vec{x}, t) . \tag{2.21}$$

Inserting this into the continuity equation

$$\frac{\partial n(\vec{x}, t)}{\partial t} = -\nabla \cdot \vec{j} + Q(\vec{x}, t) , \tag{2.22}$$

where Q is a source term, we get a simple transport equation without the momentum terms, without spatial convection and without continuous and catastrophical losses:

$$\frac{\partial n(\vec{x}, t)}{\partial t} = \nabla \cdot (\kappa \nabla n(\vec{x}, t)) + Q(\vec{x}, t) . \tag{2.23}$$

The associated Green's function for this equation reads

$$G(\vec{x}, t) = \frac{1}{8(\pi \kappa t)^{3/2}} \exp(-\frac{\vec{x}^2}{4\kappa t}) . \tag{2.24}$$

The spatial scale that emerges in the Green's function is $2\sqrt{\kappa t}$. So, if we consider diffusion away from a galactic plane into a halo (see subsequent subsections) with half-height H, the time scale for this process is in the order of

$$\boxed{T_{esc} \sim \frac{H^2}{\kappa}} \ . \tag{2.25}$$

A Leaky Box Model

In contrast to the previous subsection now we neglect spatial diffusion and convection and replace them by an escape term $-f/T_{esc}$ and consider only momentum diffusion:

$$\frac{\partial f}{\partial t} - \frac{1}{p^2}\frac{\partial}{\partial p}\left(A_2 p^2 \frac{\partial f}{\partial p}\right) - \frac{f}{T_{esc}} = Q(p) \ . \tag{2.26}$$

This type of equation is called a leaky box equation (cf. [Schlickeiser 2001] or [Gaisser 1990]), because we assume, that the particles leak out of the galaxy and no spatial diffusion takes place. From dimensional arguments the time scale T_f for momentum diffusion can be inferred:

$$\boxed{T_f \sim \frac{p^2}{A_2}} \ . \tag{2.27}$$

Propagation of Galactic Cosmic Rays

Galactic cosmic rays are confined by galactic magnetic fields and are scattered by plasma waves superimposed on these fields, thereby loosing their original direction. Thus, the measured cosmic rays on earth are isotropic up to 10^{15} eV. There is no enhancement of cosmic radiation in the direction of the galactic plane, where the bulk of the supernova remnants is located.

In this work, we are interested in the reacceleration of galactic cosmic rays by plasma waves after injection of the particles by supernova remnants. These plasma waves themselves may be induced also by supernova turbulence.

There are some hints that the confinement volume is much larger than the galactic disk itself. Around the galactic disk there is a halo filled up with magnetic fields and a hot dilute plasma, as it can be observed also in other galaxies, like that one in Fig. 2.19.
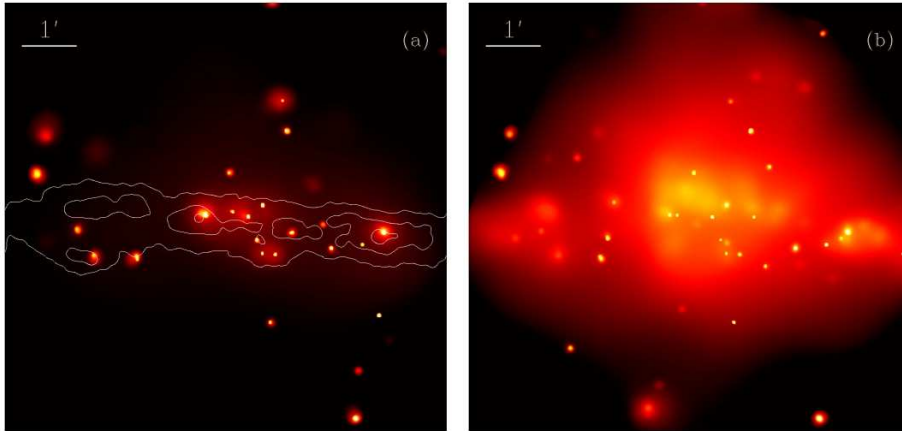
Figure 2.19: CHANDRA images of the halo of the galaxy NGC 4631 in the 1.5-7 keV
band (left) and in the 0.3-1.5 keV band (right). The far-UV intensity contours
outline the morphology of the galactic disc. Taken from [Wang et al. 2001].

Radio and optical polarization measurements provide the structure of galactic and
extragalactic magnetic fields, also in galactic halos. Measurements of radio emission
from galactic halos can be interpreted as non-thermal synchrotron radiation of en-
ergetic cosmic ray electrons gyrating around magnetic field lines.

Another evidence for a halo follows from the averaged column density λ, the cosmic
particles have penetrated when they arrive at the solar system:

$$\lambda := \bar{\rho}\,\beta\,c\,T_{esc} \tag{2.28}$$

with $\beta = v/c$. This column density can be estimated with a simple leaky box model
applied to measured primary to secondary abundance ratios. From radioactive iso-
topes possessing a half-time roughly equal to the escape time from the galaxy, we
get again within the frame of the leaky box model T_{esc}, thus the average matter
density $\bar{\rho}$ can be inferred, which is in the order of 0.4-0.6 atoms/cm^3 and therefore
less than the average density of matter in the galactic plane of ≥ 1 atoms/cm^3.
Consequently the cosmic rays have to travel a part of their lifetime through regions
with a low-density medium.

In this work we approximate the galactic disk and the halo by cylindrical volumes
and neglect second-order structures like spiral arms, etc. For a review of the prop-
erties of the galaxy refer to, e. g., the book of [Scheffler & Elsässer 1992].

Loss Processes

During their propagation particles suffer from continuous energy losses and spallation, which is important in the galactic disc, but not in the halo, where the gas density is substantial lower.

Spallation takes place in the galactic plane, which is filled up with the gaseous interstellar medium, mainly hydrogen (70%) and helium (28%). These spallation processes have to be taken into account for primary cosmic ray particles with atomic numbers $A > 1$. They enter into the transport equation by a catastrophic loss time T_c. For radioactive secondaries, we have to introduce additionally a relativistic decay time.

Continuous losses relevant for electrons are, for example, ionization and excitation of atoms, Coulomb interactions, bremsstrahlung, inverse-Compton emission and synchrotron radiation, which for nucleons are only important at energies below a few GeV, because into the cross-sections enter the Thomson cross-section, which is proportional to $(Z^4/A^2)(m_e/m_p)^2$ and, therefore, much smaller for interactions of cosmic ray nuclei (cf. [Pohl 2002]).

Details of the interaction processes can be found, for example, in the text books of [Longair 1992] and [Schlickeiser 2001]. Formula for the energy losses of nuclei, which can be applied to the transport equation, are presented in
[Mannheim & Schlickeiser 1994].

2.1.3 Extragalactic Cosmic Rays

For completeness in this subsection we deal with features and models for extragalactic cosmic rays.

Because the gyroradii

$$r_g \sim \frac{\gamma m_0 v}{ZeB} \tag{2.29}$$

for protons above 10^{15} eV are roughly equal to the scale of the galactic magnetic irregularities, which are responsible for the confinement of the particles in the galaxy, protons with higher energies have to be extragalactic. For higher elements with charge number Z the gyroradius for the same total energy is a factor $1/Z$ smaller.

The highest energies of cosmic rays exceed by orders of magnitudes the values that can be achieved at terrestrial laboratories. Energies up to about 10^{21} eV have been measured (Fig. 2.1).

To estimate roughly the maximum possible energy of particles in a magnetic field B in a source with a scale length L we take the induced electric field $\vec{E}$:

$$\nabla \times \vec{E} = -\frac{\partial \vec{B}}{\partial t} \ . \tag{2.30}$$

With the dimensions of the system we get

$$\frac{E}{L} = \frac{B}{L/c} \tag{2.31}$$

thus $E = cB$. By integration the maximum energy of a particle with charge Ze follows:

$$E_{max} = \int_0^L ZeE \, dx = ZecBL \ . \tag{2.32}$$

The possible accelerators for ultrahigh energy cosmic rays deduced from this simple criterion are shown in the famous Hillas plot in Fig. 2.20.

For the highest energetic hadronic cosmic rays the interactions with the cosmic microwave background should lead to a cutoff in the observed spectrum at $5 \cdot 10^{19}$ eV, called the GZK-cutoff (**G**reisen **Z**atsepin **K**uzmin), if the energy lies above the threshold for photo-pion production and provided that these particles are protons and that the source distribution is homogeneous in the universe:

$$p + \gamma_{2.7K} \longrightarrow p + \pi^0 \ . \tag{2.33}$$
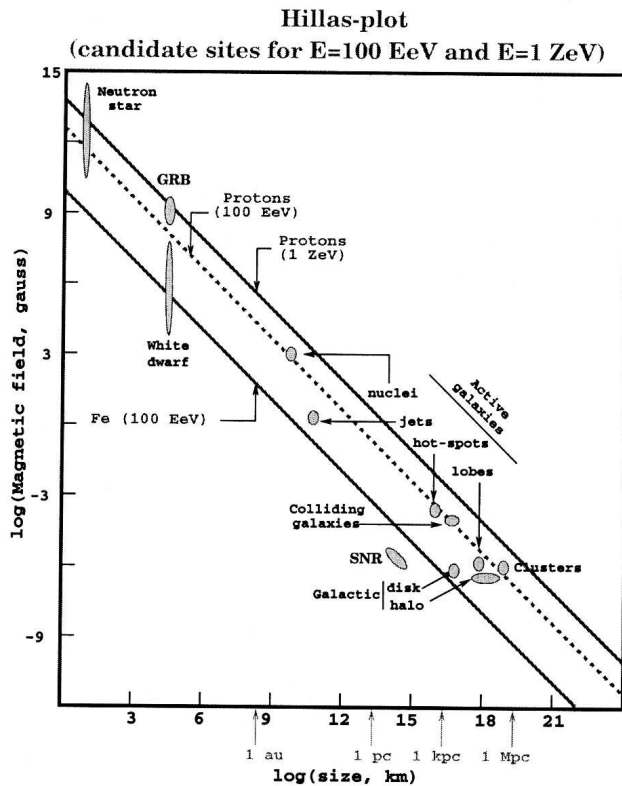
Figure 2.20: The Hillas plot. Possible accelerators for ultrahigh energy cosmic rays lie above the lines for 100 EeV (10^{17} eV) iron, 100 EeV protons and 1 ZeV (10^{18} eV) protons. (GRB = Gamma-Ray Burst, SNR = Supernova Remnant). Taken from [Lemoine & Sigl 2001].

But contrary, no cutoff is seen in the data. One could conclude, that cosmic rays with energies above about $5 \cdot 10^{19}$ eV should originate in a local volume with a radius of the order of 50-100 Mpc. On the other hand the systematic errors of the airshower experiments in this extreme energy region are still too high to determine the form of the spectrum unambiguously.

Below the GZK-cutoff energy, the dominant loss mechanism for protons is the pair production process:

$$p + \gamma_{2.7K} \longrightarrow p + e^+ + e^- \ . \tag{2.34}$$

Nuclei of atomic number A suffer - apart from the above mentioned processes - photo-disintegration at the 2.7 K photon background:

$$A + \gamma_{2.7K} \longrightarrow (A - 1) + n/p \,. \tag{2.35}$$

To explain the origin of the highest energetic cosmic rays two scenarios are imaginable:

- "top-down": the particles are decay products of remnant particles (GUT-, SUSY-, ... particles) or of topological defects (magnetic monopoles, cosmic strings, ...) created in the early universe. In this scenario the cosmic rays at the end of these fragmentation chains should be mostly photons, but there is evidence in the data, that the highest energy cosmic rays are not photons.

- "bottom-up": acceleration of particles takes place in shock fronts (termination shock of a galactic wind, active galactic nuclei (refer to the next subsection), shockfronts in galaxy clusters, shocks in gamma-ray bursts, ...). For this scenario only classical physics is used, which may be an advantage because of the partially unknown new physics needed in the top-down scenarios.

There is still a debate in scientific community about the possible theoretical mechanisms and the interpretation of the highest energy data. For an overview read, e. g., [Nagano & Watson 2000]. A short review of the recent observational results can be found in [Nagano 2002].

Extragalactic Gamma-Rays

In recent years several extragalactic sources of high energy photons for measured photon energies > 250 GeV have been detected (according to [Bojahr 2002]): Mkn 421 (confirmed), Mkn 501 (confirmed), 1ES 2344+514, 3C 66A, PKS 2155-304, 1ES 1959+650 (confirmed), 1ES 1426+428 (confirmed), BL Lacertae, NGC 253 and M 87. This TeV gamma radiation can be produced by the decay of neutral pions, as a consequence of the interaction of high energy hadronic cosmic rays, or by electron inverse Compton scattering (as mentioned in the beginning of this chapter). In the first case there would be a bump at about 70 MeV (half of the neutral pion mass) in the rest frame of the galaxy in the photon spectrum, but it could be masked by the $e^{\pm}$-bremsstrahlung of the decaying muons, stemming from the charged pions.

The above listed extragalactic sources all belong to a larger class of galaxies, the active galactic nuclei (AGN), with high nonthermal luminosities from the infrared up to gamma radiation, distinguished from normal galaxies emitting most of their energy in the optical band. The theoretical standard model of these AGN is illustrated in Fig. 2.21.
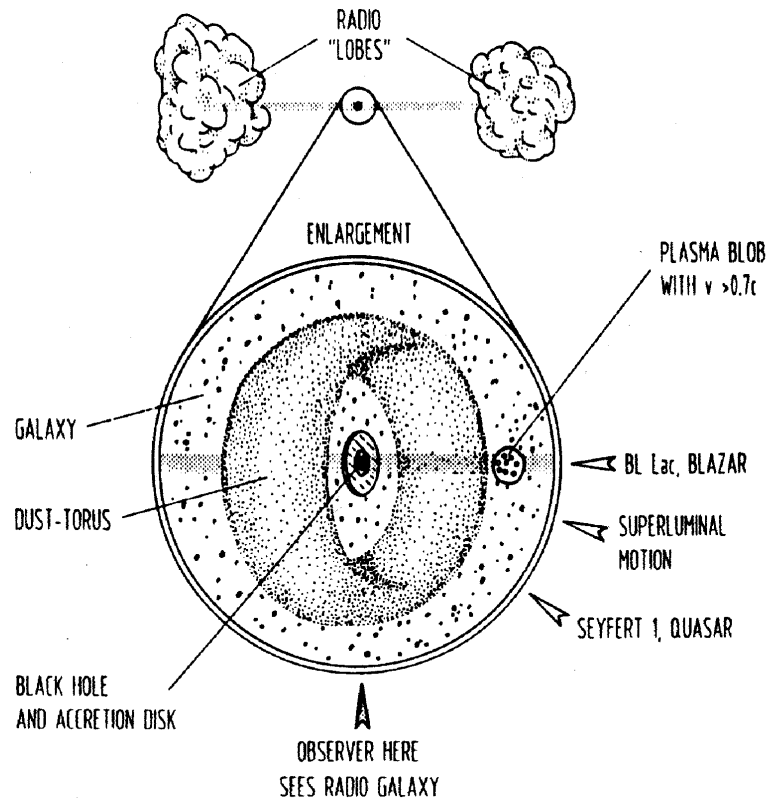
Figure 2.21: Standard model of an AGN, taken from [Mause 1996]: a galaxy with a central supermassive black hole, surrounded by an accretion disk and a dust torus. Accreted material is ejected far out of the galaxy and collides with the intergalactic medium, forming radio lobes. Depending on the viewing angle we classify the object as a BL Lac, a blazar, a Seyfert 1 galaxy, a quasar or a radio galaxy. The relativistic effect of superluminal motion of plasma blobs can be detected in a small off-axis-viewing angle.

Following from the measured short-time daily variations in the TeV-flux of, e. g., Mkn 501 ([Aharonian et al. 1999a] and [Aharonian et al. 1999b]) the only object supplying enough energy for the detected luminosities from its gravitational field can be a supermassive black hole ($10^7 - 10^{10}$ solar masses) in the center of the AGN. Material accumulates in an accretion disk around the black hole feeding two jets with plasma blobs ejected in the direction of the rotation axis of the black hole by a still not exactly known mechanism into intergalactic space, leading to radio lobes when hitting the intergalactic medium. Around the central region there might be a dust torus. Both, the accretion disk and the dust torus could deliver direct seed photons or by the broad-line region clouds rescattered photons for inverse Compton

scattering by electrons in the plasma blobs, leading to high energy photon emission ([Arbeiter 1999]), where relativistic beaming plays an important role. Instead other models state the comptonization of self-generated jet synchrotron photons (SSC models). There is still a discussion, whether and up to which energies acceleration of hadrons takes place in the jets, too. For an overview see the article of [Mannheim 1997].

Fig. 2.22 shows an example of a pair of radio jets emitted deep into intergalactic space.
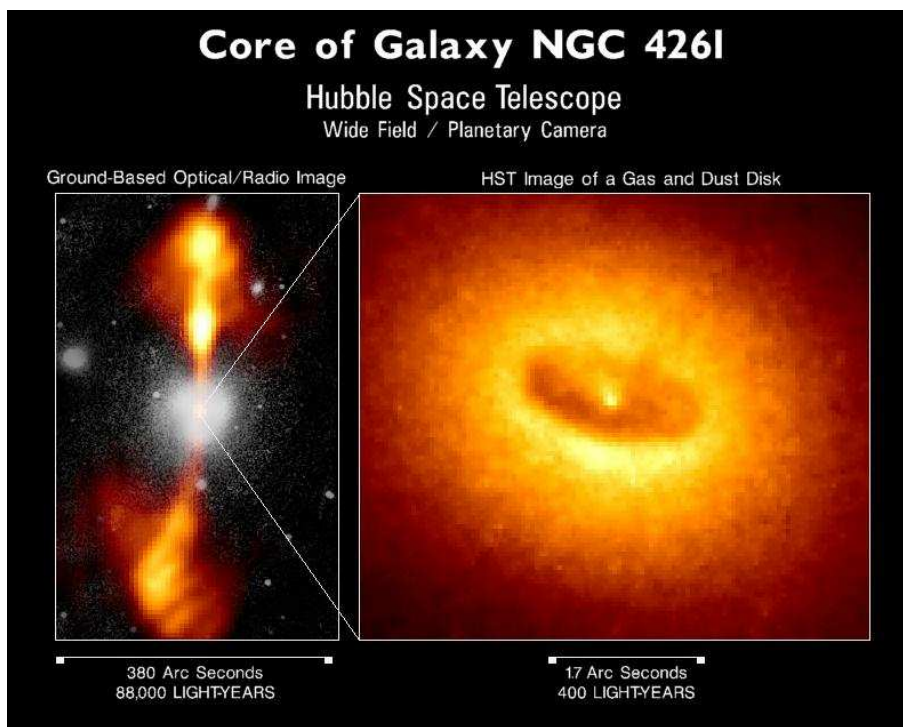
Figure 2.22: AGN NGC 4261. Left: radio lobes with superimposed optical photo, viewed with ground-based telescopes. Right: gas and dust disk in the center of the galaxy, photographed by the Hubble Space Telescope (taken from [Carroll & Ostlie 1996]).

Now it depends decisively on the direction of the jets in relation to the observer, which type of AGN is detected. If the jet axis points directly to the observer, the object is classified as the mentioned TeV-blazar.

It is speculated, that the combined gamma radiation from AGN also may make up the bulk of the cosmic diffuse gamma-ray background.

2.2   Measurement of Cosmic Rays

The first evidence of the phenomenon of cosmic rays was given by [Hess 1912] flying with a balloon and detecting an increase of the intensity of an ionizing radiation with altitude, excluding a terrestrial origin (for a historical review refer to [Federmann 2003]). This radiation, so called "Höhenstrahlung" in German, later has been identified with the energetic particles of the airshowers penetrating the earth's atmosphere induced by primary high energetic cosmic rays, as mentioned below in the Subsection 2.2.3.

2.2.1   Solar Wind

In situ measurements of (low energy) cosmic rays and of plasma parameters can be realized today by space probes travelling through the heliosphere. The first experimental confirmation of the solar wind was given 1962 by the Mariner 2 spacecraft. To investigate the sun and the interplanetary medium, SOHO (Solar and Heliospheric Observatory) recently was positioned between earth and sun. Voyager 1 measures protons up to an energy of 500 MeV and is with a distance of approximately 90 AU the outermost spacecraft to explore the outer heliosphere, perhaps crossing the termination shock of the heliospheric boundary in near future. Ulysses is the first spacecraft leaving the ecliptic plane of solar system to investigate the solar wind above the poles of the sun.

2.2.2   Direct Experiments

To detect directly the more energetic galactic cosmic rays reaching earth several balloon and satellite experiments have been launched in the past. As seen in Tab. 2.1, the highest energies that can be detected for nuclei with these methods lie in the order of 10^{14}-10^{15} eV, due to the dramatic decreasing of the flux of cosmic rays with increasing energy (cf. Fig. 2.1), which for example for protons > 10 TeV is in the order of 3 m^{-2} h^{-1} sr^{-1}.

The books of [Grupen 1993] and of [Longair 1992] explain some principles of particle detection.

An important device for direct detection of gamma-rays was EGRET onboard the Compton-Gamma-Ray-Observatory (CGRO), with an upper limit of 20 GeV for photon energies. In the future, GLAST (Gamma Ray Large Area Space Telescope) will be a successor of EGRET with a larger sensitive area.

Experiment	Type	Observed nuclei	Energy Range	Operating
ACCESS	Space station	H - U	$< 10^{15}$ eV for H	> 2007
ALICE	Balloon	Si - Fe	$3.5 \cdot 10^8 - 8 \cdot 10^8$ eV/nuc	1987
ATIC	Balloon	H - Fe	$10^{10} - 10^{14}$ eV	2000 - 2003
BACH	Balloon	Fe	$> 5 \cdot 10^{13}$ eV	1998
BESS	Balloon	H + He	$1.7 \cdot 10^8 - 3 \cdot 10^9$ eV/nuc	1993 - 1998
Bristol Cosmic Ray Detector	Satellite	Fe - Fm		1979
CAPRICE	Balloon	H	$1.5 \cdot 10^8 - 10^{11}$ eV/nuc	1994
Cosmic-Ray Charge-Isotope Telescope	Balloon	Be - Ni	$3 \cdot 10^8 - 5 \cdot 10^{10}$ eV/nuc	1974 + 1976
CRISIS	Balloon	Si - Ni	$\sim 4.3 \cdot 10^8 - 9 \cdot 10^8$ eV/nuc	1977
CRN	Satellite	C - Fe	$7 \cdot 10^{10} - 10^{12}$ eV/nuc	1985
German American High Energy Cosmic Ray Telescope	Balloon	B - Fe	$2 \cdot 10^9 - 2.5 \cdot 10^{11}$ eV/nuc	1976
HEAO-3-C2	Satellite	Be - Ni	$6 \cdot 10^8 - 3.5 \cdot 10^{10}$ eV/nuc	1979 - 1980
HEAO-3 Heavy Nuclei Experiment	Satellite	Zn - U	$> 1.5 \cdot 10^9$ eV/nuc	1979
HEAT	Balloon	H, He	$10^{10} - 10^{11}$ eV/nuc	1994
HEN	Balloon	Li - Ni	$2 \cdot 10^{10} - 10^{11}$ eV/nuc	1971 + 1972
Successor of HEN	Balloon	B - Fe	$5 \cdot 10^9 - 9 \cdot 10^{10}$ eV/nuc	1974
IMAX	Balloon	H + He	$2 \cdot 10^8 - 2 \cdot 10^{11}$ eV/nuc	1992
ISOMAX	Balloon	Be	$\sim 10^9$ eV/nuc	1998
JACEE	Balloon	H - Fe	$2 \cdot 10^{12} - 8 \cdot 10^{14}$ eV/nuc	1979 - 1995
JEM	Space Station	H - Fe	$10^{12} - 5 \cdot 10^{14}$ eV/nuc	~ 2007
LEAP	Balloon	H + He	$2 \cdot 10^8 - 10^{11}$ eV/nuc	1987
MASS	Balloon	H + He	$\sim 10^8 - 4 \cdot 10^{10}$ eV/nuc for H	1989
MUBEE	Balloon	H - Fe	$> 10^{10}$ eV/particle	1975 - 1987
Orth et al.	Balloon	Li - Fe	$2 \cdot 10^9 - 1.5 \cdot 10^{11}$ eV/nuc	1972
Proton-Satellites	Satellite	H - Fe	$10^{10} - 10^{14}$ eV	1965 - 1966
RICH	Balloon	He - O	$4 \cdot 10^{10} - 3.2 \cdot 10^{11}$ eV/nuc	1991
RUNJOB	Balloon	H - Fe	$10^{13} - 10^{15}$ eV/particle	since 1995
Ryan et al.	Balloon	H + He	$5 \cdot 10^{10} - 10^{12}$ eV/nuc	1970
Sanriku Balloon Experiment	Balloon	H - Fe	$10^{13} - 10^{14}$ eV/nuc	1989 + 1991
SMILI	Balloon	H, He	$3 \cdot 10^7 - 2 \cdot 10^8$ eV/nuc	1989 + 1991
Sokol Experiments	Satellite	H - Fe	$2 \cdot 10^{12} - 10^{14}$ eV/nuc	1984 - 1986
TIC	Balloon	H - Fe	$10^{11} - 10^{13}$ eV	1994
TRACER	Balloon	C - Fe	$10^{12} - 10^{14}$ eV	since 2000

2.1: Direct experiments for cosmic rays. Adapted from [Wiebel-Sooth 1998].

2.2.3 Indirect Experiments

In the regime of the highest cosmic ray energies one has to rely on indirect experiments and detect the secondary particles of an extended airshower emerging in the atmosphere when a primary cosmic ray particle hits an air nucleus and generates a particle cascade (cf. Fig. 2.23).
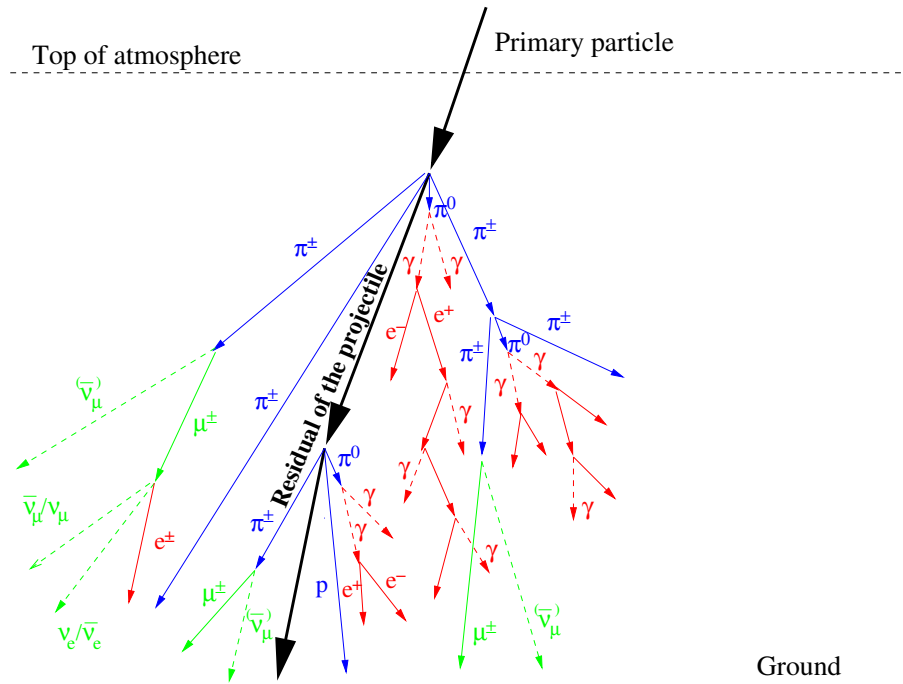
Figure 2.23: An airshower induced by a primary incident nucleus hitting earth's atmosphere. Three components can be distinguished: the electromagnetic part (red), the hadronic part (blue) and the muonic part (green). The neutrinos can be regarded as a fourth component. (Red lines: electrons/positrons; red dashed lines: photons; blue lines: hadrons; green lines: muons/antimuons; green dashed lines: electron/muon neutrinos/antineutrinos; black line: residual of the projectile.)

For a primary incident nucleus we can distinguish four components of an airshower: an electromagnetic part consisting of electrons, positrons and photons, developing by pair-production and bremsstrahlung from an originating neutral pion decay after a hadronic interaction, a hadronic part, stemming from inelastic hadronic interactions, a muonic part, due to the decay of charged pions, and neutrinos from the decay of muons and charged pions.

The evolving airshower can be investigated with ground-based experiments by dif-

ferent methods:

- scintillation detectors transform the energy losses of particles crossing the detector crystal into light emission;

- muon counters;

- Cherenkov light detectors, collecting the Cherenkov light emission of the shower particles propagating through the atmosphere;

- air / nitrogen fluorescence light detectors, which measure the fluorescence light excited by the shower particles in the atmosphere;

- hadron calorimeters for the hadronic component of the shower;

- radio antennas, catching the synchrotron emission of the cascade-electrons in the geomagnetic field;

- water Cherenkov tanks, whereby the water has a larger refractive index than air, so producing more Cherenkov light which can be detected.

Some of the most important ground-based experiments are listed in Table 2.2. Several of them combine the above mentioned detecting methods to gain complementary physical informations.

As an example for a Cherenkov telescope the MAGIC telescope on the isle La Palma is shown in Fig. 2.24.

Reconstruction of the primary energy, direction and kind of the incident particle is demanding, but possible, though it remains larger statistical and systematical errors than for the direct detection methods. For the understanding of the data it is important to simulate the evolution of the extended airshowers by Monte Carlo calculations. A serious difficulty for interpretation of the highest energy cosmic rays is the unknown physics for the ultrahigh energy hadronic interactions. The gap between these highest energies and the energies, which can be achieved by elemental particle laboratories, is some order of magnitudes. Fermilab's Tevatron Collider provides proton-antiproton collisions at a maximum center of mass energy of $2 \cdot 10^{12}$ eV, equivalent to a cosmic ray particle of about $2 \cdot 10^{15}$ eV incident on a stationary proton. The RHIC (Relativistic Heavy Ion Collider) at Brookhaven produces energies of more than 10^{11} eV per nucleon in beam-beam collisions of nuclei. For example, a nitrogen-nitrogen collision at RHIC corresponds to a $5 \cdot 10^{14}$ eV cosmic ray nitrogen nucleus incident on an air nucleus. The LHC (Large Hadron Collider) at CERN in the near future will reach a center of mass energy of proton-proton collisions of $1.4 \cdot 10^{13}$ eV, equivalent to proton projectile energy of 10^{17} eV. Another problem

Experiment	Location	Techniques	Energy Range [eV]
Akeno	Japan	S, M	$3 \cdot 10^{14} - 10^{18}$
AGASA		S, M	$> 10^{17}$
Andyrchy	Russia	S	$\sim 2 \cdot 10^{14} - 10^{16}$
ANI	Armenia	S, M, H	$10^{14} - 10^{16}$
Auger	Argentina, USA	W, A	$> 10^{19}$
BASJE	Bolivia	S	$2 \cdot 10^{13} - 10^{16}$
Buckland Park	Australia	S	$> 10^{14}$
CASA - MIA	USA	S, M	$10^{14} - 10^{16}$
- BLANCA		C	$3 \cdot 10^{14} - 3 \cdot 10^{16}$
DICE	USA	C	$5 \cdot 10^{14} - 3 \cdot 10^{16}$
EAS-TOP	Italy	S, M, C, R	$10^{14} - 10^{16}$
Fly's Eye	USA	A	$> 10^{17}$
GRAPES III	India	S, M	$3 \cdot 10^{13} - 3 \cdot 10^{16}$
Haverah Park	Great Britain	W	$> 4 \cdot 10^{17}$
HEGRA	Spain	S, M, C	$3 \cdot 10^{13} - 10^{16}$
HiRes	USA	A	$> 10^{17}$
KASCADE	Germany	S, M, H	$3 \cdot 10^{14} - 5 \cdot 10^{16}$
MAGIC	Spain	C	$3 \cdot 10^{10} - 5 \cdot 10^{13}$
MSU	Russia	S, M	$10^{15} - 10^{17}$
Mt. Norikura	Japan	S	$10^{14} - 10^{16}$
SPASE	Antarctica	S	$10^{14} - 3 \cdot 10^{16}$
- VULCAN		C	
SUGAR	Australia	M	$> 10^{17}$
Tibet ASγ	China	S	$3 \cdot 10^{12} - 2 \cdot 10^{16}$
Tien Shan	Kazakhstan	S, M, H	$10^{13} - 10^{18}$
TUNKA-13	Russia	C	$3 \cdot 10^{14} - 7 \cdot 10^{16}$
VEGA	Kazakhstan	C	$3 \cdot 10^{14} - 3 \cdot 10^{16}$
Yakutsk	Russia	S, M, C, R	$> 10^{16}$

Techniques : S = scintillator stations
M = muon counters
C = Cherenkov light detectors
A = air / nitrogen fluorescence light detectors
H = hadron calorimeters / detectors
R = radio antennas
W = water Cherenkov tanks

Table 2.2: Ground-based experiments for cosmic rays.
Adapted from [Wiebel-Sooth 1998].

is that most of the experiments are not able to measure along the direction of the particle beam. Theoretical calculations of high energy interactions in airshowers today are only possible by extrapolating empirical models up to the highest cosmic ray energies, because theoretical QCD (Quantum Chromodynamic) calculations are still not possible.

The ultrahigh energy events are very rare and new detector fields are under construction to collect more data, like the Auger experiment in Argentina.

A neutron monitor detects the nucleonic component of an airshower. If the nucleons hit a shield of lead, neutrons are generated, which are counted and are a

Figure 2.24: The MAGIC (Major Atmospheric Gamma-Ray Imaging Cherenkov) telescope on the Canarian Island La Palma site.

measure for the primary intensity.

The books of [Sokolsky 1989] and [Gaisser 1990] are, for example, dealing with airshower physics and detection methods. The methods of energy and mass determination are described in the review of [Kampert 2001].

2.2.4 Neutrino Detectors

Because Neutrinos experience only weak force processes, their detection requires large detector mediums, like huge water tanks (Super-Kamiokande detector), seas (Baikal- and ANTARES (Astronomy with a Neutrino Telescope and Abyss environmental RESearch) experiment) or the antarctic ice (AMANDA (Antarctic Muon And Neutrino Detector Array) experiment) as a detector volume to increase the possibility of an interaction. The Cherenkov light of the produced electrons, respective of the positrons, can be detected. Some other detectors are positioned deep underground to shield background particles. Solar neutrinos can also be detected by radio chemical experiments, by filtering out the converted unstable nuclei, but in this case the time, energy and direction information is lost.

2.3   The Galactic Plasma

The cosmic rays propagate through the interstellar medium and interact with plasma waves, which occur, if the interstellar medium is partially or fully ionized. The interstellar medium consists of four main constituents: molecular clouds, cold neutral HI-regions with $n \approx 10$ cm^{-3} and $T \approx 10^2$ K (cf. e. g. [Longair 1994]), the ionized inter-cloud medium, with $n \approx n_e \approx 0.1$ cm^{-3} and $T \approx 10^4$ K (cf. e. g. [Longair 1994] and [Voigt 1991]), and the hot coronal gas component with $n \approx 10^{-3}$ cm^{-3} and $T \approx 10^6$ K (cf. e. g. [Longair 1994]). The last three components are in pressure equilibrium, that means $p = nkT$ for them is roughly the same.

The energy density of the galactic cosmic rays is in the same order of magnitude as the turbulent and thermal energy density of the thermal gas and the interstellar magnetic field energy density (cf. e. g. [Unsöld & Baschek 1999]).

2.3.1   Waves in the Interstellar Medium

Waves in the interstellar medium are mainly generated by supernova explosions and the cosmic ray particles themselves. [Schlickeiser 2001] concludes from plasma instability studies, that Alfvén waves and magnetosonic waves have short growth times in the interstellar medium. In the book cited those spatial and momentum diffusion coefficients are calculated, which we use in this work.

The mean galactic magnetic field is in the order of $B \approx 3$ μG (cf. e. g. [Scheffler 1997] or [Spitzer 1978]) and the mean of the magnetic interstellar fluctuations caused by plasma turbulences is in the order of $\delta B \approx 0.9$ μG (according to [Spangler 1991] and [Minter & Spangler 1997]).

Wave Cascading

The interstellar plasma waves are assumed to be primarily induced on large scale lengths in the order of parsecs, corresponding to small wave numbers. The subsequent process of cascading to larger wave numbers can be described by a diffusion in wave number space for a 3-dimensional spectral density $\tilde{W}_i$ of a wave mode i (cf. [Schlickeiser 2001]):

$$\frac{\partial}{\partial t} \tilde{W}_i(\vec{k}) = -\frac{\partial}{\partial \vec{k}} \vec{F}(\vec{k}) \tag{2.36}$$

with the flux

$$\vec{F}(\vec{k}) = -D \frac{\partial}{\partial \vec{k}} \tilde{W}_i(\vec{k}) \tag{2.37}$$

and a diffusion coefficient in wave number space

$$D = \frac{k^2}{\tau_s(k)} \ , \tag{2.38}$$

where $\tau_s(k)$ is the spectral energy transfer time scale. For the isotropic spectral density $W_i(k) = 4\pi k^2 \tilde{W}_i(\vec{k})$ we get the one-dimensional diffusion equation

$$\frac{\partial W_i}{\partial t} = \frac{\partial}{\partial k} \left[\frac{k^4}{\tau_s(k)} \frac{\partial}{\partial k} (k^{-2} W_i) \right] + \Gamma_i W_i + S_i(k) \ . \tag{2.39}$$

Here Γ_i is the damping or growth rate of the waves and S_i is an injection or sink term. Now the spectral energy time scale provided by a special cascade phenomenology is decisive for the type of the wave spectrum. Two typical assumptions are the Kolmogorov model with

$$\tau_s(k) = \frac{1}{v_A k^{3/2}} \sqrt{\frac{2U_B}{W_i}} \tag{2.40}$$

and the Kraichnan model with

$$\tau_s(k) = \frac{2U_B}{v_A k^2 W_i} \tag{2.41}$$

including the energy density of the magnetic field $U_B = \frac{B_0^2}{4\pi}$ and the Alfvén velocity v_A. If we neglect the damping term and the source term and if we consider only the stationary diffusion equation, then we get for an ansatz

$$W_i(k) = W_0 k^{-q} \tag{2.42}$$

a spectral index of the turbulence $q = 5/3$ for a Kolmogorov spectrum and $q = 3/2$ for a Kraichnan spectrum.

While for the heliosphere a Kolmogorov index of the plasma wave spectrum has been derived directly by space probes (cf. e. g. [Marsch & Tu 1990]), for the interstellar space only indirect conclusions can be drawn. The time scale for the evolution of the plasma turbulence in the galaxy is much larger than for the solar wind driven heliosphere, thus we cannot automatically infer the same spectral behaviour. For the determination of the turbulence spectrum one assumes a connection between the electron density fluctuations of the plasma and the magnetic fluctuations induced by plasma waves:

$$\frac{\delta n_e}{n_e} \sim \frac{\delta B}{B_0} \ . \tag{2.43}$$

This topic is still under debate. In [Armstrong et al. 1995] is shown, that the electron density spectrum follows a power law with a Kolmogorov index of $q = 5/3$ across more than 10 decades with a maximum scale $\geq 10^{18}$ cm. In this work we also analyze the value of the spectral index by fitting model results from cosmic ray transport influenced by plasma wave turbulence to data.

Chapter 3

A Sketch of the Derivation of the Transport Equation

In this chapter we sketch the way from the Vlasov equation to the transport equation of the cosmic rays, which is central for this work, by applying the quasilinear and the diffusion approximations. The whole presentation can be found in the text book of [Schlickeiser 2001].

3.1   The Equations of Motion

We begin with the non-relativistic collision-free Vlasov equation for a particle j which deals with the total derivative of the phase space density:

$$\boxed{\frac{df_j(t, \vec{x}, \vec{v})}{dt} = S_j(t, \vec{x}, \vec{v})} \ . \tag{3.1}$$

The cosmic plasmas can mostly be considered as collision-free, therefore on the right hand side of the equation we can find only the source term S_j and no collision terms. Writing the left hand side explicitely provides the force term $\vec{F} = m\dot{\vec{v}}$, which is in our case the Lorentz force:

$$\begin{aligned}
\frac{df_j}{dt} &= \frac{\partial f_j}{\partial t} + \dot{\vec{x}}\frac{\partial f_j}{\partial \vec{x}} + \dot{\vec{v}}\frac{\partial f_j}{\partial \vec{v}} \\
&= \frac{\partial f_j}{\partial t} + \vec{v}\frac{\partial f_j}{\partial \vec{x}} + \frac{q}{m}\left[\vec{E}(t, \vec{x}) + \frac{\vec{v} \times \vec{B}(t, \vec{x})}{c}\right]\frac{\partial f_j}{\partial \vec{v}} \\
&= S_j(t, \vec{x}, \vec{v}) \ .
\end{aligned} \tag{3.2}$$

49

This equation is not only valid for one particle j but it describes any of the particles in the plasma, so that we omit the subscript j.

To complete the equations of motion we have to add Maxwell's equations for the electromagnetic fields generated by the collective motion of the plasma particles. The fields enter via the Lorentz force in the Vlasov equation.

The total charge density and the total current density for a particle of species a can be expressed by the phase space density:

$$\rho(t, \vec{x}) = \sum_a n_a q_a \int_{-\infty}^{\infty} d^3 v f_a(t, \vec{x}, \vec{v}) \ , \tag{3.3}$$

$$\vec{J}(t, \vec{x}) = \sum_a n_a q_a \int_{-\infty}^{\infty} d^3 v \vec{v} f_a(t, \vec{x}, \vec{v}) \ . \tag{3.4}$$

We get for the Maxwell equations:

$$\nabla \times \vec{B} = \frac{1}{c} \frac{\partial \vec{E}}{\partial t} + \frac{4\pi}{c} \sum_a n_a q_a \int_{-\infty}^{\infty} d^3 v \vec{v} f_a(t, \vec{x}, \vec{v}) + \frac{4\pi}{c} \vec{J}_{ext} \ , \tag{3.5}$$

$$\nabla \cdot \vec{B} = 0 \ , \tag{3.6}$$

$$\nabla \times \vec{E} = -\frac{1}{c} \frac{\partial \vec{B}}{\partial t} \ , \tag{3.7}$$

$$\nabla \cdot \vec{E} = 4\pi \sum_a n_a q_a \int_{-\infty}^{\infty} d^3 v f_a(t, \vec{x}, \vec{v}) + 4\pi \rho_{ext} \ . \tag{3.8}$$

The Maxwell equations include the external charge density ρ_{ext} and the external current density $\vec{J}_{ext}$.

These equations together with the Vlasov equation (3.2) are coupled nonlinearly: the electromagnetic field is generated by the particles of the plasma with the distribution function f_a, and f_a is determined by the electromagnetic field entering in the Vlasov equation.

In a first approximation, two different ansatzes can be made:
1. The *test wave approach*, where the particle distribution function f_a is given and the resulting plasma waves can be examined. In this work we do not deal with the excitation and propagation of plasma waves. Here we refer to the text book of [Schlickeiser 2001]. In our case, the waves are taken for granted in the plasma of the interstellar medium.
2. The *test particle approach*. In this case, the electromagnetic fields are initially

present and the behaviour of the particles can be discussed. The particle population in this work will be the charged hadronic cosmic rays.

The second approach will be followed in the next section.

3.2 The Quasilinear Approximation

First, we introduce the *relativistic* Vlasov equation:

$$\frac{\partial f_a}{\partial t} + \vec{v}\frac{\partial f_a}{\partial \vec{x}} + \dot{\vec{p}}\frac{\partial f_a}{\partial \vec{p}} = S_a(t, \vec{x}, \vec{p}) \tag{3.9}$$

with

$$\dot{\vec{p}} = q_a \left[\vec{E}_T(t, \vec{x}) + \frac{\vec{v} \times \vec{B}_T(t, \vec{x})}{c} \right] \tag{3.10}$$

and

$$\dot{\vec{x}} = \vec{v} = \frac{\vec{p}}{\gamma m_a} \ . \tag{3.11}$$

Because of the high conductivity of the cosmic plasma there is no background electric field, only a background magnetic field $\vec{B}_0 = B_0\vec{e}_z$. The plasma turbulence is superposed onto these fields and the total fields are consequently:

$$\vec{B}_T = \vec{B}_0 + \delta\vec{B}(t, \vec{x}) \ , \tag{3.12}$$

$$\vec{E}_T = \delta\vec{E}(t, \vec{x}) \ . \tag{3.13}$$

Now we transform the Vlasov equation into a new set of coordinates. The new spatial coordinates are the coordinates of the guiding center of the gyrorotating particles:

$$\vec{R} = (X, Y, Z) = \vec{x} + \frac{\vec{v} \times \vec{e}_z}{\epsilon\Omega} \tag{3.14}$$

with $\epsilon\Omega = \frac{q_a B_0}{m_a c\gamma}$, the gyrofrequency Ω in the uniform field and ϵ the charge sign.

In momentum space, we introduce spherical coordinates (p, μ, ϕ):

$$p_x = p\cos\phi\sqrt{1 - \mu^2} \ , \tag{3.15}$$

$$p_y = p\sin\phi\sqrt{1 - \mu^2} \ , \tag{3.16}$$

$$p_z = p\mu \, , \tag{3.17}$$

with $\mu = \cos\theta$.

Now the spatial coordinates read:

$$X = x + \frac{v\sqrt{1-\mu^2}}{\epsilon\Omega} \sin\phi \, , \tag{3.18}$$

$$Y = y - \frac{v\sqrt{1-\mu^2}}{\epsilon\Omega} \cos\phi \, , \tag{3.19}$$

$$Z = z \, . \tag{3.20}$$

Changing to the new coordinates $x_\sigma = (p, \mu, \phi, X, Y, Z)$ yields the Vlasov equation (using Einstein's summation convention)

$$\frac{\partial f_a}{\partial t} + v\mu\frac{\partial f_a}{\partial Z} - \epsilon\Omega\frac{\partial f_a}{\partial\phi} + \frac{1}{p^2}\frac{\partial}{\partial x_\sigma}(p^2 g_{x_\sigma} f_a) = S_a(t, \vec{x}, \vec{p}) \tag{3.21}$$

with the generalized force term g_{x_σ} which includes the effects of the electromagnetic fluctuations $(\delta\vec{E}, \delta\vec{B})$.

We are interested only in the expectation value of f_a:

$$\langle f_a(t, \vec{x}, \vec{p})\rangle =: F_a(t, \vec{x}, \vec{p}) \, , \tag{3.22}$$

where we consider the average over all members of an ensemble of distribution functions. For the average of the magnetic fields we obtain

$$\langle \delta\vec{B}(t, \vec{x})\rangle = \langle \delta\vec{E}(t, \vec{x})\rangle = 0 \, , \tag{3.23}$$

consequently for the average of the electromagnetic fields:

$$\langle \vec{B}_T(t, \vec{x})\rangle = \vec{B}_0 \, , \ \langle \vec{E}_T(t, \vec{x})\rangle = 0 \, . \tag{3.24}$$

Averaging the Vlasov equation provides:

$$\frac{\partial F_a}{\partial t} + v\mu\frac{\partial F_a}{\partial Z} - \epsilon\Omega\frac{\partial F_a}{\partial\phi} = S_a(t, \vec{x}, \vec{p}) - \frac{1}{p^2}\frac{\partial}{\partial x_\sigma}\left(\langle p^2 g_{x_\sigma} \delta f_a\rangle\right) \tag{3.25}$$

with

$$\delta f_a(t, \vec{x}, \vec{p}) := f_a(t, \vec{x}, \vec{p}) - F_a(t, \vec{x}, \vec{p}) \, . \tag{3.26}$$

Subtracting Eq. (3.25) from Eq. (3.21) yields an equation for the fluctuation function

$$\frac{\partial \delta f_a}{\partial t} + v\mu \frac{\partial \delta f_a}{\partial Z} - \epsilon\Omega \frac{\partial \delta f_a}{\partial \phi} = -g_{x_\sigma} \frac{\partial F_a}{\partial x_\sigma} - g_{x_\sigma} \frac{\partial \delta f_a}{\partial x_\sigma} - \left\langle g_{x_\sigma} \frac{\partial \delta f_a}{\partial x_\sigma} \right\rangle . \qquad (3.27)$$

Here we used (cf. [Shalchi 2003])

$$\frac{1}{p^2} \frac{\partial}{\partial x_\sigma} (p^2 g_{x_\sigma}) = 0 . \qquad (3.28)$$

We assume as the quasilinear approximation, that the variation δf_a is much smaller than F_a, so we can neglect the two last terms on the right hand side:

$$\frac{\partial \delta f_a}{\partial t} + v\mu \frac{\partial \delta f_a}{\partial Z} - \epsilon\Omega \frac{\partial \delta f_a}{\partial \phi} \simeq -g_{x_\sigma} \frac{\partial F_a}{\partial x_\sigma} . \qquad (3.29)$$

This differential equation can be solved by the method of characteristics, that means by the integration along the unperturbed particle orbits.

Then we get:

$$\begin{aligned}
\frac{\partial F_a}{\partial t} + v\mu \frac{\partial F_a}{\partial Z} - \epsilon\Omega \frac{\partial F_a}{\partial \phi} &= S_a(t, \vec{x}, \vec{p}) \qquad\qquad\qquad (3.30) \\
&+ \frac{1}{p^2} \frac{\partial}{\partial x_\sigma} \left(\left\langle p^2 g_{x_\sigma} \int_{t_0}^{t} ds \left[g_{x_\nu}(x_\nu, s) \frac{\partial F_a(x_\nu, s)}{\partial x_\nu} \right]' \right\rangle \right) .
\end{aligned}$$

After some rearrangements (cf. [Schlickeiser 2001]) of the second term on the right hand side we obtain the *Fokker-Planck equation*

$$\boxed{\frac{\partial F_a}{\partial t} + v\mu \frac{\partial F_a}{\partial Z} - \epsilon\Omega \frac{\partial F_a}{\partial \phi} = S_a(t, \vec{x}, \vec{p}) + \frac{1}{p^2} \frac{\partial}{\partial x_\sigma} \left(p^2 D_{x_\sigma x_\nu} \frac{\partial F_a}{\partial x_\nu} \right)} \qquad (3.31)$$

with the 25 Fokker-Planck coefficients

$$D_{x_\sigma x_\nu}(t, \vec{x}, \vec{p}) = \mathrm{Re} \int_0^\infty d\xi \langle \bar{g}_{x_\sigma}(t) \bar{g}_{x_\nu}^*(t+\xi) \rangle \qquad (3.32)$$

where the bars indicate, that the functions have to be taken along the unperturbed particle orbits.

3.3 The Diffusion Approximation

The fastest particle-wave interaction processes are diffusion in gyrophase ϕ and in pitch angle μ, so that we average over ϕ and μ. Furthermore, the diffusion approximation holds, if the particle densities are slowly varying in time and space.

3.4 The Transport Equation

After some calculations we get the *diffusion-convection transport equation* for the isotropic pitch angle averaged particle distribution function $f(t, \vec{x}, p)$ (where we now omit the index a):

$$
\begin{aligned}
\frac{\partial f}{\partial t} - S(t, \vec{x}, p) = \ & \frac{\partial}{\partial z} \kappa_{zz} \frac{\partial f}{\partial z} \\
& + \frac{\partial}{\partial X} \left[\kappa_{XX} \frac{\partial f}{\partial X} + \kappa_{XY} \frac{\partial f}{\partial Y} \right] \\
& + \frac{\partial}{\partial Y} \left[\kappa_{YY} \frac{\partial f}{\partial Y} + \kappa_{YX} \frac{\partial f}{\partial X} \right] \\
& - \frac{1}{4p^2} \frac{\partial(p^2 v A_1)}{\partial p} \frac{\partial f}{\partial z} \\
& + \frac{1}{p^2} \frac{\partial}{\partial p} \left(p^2 A_2 \frac{\partial f}{\partial p} \right) + \frac{v}{4} \frac{\partial A_1}{\partial z} \frac{\partial f}{\partial p}
\end{aligned}
\tag{3.33}
$$

depending on the pitch angle averaged Fokker-Planck coefficients:

$$
\kappa_{zz} = \frac{v^2}{8} \int_{-1}^{1} d\mu \frac{(1 - \mu^2)^2}{D_{\mu\mu}(\mu)} \, ,
\tag{3.34}
$$

$$
\kappa_{XX} = \frac{1}{2} \int_{-1}^{1} d\mu D_{XX}(\mu) \, ,
\tag{3.35}
$$

$$
\kappa_{XY} = \frac{1}{2} \int_{-1}^{1} d\mu D_{XY}(\mu) \, ,
\tag{3.36}
$$

$$
\kappa_{YY} = \frac{1}{2} \int_{-1}^{1} d\mu D_{YY}(\mu) \, ,
\tag{3.37}
$$

$$
\kappa_{YX} = \frac{1}{2} \int_{-1}^{1} d\mu D_{YX}(\mu) \, ,
\tag{3.38}
$$

$$
A_1 = \int_{-1}^{1} d\mu \frac{(1 - \mu^2) D_{\mu p}(\mu)}{D_{\mu\mu}} \, ,
\tag{3.39}
$$

$$
A_2 = \frac{1}{2} d\mu \left[D_{pp}(\mu) - \frac{D_{\mu p}^2(\mu)}{D_{\mu\mu}(\mu)} \right] \, .
\tag{3.40}
$$

We interpret the terms on the right hand side of Eq. (3.33): the first 5 terms represent the spatial diffusion, the 6th term spatial convection, the 7th term decribes the momentum diffusion and the 8th term momentum convection.

For slab Alfvénic wave turbulence we can omit the perpendicular diffusion terms (cf. e. g. [Shalchi & Schlickeiser 2004]), i. e. the 2nd to the 5th term on the right hand side.

Introducing the cosmic ray bulk speed

$$V := \frac{1}{4p^2} \frac{\partial(p^2 v A_1)}{\partial p} \tag{3.41}$$

provides

$$\frac{\partial f}{\partial t} - S(t, \vec{x}, p) = \frac{\partial}{\partial z} \kappa_{zz} \frac{\partial f}{\partial z} - V \frac{\partial f}{\partial z}$$
$$+ \frac{1}{p^2} \frac{\partial}{\partial p} \left(p^2 A_2 \frac{\partial f}{\partial p} \right) + \frac{p}{3} \frac{\partial V}{\partial z} \frac{\partial f}{\partial p} . \tag{3.42}$$

Combining

$$\frac{p}{3} \frac{\partial V}{\partial z} \frac{\partial f}{\partial p} - V \frac{\partial f}{\partial z} = -\frac{\partial}{\partial z}[V f] + \frac{1}{p^2} \frac{\partial}{\partial p} \left[\frac{p^3}{3} \frac{\partial V}{\partial z} f \right] \tag{3.43}$$

we get

$$\frac{\partial f}{\partial t} - S(t, \vec{x}, p) = \frac{\partial}{\partial z} \left[\kappa_{zz} \frac{\partial f}{\partial z} - V f \right]$$
$$+ \frac{1}{p^2} \frac{\partial}{\partial p} \left(p^2 A_2 \frac{\partial f}{\partial p} + \frac{p^3}{3} \frac{\partial V}{\partial z} f \right) . \tag{3.44}$$

Including continuous loss processes (like synchrotron radiation) by the term

$$-\frac{1}{p^2} \frac{\partial}{\partial p} (p^2 \dot{p} f) \tag{3.45}$$

with a loss rate $\dot{p} = \dot{p}(p, \vec{x})$ and catastrophic loss processes (like spallation) by the term

$$-\frac{f}{T_c} \tag{3.46}$$

with a catastrophic loss time $T_c = T_c(p, \vec{x})$ in general, we can write for the transport equation

$$\frac{\partial f}{\partial t} - S(t,\vec{x},p) \;=\; \frac{\partial}{dz}\left[\kappa_{zz}\frac{\partial f}{\partial z} - Vf\right]$$
$$+\frac{1}{p^2}\frac{\partial}{\partial p}\left(p^2 A_2\frac{\partial f}{\partial p} + \frac{p^3}{3}\frac{\partial V}{\partial z}f - p^2\dot{p}f\right)$$
$$-\frac{f}{T_c} \;. \tag{3.47}$$

In the following we assume that T_c is independent of space and momentum. We want to investigate the stationary transport equation ($\frac{\partial}{\partial t}f = 0$), for the treatment of the time-dependent equation see e. g. [Büsching 2004]. In this work, we neglect continuous loss processes and spatial and momentum convection (cf. Subsection 2.1.2), so the transport equation we analyze reads

$$\boxed{\frac{\partial}{\partial z}\left(\kappa_{zz}\frac{\partial f}{\partial z}\right) + \frac{1}{p^2}\frac{\partial}{\partial p}\left(p^2 A_2\frac{\partial f}{\partial p}\right) - \frac{f}{T_c} = -S(\vec{x},p)} \;. \tag{3.48}$$

We remind that we also do not take into account a moving background medium.

Now we assume that the two diffusion coefficients (spatial and momentum, respectively) are independent of position

$$\kappa_{zz} = \kappa_0\kappa(p) \tag{3.49}$$

$$A_2 = A_2(p) \tag{3.50}$$

and we define the two operators

$$L_{\vec{x}} \;:=\; \kappa_0\nabla^2 \tag{3.51}$$
$$L_p \;:=\; \frac{1}{\kappa(p)}\left(\frac{1}{p^2}\frac{\partial}{\partial p}\left(p^2 A_2(p)\frac{\partial}{\partial p}\right) - \frac{1}{T_c}\right) \tag{3.52}$$

separated in space and momentum, where we generalize the spatial operator for the present to three dimensions in arbitrary coordinates.

Additionally, the source function is assumed to be separable

$$S(\vec{x},p) = Q_1(\vec{x})Q_2(p) \;, \tag{3.53}$$

which is reasonable, because the cosmic ray intensity has hardly varied at earth over the last 10^9 years while the earth has rotated 5-times around the galactic center (cf. [Schaeffer 1975]), so we get for the transport equation:

$$L_{\vec{x}} f(\vec{x}, p) + L_p f(\vec{x}, p) = -Q_1(\vec{x}) \frac{Q_2(p)}{\kappa(p)} \quad . \tag{3.54}$$

We note that $f(\vec{x}, p)$ is the phase space distribution function of the charged cosmic ray particles. By solving Eq. (3.54) and inserting special spatial and momentum source functions we are able to calculate the spectra of the cosmic rays at any point in our galaxy, especially at the position of the solar system, after they diffused through the galaxy and the galactic halo and after they were accelerated by the plasma waves superimposed on the galactic plasma. Consequently, the results can be compared to data, as we will do later in Chapter 7.

Chapter 4

Analytical Solution of the Transport Equation

In this chapter we present the complete solution of the transport equation in cylindrical coordinates after introducing a dimensionless momentum variable x and special forms of the diffusion coefficients.

The transport equation can be separated in a spatial and momentum part by applying the "scattering time method" (see Appendix A.1).

The complete solution is an infinite double sum (see Eq. (A.64)):

$$\boxed{f(\vec{x}, p) = \sum_{m=1}^{\infty} \sum_{n=1}^{\infty} c_{mn} t_{mn}(\vec{x}) N_{mn}(p)} \tag{4.1}$$

respectively

$$f(\vec{x}, Am_p cx) = \frac{1}{(m_p cA)^3} \sum_{m=1}^{\infty} \sum_{n=1}^{\infty} c_{mn} t_{mn}(\vec{x}) N_{mn}(x) \tag{4.2}$$

with the dimensionless momentum variable x defined subsequently.

We introduce cylindrical coordinates and assume a cylindrical halo with half-height H and radius L as the confinement region (see Fig. 4.1) with "free-escape-boundary conditions". These are appropriate if the majority of the cosmic ray sources do not concentrate at the halo boundary, which is indeed the case, as we will see in Chapter 6.

For the spatial functions then we get (see Appendix A.2):
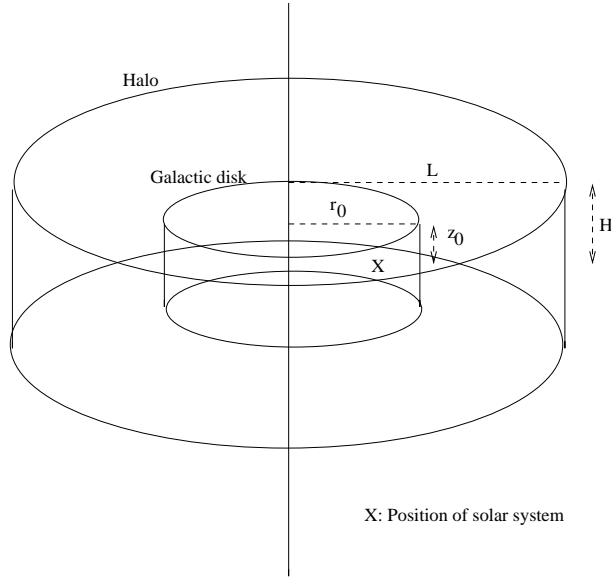
Figure 4.1: Geometry of the galaxy.

$$t_{mn}(r, z) = \frac{\sqrt{2}}{\sqrt{H} L J_1(y_n)} \cos\left(\frac{(2m-1)\pi}{2H} z\right) J_0\left(\frac{y_n}{L} r\right) \qquad (4.3)$$

where y_n are the zeros of the Bessel function J_0.

The corresponding eigenvalues are:

$$\lambda_{mn}^2 = \kappa_0 \left(\frac{y_n^2}{L^2} + \frac{(2m-1)^2 \pi^2}{4H^2}\right) . \qquad (4.4)$$

The expansion coefficients depend on the spatial functions and the spatial source function:

$$c_{mn} = \int_0^L dr\, r \int_{-H}^H dz\, Q_1(r, z) t_{mn}(r, z) . \qquad (4.5)$$

For the momentum problem remains an infinite set of equations:

$$\left[\kappa(p) L_p - \lambda_{mn}^2 \kappa(p)\right] N_{mn}(p) = -Q_2(p) . \qquad (4.6)$$

Explicitely they read:

$$\frac{1}{p^2}\frac{d}{dp}\left(p^2 A_2(p)\frac{dN_{mn}(p)}{dp}\right) - \left[\frac{1}{T_c} + \lambda_{mn}^2\kappa(p)\right]N_{mn}(p) = -Q_2(p) \ . \tag{4.7}$$

The following part is taken from [Schlickeiser 2001]. We introduce the particle momentum per nucleon

$$\tilde{p} := p/A = R/\alpha \tag{4.8}$$

with the mass to charge number

$$\alpha := A/Z \tag{4.9}$$

and the rigidity R thus changing

$$F_{mn}(\tilde{p}) := A^3 N_{mn}(p) \tag{4.10}$$

and

$$Q(\tilde{p}) := A^3 Q_2(p) \tag{4.11}$$

and we get

$$\frac{1}{\tilde{p}^2}\frac{d}{d\tilde{p}}\left(\tilde{p}^2 D(\tilde{p})\frac{dF_{mn}(\tilde{p})}{d\tilde{p}}\right) - \left[\frac{1}{T_c} + \lambda_{mn}^2\kappa(\tilde{p})\right]F_{mn}(\tilde{p}) = -Q(\tilde{p}) \tag{4.12}$$

with

$$D(\tilde{p}) = A_2(p)/A^2 \ . \tag{4.13}$$

Now we make an ansatz for the momentum dependence of the two diffusion coefficients:

$$\boxed{\kappa_0\kappa(\tilde{p}) = K_1(\alpha\tilde{p})^{2-q}} \tag{4.14}$$

and

$$\boxed{D(\tilde{p}) = D_1\alpha^{q-2}\tilde{p}^q} \tag{4.15}$$

where the power law index q of the wave number distribution of the turbulence spectrum enters (cf. Subsection 2.3.1):

$$I(k) = I_0 k^{-q} \ . \tag{4.16}$$

We define the dimensionless momentum variable

$$x := \tilde{p}/(m_p c) = p/(mc) \tag{4.17}$$

and therefore

$$f_{mn}(x) := (m_p c)^3 F_{mn}(\tilde{p}) \tag{4.18}$$

$$q(x) := (m_p c)^3 Q(\tilde{p}) \, . \tag{4.19}$$

Introducing the two time scales for momentum diffusion and spatial diffusion

$$T_f := (m_p c)^{2-q}/D_1 \tag{4.20}$$

and

$$T_{mn} := (m_p c)^{q-2} \kappa_0 / (K_1 \lambda_{mn}^2) \tag{4.21}$$

then for the differential equation follows

$$\frac{\alpha^{q-2}}{T_f x^2} \frac{d}{dx} \left(x^{q+2} \frac{df_{mn}(x)}{dx} \right) - \left[\frac{1}{T_c} + \frac{\alpha^{2-q} x^{2-q}}{T_{mn}} \right] f_{mn}(x) = -q(x) \, . \tag{4.22}$$

We introduce

$$\boxed{\chi := 2 - q} \tag{4.23}$$

and the ratios of the characteristic time scales

$$\boxed{\psi := \frac{T_f}{T_c} \alpha^{2-q}} \tag{4.24}$$

$$\boxed{\phi_{mn} := \frac{T_f}{T_{mn}} \alpha^{2(2-q)}} \tag{4.25}$$

and obtain the self-adjoint form of the differential equation

$$\boxed{\left[\frac{d}{dx} \left(x^{4-\chi} \frac{d}{dx} \right) - (\psi x^2 + \phi_{mn} x^{2+\chi}) \right] f_{mn}(x) = -T_f \alpha^\chi x^2 q(x)} \, . \tag{4.26}$$

f_{mn} can be expressed by a Green's function

$$f_{mn}(x) = T_f \alpha^\chi \int_0^\infty dx_0 x_0^2 q(x_0) G_{mn}(x, x_0) \tag{4.27}$$

with the momentum source function $q(x_0)$. G_{mn} is the solution of

$$\left[\frac{d}{dx}\left(x^{4-\chi}\frac{d}{dx}\right) - (\psi x^2 + \phi_{mn}x^{2+\chi})\right] G_{mn}(x, x_0) = -\delta(x - x_0) . \tag{4.28}$$

In the next two sections we present the Green's functions for the momentum solution with and without catastrophic losses.

4.1 Green's Function for the Solution Without Catastrophic Losses

The Green's function for no catastrophic losses, that means the case $\psi = 0$ (see Appendix A.3.1), contains modified Bessel functions I and K (cf. Appendix H):

$$G_{mn}(x, x_0) = \frac{1}{\chi} x^{\frac{\chi-3}{2}} x_0^{\frac{\chi-3}{2}} \begin{cases} I_{\frac{3-\chi}{2\chi}}(\frac{\sqrt{\phi_{mn}}}{\chi}x^\chi)K_{\frac{3-\chi}{2\chi}}(\frac{\sqrt{\phi_{mn}}}{\chi}x_0^\chi) & ; \ 0 \leq x \leq x_0 \\ I_{\frac{3-\chi}{2\chi}}(\frac{\sqrt{\phi_{mn}}}{\chi}x_0^\chi)K_{\frac{3-\chi}{2\chi}}(\frac{\sqrt{\phi_{mn}}}{\chi}x^\chi) & ; \ x_0 \leq x < \infty \end{cases} .$$

$$\tag{4.29}$$

This function is used in the Chapters 5 and 7.

4.2 Green's Function for the Solution With Catastrophic Losses

In consideration of catastrophic losses ($\psi \neq 0$) we get (cf. [Schlickeiser 2001]) a Green's function involving the confluent hypergeometric functions M and U (see [Abramowitz & Stegun 1984], Chapter 13):

$$G_{mn}(x, x_0) = \frac{\left(2\sqrt{\phi_{mn}}\right)^{\frac{3}{\chi}-1}}{\chi^{\frac{3}{\chi}}} \frac{\Gamma\left[\frac{3}{2\chi} + \frac{\psi}{2\chi\sqrt{\phi_{mn}}}\right]}{\Gamma\left[\frac{3}{\chi}\right]} \exp\left[-\frac{\sqrt{\phi_{mn}}(x^\chi + x_0^\chi)}{\chi}\right] \times$$

$$\times \begin{cases} M\left(\frac{3}{2\chi} + \frac{\psi}{2\chi\sqrt{\phi_{mn}}}, \frac{3}{\chi}, \frac{2\sqrt{\phi_{mn}}x^\chi}{\chi}\right) U\left(\frac{3}{2\chi} + \frac{\psi}{2\chi\sqrt{\phi_{mn}}}, \frac{3}{\chi}, \frac{2\sqrt{\phi_{mn}}x_0^\chi}{\chi}\right) & ; \ 0 \leq x \leq x_0 \\ U\left(\frac{3}{2\chi} + \frac{\psi}{2\chi\sqrt{\phi_{mn}}}, \frac{3}{\chi}, \frac{2\sqrt{\phi_{mn}}x^\chi}{\chi}\right) M\left(\frac{3}{2\chi} + \frac{\psi}{2\chi\sqrt{\phi_{mn}}}, \frac{3}{\chi}, \frac{2\sqrt{\phi_{mn}}x_0^\chi}{\chi}\right) & ; \ x_0 \leq x < \infty \end{cases} \tag{4.30}$$

We investigate this solution in Chapter 8.

Chapter 5

Studies of the Momentum Solution

In the following we deal with the momentum solution without catastrophic losses, as it is valid for the protons ($\alpha = 1$) of the cosmic rays. We study the I-K-Bessel function solution by performing some theoretical consistency checks and by varying the parameters for different momentum source functions.

5.1 Theoretical Consistency Checks

5.1.1 Inserting the Solution Into the Differential Equation

By inserting the momentum solution into the differential equation its correctness is proved, as shown in Appendix B.

5.1.2 Transition From the Solution With to That Without Catastrophic Losses

The M-U-solution for the case with catastrophic losses with a time scale T_c transforms into the I-K-solution, if we neglect catastrophic losses by setting

$$\boxed{\psi \to 0} \tag{5.1}$$

because

$$\psi \sim \frac{T_f}{T_c} \to 0 \qquad \text{for} \quad T_c \to \infty \ . \tag{5.2}$$

The calculation can be found in Appendix C.

5.2 A δ Momentum Injection Function

If we insert a δ momentum source function with the injection momentum x_i

$$q(x_0) = q_0 x_0^{-2} \delta(x_0 - x_i) \,, \tag{5.3}$$

we get for the momentum part of the phase space distribution function:

$$f_{mn}(x) = \begin{cases} q_0 T_F \frac{1}{\chi} \, x^{\frac{\chi-3}{2}} \, K_\nu \left(\frac{\sqrt{\phi_{mn}}}{\chi} x^\chi \right)^\chi I_\nu \left(\frac{\sqrt{\phi_{mn}}}{\chi} x_i^\chi \right)^\chi & ; \text{ for } x > x_i \\ q_0 T_F \frac{1}{\chi} \, x^{\frac{\chi-3}{2}} \, I_\nu \left(\frac{\sqrt{\phi_{mn}}}{\chi} x^\chi \right)^\chi K_\nu \left(\frac{\sqrt{\phi_{mn}}}{\chi} x_i^\chi \right)^\chi & ; \text{ for } x < x_i \end{cases}, \tag{5.4}$$

with the abbreviation $\nu := \frac{3-\chi}{2\chi}$.

5.3 The Limit $q \to 2$

In the limit $q \to 2$ of the index of the turbulence spectrum, we obtain singularities in the solutions of the momentum equations. Starting directly with the momentum differential equation for $q = 2$, that means $\chi = 0$, we get for each eigenvalue the following Green's function of the momentum solution (see Appendix D):

$$\boxed{G_{mn}(x, x_0) = \frac{(xx_0)^{-\frac{3}{2}}}{2\sqrt{\frac{9}{4} + \psi + \phi_{mn}}} \begin{cases} (x/x_0)^{\sqrt{\frac{9}{4}+\psi+\phi_{mn}}} & ; \ 0 \le x \le x_0 < \infty \\ (x/x_0)^{-\sqrt{\frac{9}{4}+\psi+\phi_{mn}}} & ; \ 0 < x_0 \le x < \infty \end{cases}}.$$
$$\tag{5.5}$$

We insert a δ momentum source function like Eq. (5.3). The appropriately calculated phase space distribution function for $q < 2$ converges towards this limiting curve for each eigenvalue ϕ_{mn}, as it should be expected (see Fig. 5.1 for a special eigenvalue).

5.4 A Power Law Momentum Injection Function

Now we study the response of the momentum solution for a power law injection spectrum (refer to Subsection 2.1.2)

$$\boxed{q(x_0) = q_0 x_0^{-\beta-2}} \tag{5.6}$$

covering the interval from x_{min} to x_{max} by varying the spectral index q of the plasma turbulence, the ratio T_f/T_0 of the momentum to the spatial diffusion time scale (T_0
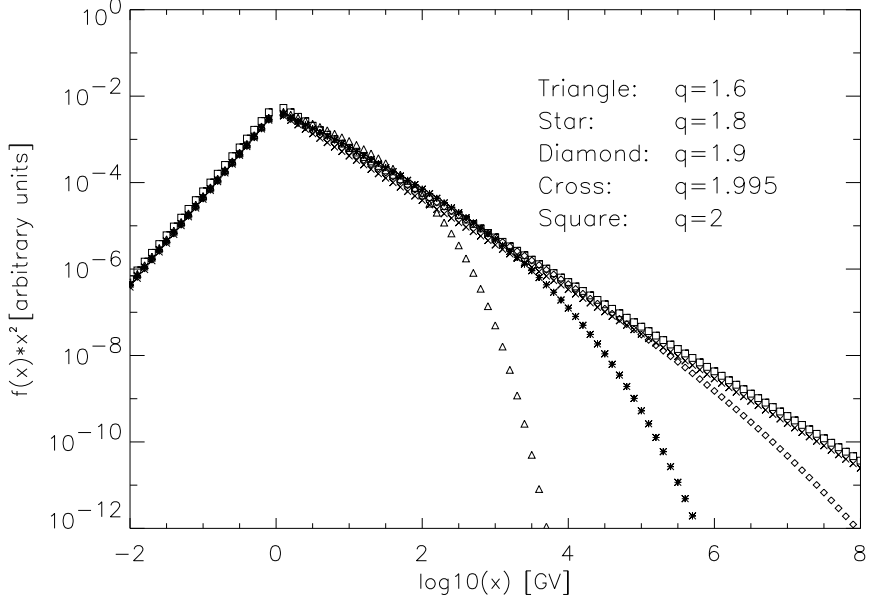
Figure 5.1: Momentum solution for a δ-injection at 1 GV for different spectral indices of the plasma wave spectrum. The numerically calculated functions for $q < 2$ converge towards the limiting curve (Eq. (5.5)) for $q = 2$ for one special eigenvalue ϕ_{mn}.

is the time for the first eigenvalue ϕ_{11}) and the spectral index β of the initial spectrum. Here, x_{max} was set to 10^6 GV (cf. Subsection 2.1.2).

A further test of the analytical solution and especially of the numerical code are the following approximations (see Appendix E) for the momentum solution:

$$f_{mn}(x) \simeq \frac{q_0 T_f}{\beta - 1} \frac{1}{3 - \chi} x_{min}^{1-\beta} x^{\chi - 3} \qquad (5.7)$$

for $x \ll x_c$ (see case 1, Eq. (E.25), and 2, Eq. (E.38)) and

$$f_{mn}(x) \simeq q_0 T_f \frac{1}{\phi_{mn}} x^{-\chi - \beta - 2} \qquad (5.8)$$

for $x \gg x_c$ (see case 3, Eq. (E.48), and 4, Eq. (E.52)) according to the characteristic momentum

$$x_c := \left(\frac{\chi}{\sqrt{\phi_{mn}}} \right)^{\frac{1}{\chi}} , \tag{5.9}$$

which appears in the argument of the Bessel functions. x_c contains the ratio T_f/T_0.

In the case $x \ll x_c$, the influence of the source function disappears and momentum diffusion dominates, and in the case $x \ll x_c$, the initial power law is only steepened by $q - 2$ and momentum diffusion plays a minor role.

Above the maximum injection momentum x_{max} all spectra cut off exponentially, independent of the source index β (see Appendix E.2.5):

$$f_{mn}(x) \sim x^{-\frac{3}{2}} e^{-\left(\frac{x}{x_c} \right)^{\chi}} . \tag{5.10}$$

The approximating curves from Eqs. (5.7) and (5.8) are superimposed in the Figs. 5.2, 5.3 and 5.4.

The strong effect of the wave number distribution of the turbulence spectrum shows Fig. 5.2. For larger values of q the momentum diffusion process can accelerate particles to higher momenta, exceeding the upper momentum injection limit x_{max}.

A similar consequence has the increase of T_f/T_0 (see Fig. 5.3). If the time scale for momentum diffusion in comparison to the spatial diffusion is small, more particles can reach higher momenta.

From Fig. 5.4 one notices that a flatter injection spectrum, of course, results in a flatter processed spectrum. If momentum acceleration dominates, the influence of the primary distribution vanishes for larger momenta.

5.5   A Source Spectrum With a Dispersive Index

Assuming a superposition of source spectra with different spectral indices, as it can occur if the sources are supernova remnants producing power law injection spectra with variable steepnesses, we insert the dispersive source function

$$q(x_0) = q_0 x_0^{-<\beta>-2+\frac{1}{2}\sigma^2 \ln(\frac{x_0}{x_r})} \tag{5.11}$$

with a mean index $< \beta >$ and a dispersion parameter σ at a reference momentum x_r (for a derivation see, e. g., [Schlickeiser 2001]; the proton source spectral indices are inferred from the radio spectral indices, which show a dispersion, cf. [Green 2000]).
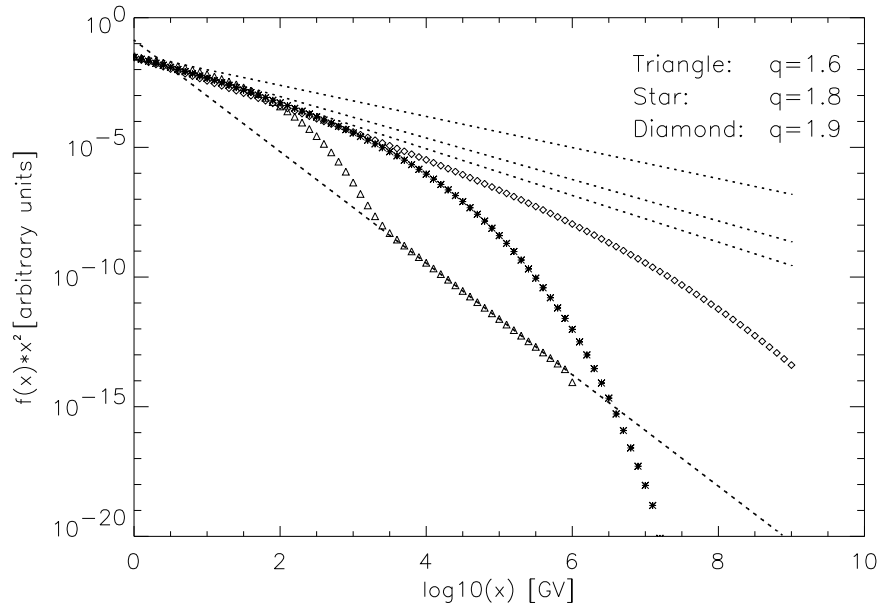
Figure 5.2: Phase space distribution function for a power law momentum source function (Eq. (5.6)) with spectral index $\beta = 1.75$ extending to $x_{max} = 10^6$ GV for different spectral indices q of the plasma turbulence spectrum and $\phi = T_f/T_0 = 1/10$. The three upper flat dotted lines are the power law approximations (Eq. (5.7)) for small x with the mentioned parameters β and ϕ and the quoted values of q. The lower steeper dashed line is the respective approximation (Eq. (5.8)) for large x for the case $q = 1.6$.

A comparison to the single power law distribution is shown in Fig. 5.5. A typical dispersion parameter is in the order of $\sigma = 0.25$ ([Büsching et al. 2001]). To see an effect, here we take also an extreme value of $\sigma = 0.55$. As expected, the flattest source spectrum of the sample dominates for large values, thereby shifting the particles to higher momenta.

For typical realistic dispersion parameters like mentioned above the effect of dispersion can be neglected in the first order in the following studies.
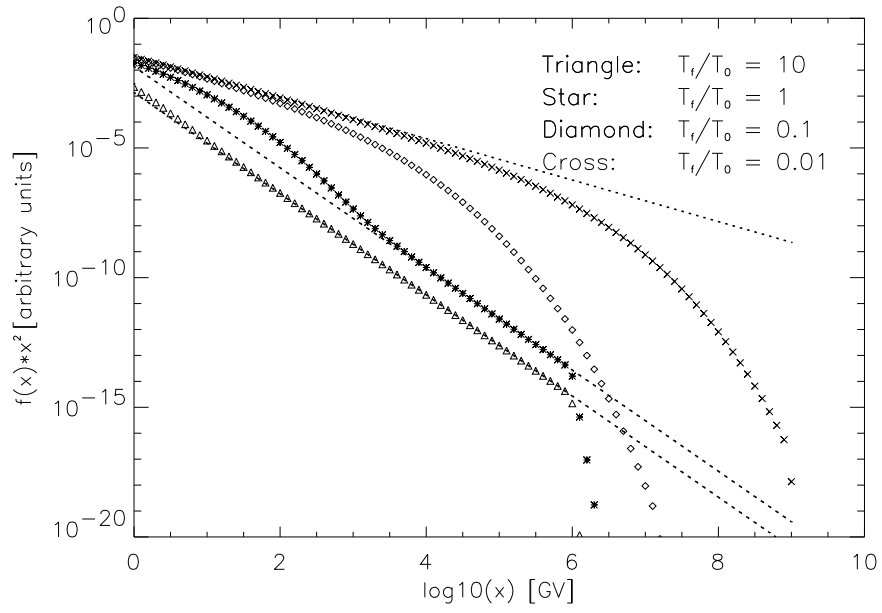
Figure 5.3: Phase space distribution function with an injection power law (Eq. (5.6)) extending to $x_{max} = 10^6$ GV for $q = 1.8$ and different ratios of the momentum to the spatial diffusion time scale T_f/T_0. The upper flat dotted curve is the approximation (5.7) for small x, the two lower steeper dashed curves are the approximations (5.8) for large x for the cases $T_f/T_0 = 10$ and $T_f/T_0 = 1$.
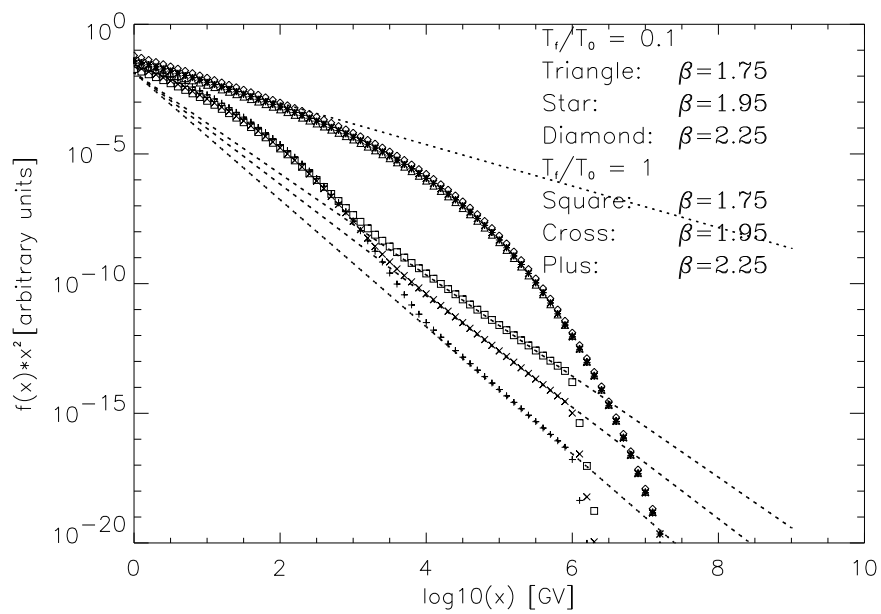
Figure 5.4: Phase space distribution function for $q = 1.8$ and a source function (5.6) extending to $x_{max} = 10^6$ GV, but with varying β. The curves are calculated for two different time scale ratios. Again the upper dotted curve is yielded with Eq. (5.7) for small x and $T_f/T_0 = 0.1$ and the lower steeper dashed curves (5.8) approximate the three cases for $T_f/T_0 = 1$ for large x.
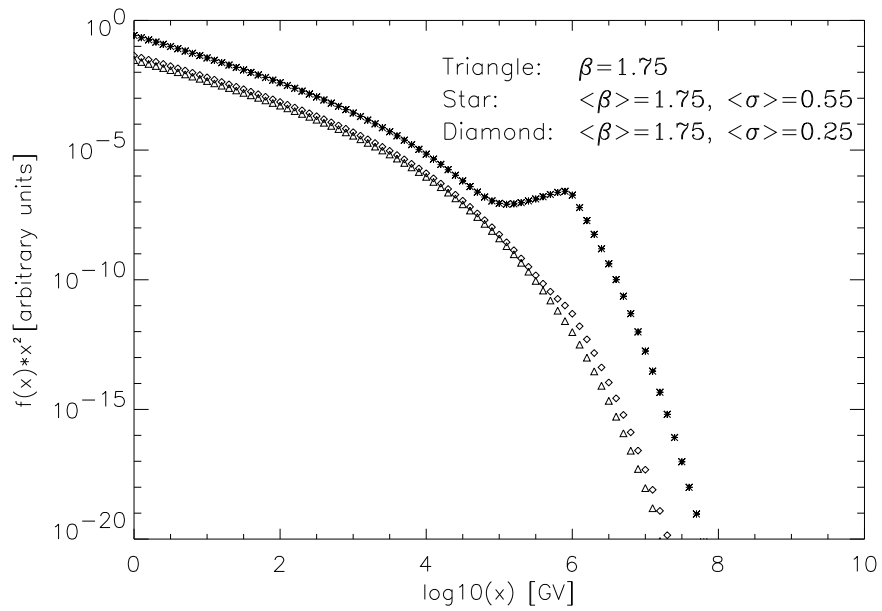
Figure 5.5: Source distribution with dispersion as in Eq. (5.11) with $\sigma = 0.25$ and $\sigma = 0.55$, and $<\beta> = 1.75$. Additionally drawn is the result for a single power law (Eq. (5.6)) with $\beta = 1.75$.

Chapter 6

The Spatial Source Function

As a first approximation a cylindrical and subsequently a more realistic spatial source function for the supernova remnants (refer to Subsection 2.1.2) are introduced. The spatial source function is inserted into Eq. (4.5):

$$c_{mn} = \int_0^L dr\, r \int_{-H}^{H} dz\, Q_1(r,z) t_{mn}(r,z) \,. \qquad (6.1)$$

6.1 Cylindrical Spatial Source Function

For the spatial distribution of the cosmic ray sources for a crude approximation we make the assumption that it is homogeneous in the galactic disk in a cylinder with radius $r_0 < L$ and a height $2z_0 < 2H$ (cf. Fig. 4.1), so it can be described by a double Heaviside function θ with a medium spatial density $Q_{1,0}$:

$$\boxed{Q_1(r,z) = Q_{1,0}\, \theta(r_0 - r)\, \theta(z_0 - |z|)} \,. \qquad (6.2)$$

The integrals separate, and c_{mn} is calculated as follows:

$$c_{mn} = Q_{1,0} \frac{\sqrt{2}}{\sqrt{H} L J_1(y_n)} \int_0^{r_0} dr\, r J_0\left(\frac{y_n}{L} r\right) \int_{-z_0}^{z_0} dz\, \cos\left(\frac{2m-1}{2H}\pi z\right) \,. \qquad (6.3)$$

With the substitution $z' = \frac{2m-1}{2H}\pi z$ we get:

$$c_{mn} = Q_{1,0} \frac{\sqrt{2}}{\sqrt{H} L J_1(y_n)} \frac{2H}{(2m-1)\pi} \int_0^{r_0} dr\, r J_0\left(\frac{y_n}{L} r\right) \int_{-z_0'}^{z_0'} dz'\, \cos z' \qquad (6.4)$$

and thus

$$c_{mn} = Q_{1,0} \frac{2\sqrt{2}\sqrt{H}}{LJ_1(y_n)(2m-1)\pi} 2\sin\left(\frac{2m-1}{2H}\pi z_0\right) \int_0^{r_0} dr\, r J_0\left(\frac{y_n}{L}r\right). \tag{6.5}$$

According to [Magnus et al. 1966], chapter 3.8.1 one obtains for the radial integral:

$$\int dz\, z^{\nu+1} J_\nu(z) = z^{\nu+1} J_{\nu+1}(z). \tag{6.6}$$

Here for $\nu = 0$:

$$\int_0^{r_0} dr\, r J_0\left(\frac{y_n}{L}r\right)$$

$$\overset{r'=\frac{y_n}{L}r}{=} \left(\frac{L}{y_n}\right)^2 \int_0^{r_0'} dr'\, r' J_0(r')$$

$$= \left(r_0\frac{L}{y_n}\right) [J_1(r')]_0^{r_0'} \tag{6.7}$$

$$= \left(r_0\frac{L}{y_n}\right) J_1\left(\frac{y_n}{L}r_0\right) \quad \text{with} \quad J_1(0) = 0. \tag{6.8}$$

For the coefficients follows:

$$\boxed{c_{mn} = Q_{1,0} \frac{4\sqrt{2}\sqrt{H}\, r_0 J_1\left(\frac{y_n}{L}r_0\right)}{J_1(y_n)y_n(2m-1)\pi} \sin\left(\frac{(2m-1)\pi}{2H}z_0\right).} \tag{6.9}$$

6.1.1 Normalization

The following condition should hold:

$$2\pi \int_0^L dr\, r \int_{-H}^{H} Q_1(r,z) \overset{!}{=} 1 \tag{6.10}$$

$$Q_{1,0} 2\pi \int_0^{r_0} dr\, r \int_{-z_0}^{z_0} dz = Q_{1,0} 2\pi z_0 r_0^2. \tag{6.11}$$

The normalization factor is the reciprocal value of the cylinder volume:

$$\boxed{Q_{1,0} = \frac{1}{2\pi z_0 r_0^2}.} \tag{6.12}$$

6.1.2 Phase Space Distribution Function for Different Volumes and Different Number of Terms in the Sum

In Fig. 6.1 we have plotted the processed phase space distribution function for different spatial injection source functions.
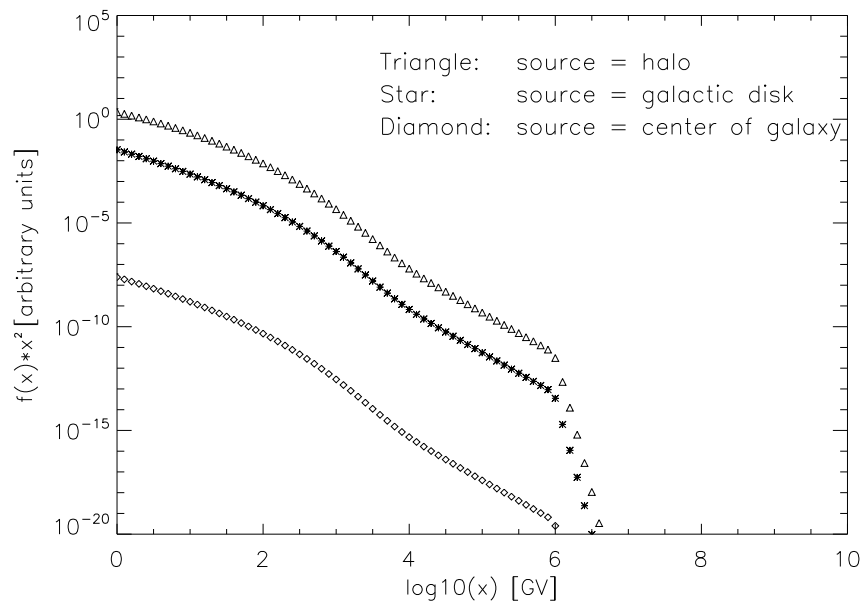
Figure 6.1: Phase space distribution function for different spatial source functions.

If the sources are surrounding the solar system, like in the galactic disc case or the halo case, more particles can reach the solar system by diffusion and can be measured at the position of the earth. The shapes of the spectra remain the same.

Fig. 6.2 shows f (Eq. (4.1)) for different number of terms of the eigenvalue expansion. Taking into account more than $m_{max} = n_{max} = 3$ terms of the double sum is not necessary, because of the fast convergence of the sum.

6.2 Realistic Spatial Source Function

Now we refine the model and follow a more general ansatz for the spatial distribution function:
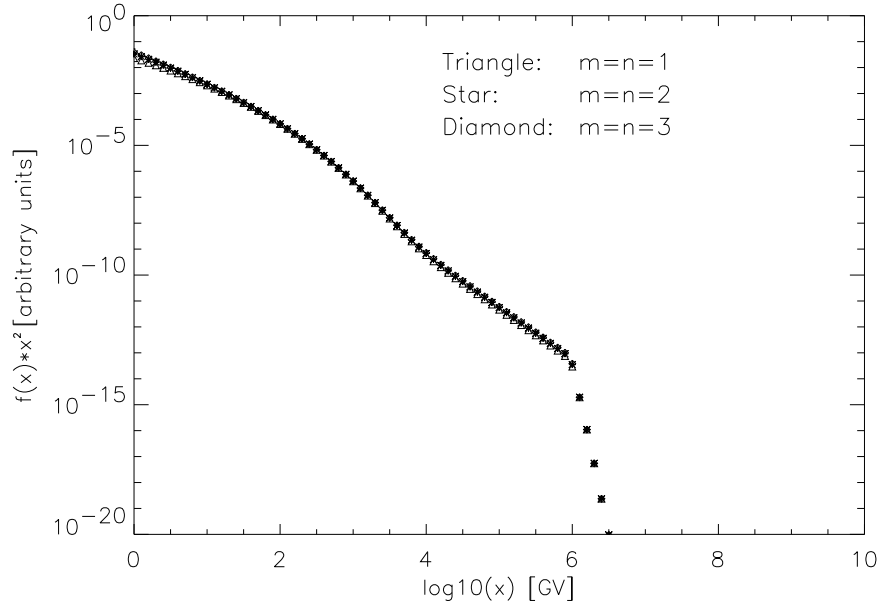
Figure 6.2: Phase space distribution function for different number of terms of the eigen-value expansion.

$$Q_1(r,z) = Q_{1,0}\theta(r_0 - r)\theta(z_0 - |z|)\left(\frac{r}{r_s}\right)^a e^{-b\frac{r-r_s}{r_s}}e^{-c\frac{|z|}{z_k}}. \qquad (6.13)$$

Here r_s is the radius of the position of the solar system, z_k is a constant and a, b and c are free parameters of the model. At the radius r_0 and the half-height z_0 the source distribution cuts off.

Typical values are:

$$a = 1.7,\ b = 3.3,\ c = 1,\ z_k = 200pc, \qquad (6.14)$$

taken from [Strong & Moskalenko 1998], where the radial values have been adopted by [Case & Bhattacharya 1996], which are similar to the values chosen by [Case & Bhattacharya 1998]. Other radial parameter sets stem from [Stecker & Jones 1977]:

$$a = 1.20,\ b = -6.44, \qquad (6.15)$$

and from [Lyne et al. 1985]:

$$a = 0.6, \ b = 1.20, \tag{6.16}$$

cited in [Webber et al. 1992].

We again only consider a cylindrical symmetry and neglect the correlation of galactic supernova remnants and spiral arms; for this topic refer to [Li et al. 1991].

For the coefficients of the eigenvalue expansion we now have to calculate the following two integrals:

1.

$$I_1 := \int_0^{r_0} dr \, r J_0 \left(\frac{y_n}{L} r \right) \left(\frac{r}{r_s} \right)^a e^{-b\frac{r}{r_s}} \tag{6.17}$$

and

2.

$$I_2 := \int_{-z_0}^{z_0} dz \cos \left(\frac{(2m-1)\pi}{2H} z \right) e^{-c\frac{|z|}{z_k}} \ . \tag{6.18}$$

6.2.1 The Radial Integral

The evaluation of the integral I_1 is known, if the upper limit converges to infinity (see [Gradshteyn & Ryzhik 1994] (6.621).1):

$$\int_0^{\infty} dt \, t^{\mu} e^{-\beta t} J_{\nu}(\alpha t) = \Gamma(\nu + \mu + 1)(\beta^2 + \alpha^2)^{-\frac{1}{2}\mu - \frac{1}{2}} P_{\mu}^{-\nu} \left[\beta(\beta^2 + \alpha^2)^{-\frac{1}{2}} \right] \ . \tag{6.19}$$

Here $P_{\mu}^{-\nu}$ are the associated Legendre functions of the first kind; for our case $\nu = 0$.

This limit serves as a test for the numerical calculations. If generating numerically the limit "infinity" at the upper boundary, it provides the same result as the direct calculation of the right hand side.

6.2.2 The z-integral

The integrand of I_2 is an even function of z, thus we can write:

$$\int_{-z_0}^{z_0} dz... = 2 \int_0^{z_0} dz... \ . \tag{6.20}$$

The integral has the form

$$\int dx \, e^{a'x} \cos(b'x) \tag{6.21}$$

with $a' := -c/z_k$ and $b' = \frac{(2m-1)\pi}{2H}$ and can be solved by considering the integrand as a complex function:

$$
\begin{aligned}
\int dx\, e^{a'x}\cos(b'x) &= Re \int dx\ e^{a'x}e^{ib'x} \\
&= Re \int dx\ e^{(a'+ib')x} \\
&= Re\left(\frac{1}{a'+ib'}\left[e^{(a'+ib')x}\right]\right) \\
&= Re\left(\frac{a'-ib'}{a'^2+b'^2}\left[e^{(a'+ib')x}\right]\right) \\
&= Re\left(\frac{e^{a'x}}{a'^2+b'^2}(a'-ib')(\cos(b'x)+i\sin(b'x))\right) \\
&= \frac{e^{a'x}}{a'^2+b'^2}(a'\cos(b'x)+b'\sin(b'x))\ . \quad (6.22)
\end{aligned}
$$

This agrees with [Gradshteyn & Ryzhik 1994] (2.663).3.

6.2.3 Normalization

Normalizing means:

$$
2\pi\int_0^L dr\ r\int_{-H}^H dz\ Q_{1,0}\theta(r_0-r)\theta(z_0-|z|)\left(\frac{r}{r_s}\right)^a e^{-b\frac{r-r_s}{r_s}}e^{-c\frac{|z|}{z_k}}
$$

$$
= Q_{1,0}2\pi\frac{e^b}{r_s^a}\int_0^{r_0} dr\ r^{a+1}e^{-b\frac{r}{r_s}}\int_{-z_0}^{z_0} dz\ e^{-c\frac{|z|}{z_k}} \overset{!}{=} 1\ . \quad (6.23)
$$

The z-integral gives:

$$
I_z = -2\frac{z_k}{c}\left[e^{-c\frac{z_0}{z_k}}-1\right]\ . \quad (6.24)
$$

The radial integral has to be solved numerically. So the normalization factor can be noted as

$$
Q_{1,0} = \frac{1}{I_z\ 2\pi\frac{e^b}{r_s^a}\int_0^{r_0} dr\, r^{a+1}e^{-b\frac{r}{r_s}}}\ . \quad (6.25)
$$

Chapter 7

Calculating Spectra and Comparison With Data

Now we introduce spatial and momentum diffusion coefficients determining the eigenvalues ϕ_{mn}, which will be examined for different parameters. After taking into account solar modulation, we fit the calculated spectra to the data for protons (no catastrophic losses) for different parameter sets by computing the eigenfunction sum solution (4.1) with the momentum integrals (4.27), including the Green's functions (4.29), and by using the realistic spatial source function and the eigenfunction coefficients derived in Chapter 6.

7.1 Diffusion Coefficients and the Corresponding Eigenvalues

The diffusion coefficients for a mixture of slab Alfvén waves and fast magnetosonic waves (cf. Subsection 2.3.1) with a Kolmogorov-type power law spectrum - already used in Chapter 4 - read [Schlickeiser 2001]

$$\kappa_0 \kappa(\tilde{p}) = K_1 (\alpha \tilde{p})^{2-q} \tag{7.1}$$

$$D(\tilde{p}) = D_1 \alpha^{q-2} \tilde{p}^q \tag{7.2}$$

where

$$K_1 = \frac{2}{3} \frac{\eta(q)c}{(2-q)(4-q)} \left(\frac{v_A}{c}\right)^{2-q} \tag{7.3}$$

and

$$D_1 = \frac{3}{2} \frac{v_A^2}{q(q+2)c\eta(q)} \ln(c/v_A) \tag{7.4}$$

with

$$\eta(q) = \frac{3}{2\pi(q-1)} \left(\frac{B_0}{\delta B}\right)^2 \left(\frac{c}{eB_0}\right)^{2-q} k_{min}^{1-q} . \tag{7.5}$$

Here, v_A is the Alfvén velocity, k_{min} is the minimum wave number of the turbulence, B_0 is the magnitude of the background magnetic field and δB the typical strength of the plasma waves. c is the speed of light, e the elementary charge.

In Chapter 4 we have introduced the ratio of the momentum to the spatial diffusion time scale including the eigenvalues (Eq. (4.25) with $\alpha = 1$ for protons):

$$
\begin{aligned}
\phi_{mn} &= \frac{T_f}{T_{mn}} \tag{7.6}\\
&= (m_p c)^{2(2-q)} \frac{K_1}{D_1} \left(\frac{y_n^2}{L^2} + \frac{(2m-1)^2\pi^2}{4H^2}\right)\\
&= (m_p c)^{2(2-q)} \frac{\frac{2}{3}\eta(q)c\left(\frac{v_A}{c}\right)^{2-q} q(q+2)c\eta(q)}{(2-q)(4-q)\frac{3}{2}v_A^2 \ln(c/v_A)} \left(\frac{y_n^2}{L^2} + \frac{(2m-1)^2\pi^2}{4H^2}\right)\\
&= (m_p c)^{2(2-q)} \left(\frac{2}{3}\right)^2 \frac{q(q+2)}{(2-q)(4-q)} \frac{\left(\frac{c}{v_A}\right)^q}{\ln\left(\frac{c}{v_A}\right)} \eta(q)^2 \left(\frac{y_n^2}{L^2} + \frac{(2m-1)^2\pi^2}{4H^2}\right) .
\end{aligned}
$$

Here we have inserted the above listed formulas for the diffusion coefficients.

7.1.1 Typical Values

The Value of η

Typical values of the parameters for η are e.g.:

$$k_{min} \approx 10^{-18} \text{ cm}^{-1} \text{ corresponding to a scale length of } l_{max} \approx 1 \text{ pc} \approx 3.1 \cdot 10^{18} \text{ cm}, \tag{7.7}$$

as it is mentioned in Subsection 2.3.1.
The magnetic field strength is of the order of (cf. Section 2.3):

$$B_0 \approx 3 \ \mu\text{G} \quad \text{and} \quad \delta B \approx 0.9 \ \mu\text{G} \quad \longrightarrow \quad \frac{\delta B}{B_0} \approx 0.3 . \tag{7.8}$$

With the constants

$$c \approx 3 \cdot 10^{10} \ \frac{\text{cm}}{\text{s}} \tag{7.9}$$

and

$$e \approx 4.8 \cdot 10^{-10} \ \text{g}^{1/2} \ \text{cm}^{3/2} \ \text{s}^{-1} \tag{7.10}$$

we get typically with $q = 1.8$:

$$\eta(1.8) \approx 2.0 \cdot 10^{20} \ \text{g}^{q-2} \ \text{cm}^{q-1} \ \text{s}^{2-q} \ . \tag{7.11}$$

The Value of v_A

The Alfvén velocity is calculated by

$$v_A = \frac{B_0}{\sqrt{4\pi(m_p + m_e)n_e}} \approx 2.18 \cdot 10^{11} \left(\frac{B_0}{1 \ \text{G}} \right) \left(\frac{n_e}{1 \ \text{cm}^{-3}} \right)^{-\frac{1}{2}} \ \frac{\text{cm}}{\text{s}} \tag{7.12}$$

(m_p and m_e are the proton and the electron mass, respectively, and n_e is the electron density), where with typical values for the interstellar medium (refer to Section 2.3)

$$n_e \approx 0.1 \ \text{cm}^{-3} \tag{7.13}$$

and

$$B_0 \approx 3 \cdot 10^{-6} \ \text{G} \tag{7.14}$$

the value

$$v_A \approx 7 \cdot 10^5 \ \frac{\text{cm}}{\text{s}} \tag{7.15}$$

is obtained.

The Resulting Value for ϕ_{11}

With an assumed halo radius of

$$L = 15000 \ \text{pc} \ , \tag{7.16}$$

an assumed half-height of the halo

$$H = 10000 \ \text{pc} \tag{7.17}$$

and with the zero of the Bessel function

$$y_1 \approx 2.4 \ , \tag{7.18}$$

the value

$$\phi_{11} \approx 0.1 \tag{7.19}$$

is obtained as the first eigenvalue.

7.1.2 Eigenvalues for Variation of the Parameters

In the following the ratios of the time scales, i. e. the eigenvalues, subject to the different parameters are listed:

$q = 1.8,\ B_0 = 3 \cdot 10^{-6}$ G, $v_A = 7 \cdot 10^5$ cm/s, $k_{min} = 10^{-18}$ cm^{-1}				
	$m = 1, n = 1$	$m = 1, n = 2$	$m = 2, n = 1$	$m = 2, n = 2$
$H = 10$ kpc, $L = 15$ kpc	0.14	0.45	0.69	1.00
$H = 10$ kpc, $L = 20$ kpc	0.11	0.23	0.67	0.81
$H = 15$ kpc, $L = 15$ kpc	0.10	0.41	0.35	0.65
$H = 15$ kpc, $L = 20$ kpc	0.07	0.24	0.32	0.45

Table 7.1: Eigenvalues ϕ_{mn} for different halo sizes.

$q = 1.8,\ H = 10$ kpc, $L = 15$ kpc, $v_A = 7 \cdot 10^5$ cm/s, $k_{min} = 10^{-18}$ cm^{-1}				
	$m = 1, n = 1$	$m = 1, n = 2$	$m = 2, n = 1$	$m = 2, n = 2$
$B_0 = 1 \cdot 10^{-6}$ G	0.027	0.086	0.13	0.19
$B_0 = 3 \cdot 10^{-6}$ G	0.14	0.45	0.69	1.00
$B_0 = 10 \cdot 10^{-6}$ G	10.7	34.1	52.7	76.1

Table 7.2: Eigenvalues ϕ_{mn} for different strengths of the background magnetic field.

$q = 1.8,\ H = 10$ kpc, $L = 15$ kpc, $B_0 = 3 \cdot 10^{-6}$ G, $k_{min} = 10^{-18}$ cm^{-1}				
	$m = 1, n = 1$	$m = 1, n = 2$	$m = 2, n = 1$	$m = 2, n = 2$
$v_A = 1 \cdot 10^5$ cm/s	3.95	12.5	19.4	28.0
$v_A = 7 \cdot 10^5$ cm/s	0.14	0.45	0.69	1.00
$v_A = 15 \cdot 10^5$ cm/s	0.38	0.12	0.19	0.27

Table 7.3: Eigenvalues ϕ_{mn} for different Alfvén velocities.

$q = 1.8,\ H = 10$ kpc, $L = 15$ kpc, $B_0 = 3 \cdot 10^{-6}$ G, $v_A = 7 \cdot 10^5$ cm/s				
	$m = 1, n = 1$	$m = 1, n = 2$	$m = 2, n = 1$	$m = 2, n = 2$
$k_{min} = 10^{-17}$ cm^{-1}	0.035	0.11	0.17	0.25
$k_{min} = 10^{-18}$ cm^{-1}	0.14	0.45	0.69	1.00
$k_{min} = 10^{-19}$ cm^{-1}	5.59	17.8	27.5	39.7

Table 7.4: Eigenvalues ϕ_{mn} for different minimum turbulence wave numbers.

$H = 10$ kpc, $L = 15$ kpc, $B_0 = 3 \cdot 10^{-6}$ G, $v_A = 7 \cdot 10^5$ cm/s, $k_{min} = 10^{-18}$ cm^{-1}				
	$m = 1, n = 1$	$m = 1, n = 2$	$m = 2, n = 1$	$m = 2, n = 2$
$q = 1.6$	0.000046	0.00015	0.00023	0.00033
$q = 1.8$	0.14	0.45	0.69	1.00
$q = 1.9$	11.5	36.57	56.6	81.6

Table 7.5: Eigenvalues ϕ_{mn} for different spectral indices of the wave spectrum.

From the Tables 7.1 to 7.5 we see that the range of the values of ϕ_{mn} can be strongly dependent on the parameter sets. Because the parameters are not known exactly, it is also possible to vary only ϕ_{mn} alone, the ratio of the two diffusion time scales.

7.2 Solar Modulation

The galactic cosmic rays are influenced by the solar wind when they enter the heliosphere, as we discussed already in 2.1.1. This modulation on their flight through the heliosphere (cf. [Gleeson & Axford 1968]) is taken into account to first order by the following simple rule deduced by the so called "force field approximation", where one assumes that the particles move through an electric field with a potential ϕ_{SM}:

$$\Phi_{IM} = \Phi_{TOA} \left(\frac{p_{IM}}{p_{TOA}} \right)^2 \tag{7.20}$$

where

$$p_{TOA} = p_{IM} - Ze\phi_{SM} \ . \tag{7.21}$$

Here, Φ_{IM} and Φ_{TOA} are the flux of galactic cosmic rays in the interstellar medium and at the top of the atmosphere, respectively, and p_{IM} and p_{TOA} are the momentum of galactic cosmic rays at the same locations. Z is the charge number of the cosmic rays and e is the electron charge.

ϕ_{SM} is the solar modulation parameter, measured by neutron monitors (refer to Subsection 2.2.3) at the corresponding time. The respective modulation parameters for the data sets listed below are used to model the influence of the heliosphere.

7.3 Data Sets Used

In the following, we use data sets from measured proton spectra at the top of the atmosphere from different experiments, balloon-borne and ground-based (cf. Section 2.2). In Table 7.6 the considered experiments are listed. From List 2.1 we take only in consideration data sets of recent experiments. The balloon experiments cover the low energy regime, while the airshower arrays measure the cosmic rays at higher energies (cf. Table 2.2). A mediator of both energy ranges is the balloon-borne mission JACEE. The symbols are used in the subsequent figures.

Symbol	Experiment	Type	Publication	Energy range for protons
Star	IMAX	Balloon	[Menn et al. 2000]	0.2-200 GeV
Diamond	BESS	Balloon	[Wang et al. 2002]	0.2-10 GeV
Cross	BESS	Balloon	[Sanuki et al. 2000]	1-120 GeV
Square	CAPRICE	Balloon	[Boezio et al. 1999]	0.4-200 GeV
Plus	JACEE	Balloon	[Asakimori et al. 1998]	20-800 TeV
Triangle	TIBET	Airshower array	[Amenomori et al. 2000]	200-1000 TeV

Table 7.6: Data sets used for measured proton spectra.

7.4 Comparison of the Calculated Spectra With Data

Now we have completed all preparations to calculate the proton spectra with the realistic spatial source function from Chapter 6 and for a power law momentum injection function (see Chapter 5) and can compare the results with the above-mentioned data sets.

The effect of solar modulation is taken into account in the way described in Section 7.2.

In order to avoid boundary effects, we set the lower momentum limit of the injection power law to $x_{min} = 0.01$ GV. The graphs in this section are plotted for momenta higher than 1 GeV, because in this regime the relative contribution of cosmic rays

originating from the sun is small. The maximum momentum of the particles injected by, for example, supernovae is assumed to be in the order of $x_{max} = 10^6$ GV (cf. Subsection 2.1.2).

The position of the solar system in the galaxy is taken to be as $z = 0$ pc and $r = 8500$ pc (refer to [Alves 2000]). For the galactic halo dimensions the values $L = 15$ kpc and $H = 10$ kpc are inserted and for the galactic disk boundary we take $r_0 = 15$ kpc and $z_0 = 0.5$ kpc.

In the following graphs the isotropic phase space distribution function $f(x)x^2$ is plotted after multiplying it with $x^{2.5}$ to flatten the graphs and to better recognize the features.

As we have seen in Chapter 6, the restriction of the number of eigenvalue terms to $m_{max} = n_{max} = 3$, i. e. to 9 terms, is sufficient and results in a reasonable calculation time.

Figure 7.1: Calculated spectra for a power law momentum source function for different turbulence spectral indices q in comparison with data. The parameters used are: $\beta = 2.4$, $x_{min} = 0.01$ GV, $x_{max} = 10^6$ GV, $m_{max} = n_{max} = 3$.

In Fig. 7.1 we compare the spectra for different spectral indices q of the turbu-

lence spectrum, where we used the eigenvalues for a mixture of slab Alfvén waves and fast magnetosonic waves as introduced in Section 7.1.

From the results we can state a very strong dependence of q, because q does not only enter in the argument of the Bessel functions I and K but also enters in the eigenvalues ϕ_{mn}.

To filter out this strong q-dependence of the eigenvalue ϕ_{mn} in Fig. 7.2 we adjust k_{min} (occuring in the parameter η, cf. Eq. (7.5)) in all cases such that the ratio of the momentum diffusion time and the spatial diffusion time is set equal at 1 GV for different q.
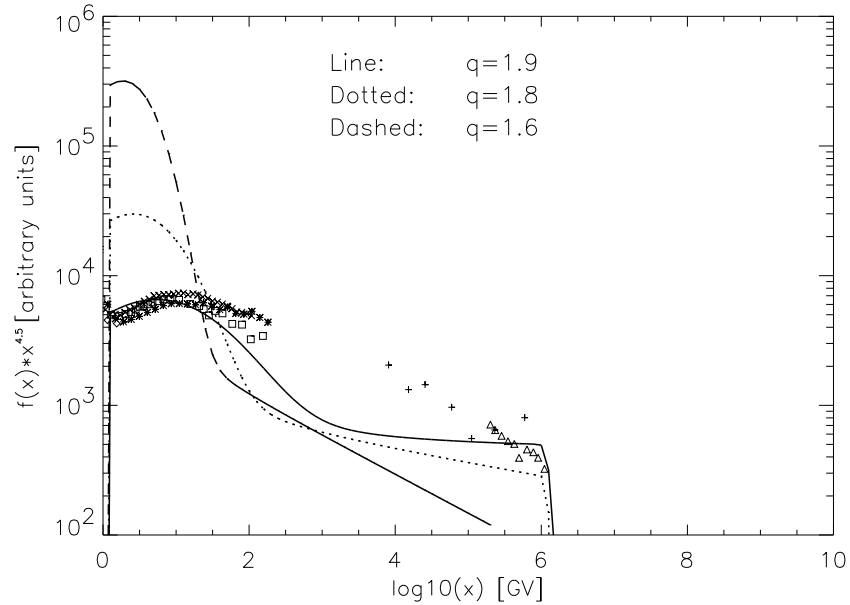
Figure 7.2: Phase space distribution function $f(x)x^{4.5}$ for different turbulence spectral indices q. k_{min} was adjusted such that the ratio of the momentum diffusion time and the spatial diffusion time is set equal at 1 GV for the three cases of different q. The parameters used are: $\beta = 2.4$, $x_{min} = 0.01$ GV, $x_{max} = 10^6$ GV, $m_{max} = n_{max} = 3$.

The best fit in both of the above cases we find for $q = 1.9$, especially in the low energy range, but the fit for higher energies is not very good, especially the steepness of the graph differs from that of the data.

In the energy region close to 1 GV we register the influence of the solar modulation. The solar wind pushes away the low energy galactic cosmic rays.

Now we vary the spectral index β of the initial momentum spectrum. The results we obtain are drawn in Fig. 7.3.

Here the best values are $\beta = 2.35 - 2.4$.

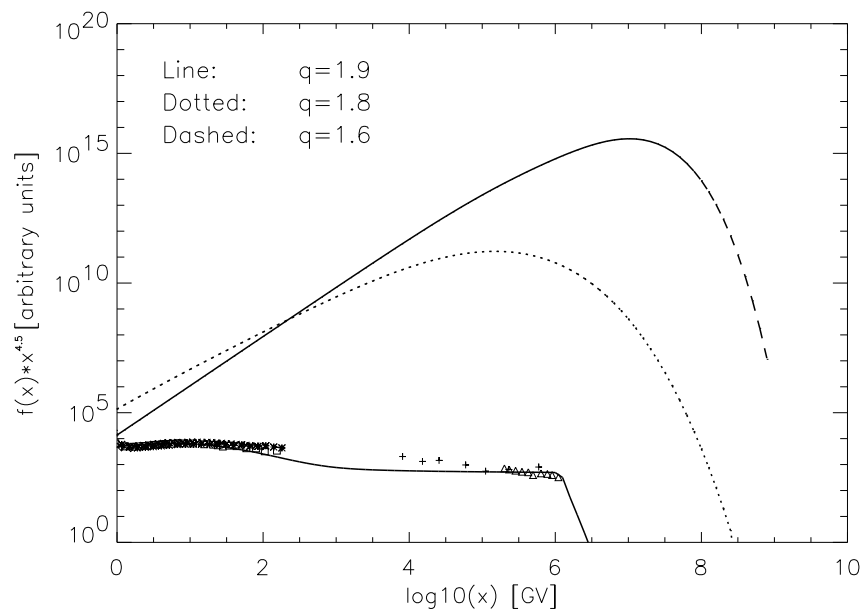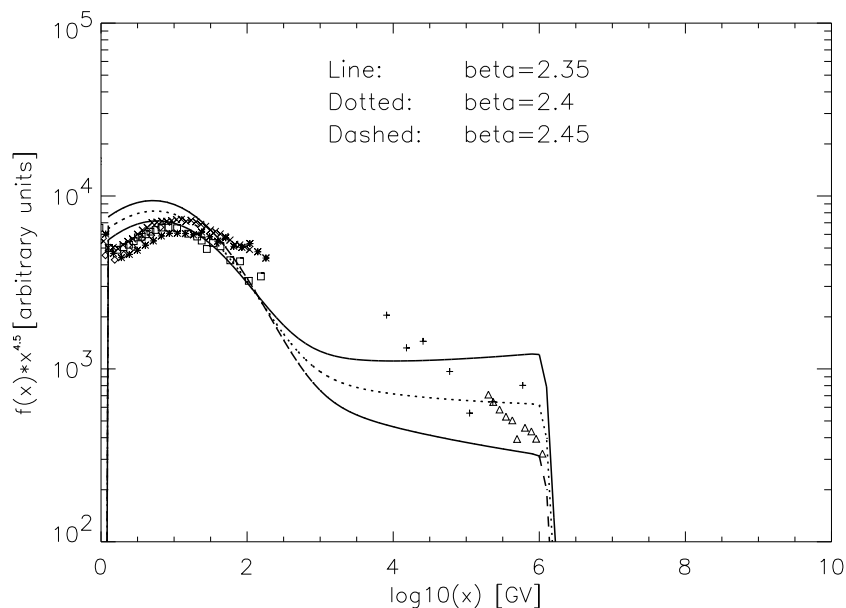*Figure 7.3:* Calculated spectra for a power law momentum source function for different source spectral indices β. The parameters used are: $q = 1.9$, $x_{min} = 0.01$ GV, $x_{max} = 10^6$ GV, $m_{max} = n_{max} = 3$.

If we regard the eigenvalue $\phi_{11} =: \phi$ as a free parameter, we obtain Fig. 7.4 for $q = 1.6$ and Fig. 7.5 for $q = 1.9$ for the first term of the eigenvalue expansion.

In the first case, ϕ has to be greater than 30, in the second case $\phi \approx 5$.

Fig. 7.4 with $q = 1.6$ provides a steepness of the resulting spectrum for large x as

$$f(x)x^2 \sim x^{-2.75} \,, \tag{7.22}$$

as it should be, according to Eq. (5.8) but the fit does not apply to small values of

Figure 7.4: Calculated spectra for a power law momentum source function and different $\phi_{11} =: \phi$ in comparison with data. The parameters used are: $\beta = 2.35$, $q = 1.6$, $x_{min} = 0.01$ GV, $x_{max} = 10^6$ GV, $m_{max} = n_{max} = 1$.

x. The power law index 2.75 is in agreement with the measured proton spectrum below the knee, cf. for example [Wiebel-Sooth et al. 1998] with a power law index for the proton spectrum measured at the earth of 2.77 ± 0.02.

An inspection of Fig. 7.5 shows, that we get a better fit for small x with $q = 1.9$ and $\beta = 2.35$, but now, the curve does not match the large values of x appropriately.

The strong influence of the spatial source function is represented in Fig. 7.6.

The more realistic source function introduced in Chapter 6 allows a substantial better fit to the data.

In Fig. 7.7 we compare the calculation with only one eigenvalue term with the calculation with more terms of the sum ($m_{max} = n_{max} = 3$ means 9 terms) to demonstrate that the first term is the dominant one.
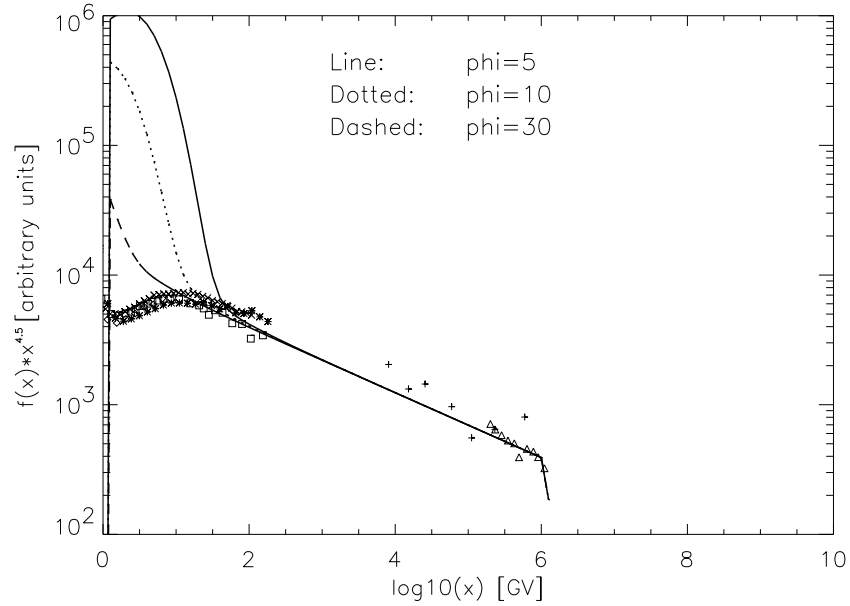
Figure 7.5: Calculated spectra for a power law momentum source function and different $\phi_{11} =: \phi$ in comparison with data. The parameters used are: $\beta = 2.35$, $q = 1.9$, $x_{min} = 0.01$ GV, $x_{max} = 10^6$ GV, $m_{max} = n_{max} = 1$.

7.4.1 Discussion of the results

In conclusion, it can be stated that the best data fit for a mixture of slab Alfvén waves and fast magnetosonic waves is obtained for the parameters $q = 1.9$ and $\beta \approx 2.4$. For smaller values of q we have some orders of magnitude differences to the data.

If we filter out the effect of the q-dependence in the eigenvalues ϕ_{mn}, and thus do not consider diffusion coefficients for special wave modes, $q = 1.9$ and $\beta \approx 2.35$ are also the best choice in the low energy regime, where the spectrum is still influenced by the solar wind. Contrary, the parameters $q = 1.6$ and $\beta \approx 2.35$ provide the expected steepness of the spectrum above about 100 GV, like it has been approximated in Chapter 5. The value $\beta \approx 2.35$ is in good agreement with the value of $\beta \approx 2.4$ provided by purely numerical models of other groups, which take into account stochastic reacceleration (cf. Subsection 2.1.2). [Jones et al. 2001], for example, give a value range of $\beta = 2.3 - 2.4$. The value $q = 1.6$ is in the order of the Kolmogorov index, as introduced in Subsection 2.3.1. This value is also consistent with results by the groups [Heinbach & Simon 1995] and [Jones et al. 2001], which in contrast use numerical models.

Figure 7.6: Calculated spectra for a power law momentum source function and different spatial source functions in comparison with data. The parameters used are: $\beta = 2.35$, $q = 1.9$, $x_{min} = 0.01$ GV, $x_{max} = 10^6$ GV, $m_{max} = n_{max} = 3$.

Other groups have fitted different values for q, like, for example, in the numerical treatment of [Maurin et al. 2002]. The value of the turbulence index is an important open question, which is still under debate. In some studies the Kolmogorov index is inserted as a fixed value into the model, like e. g. in [Seo & Ptuskin 1994], and is not treated as a free fit parameter, like in this work.

The ratio of the momentum and the spatial time scale ϕ_{11} can be fixed only if we consider the eigenvalue expansion to first order, because for more terms of the sum we have a respective number of eigenvalues ϕ_{mn}. For $q = 1.6$, ϕ has to be at least larger than 30, for $q = 1.9$ we get a value of $\phi \approx 5$.

A good fit for the whole energy range can not be achieved in this model so far. But pay attention: The differences of the calculated curves and the data sets also seem to be larger, because of the chosen scaling factor of $x^{2.5}$ in the plots of the spectra.

Including a source function with a realistic distribution of supernova remnants, the
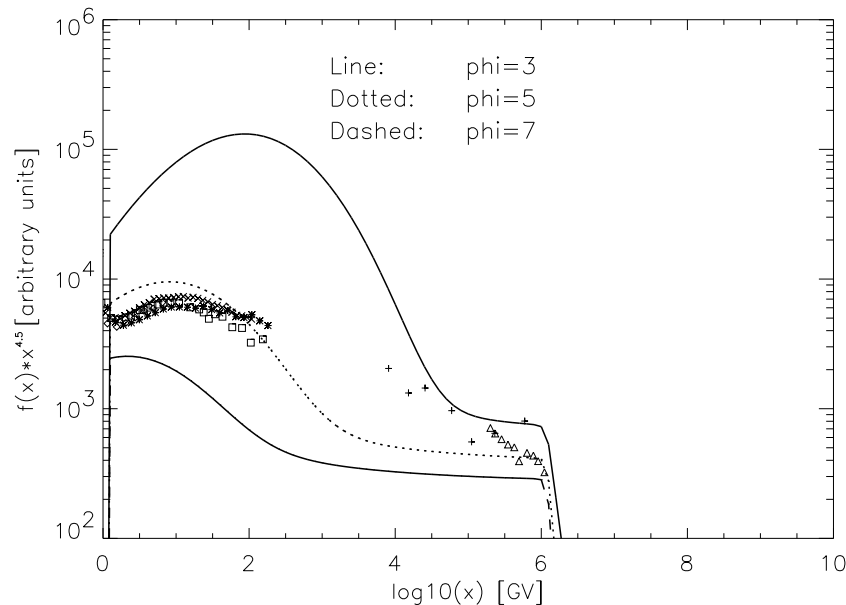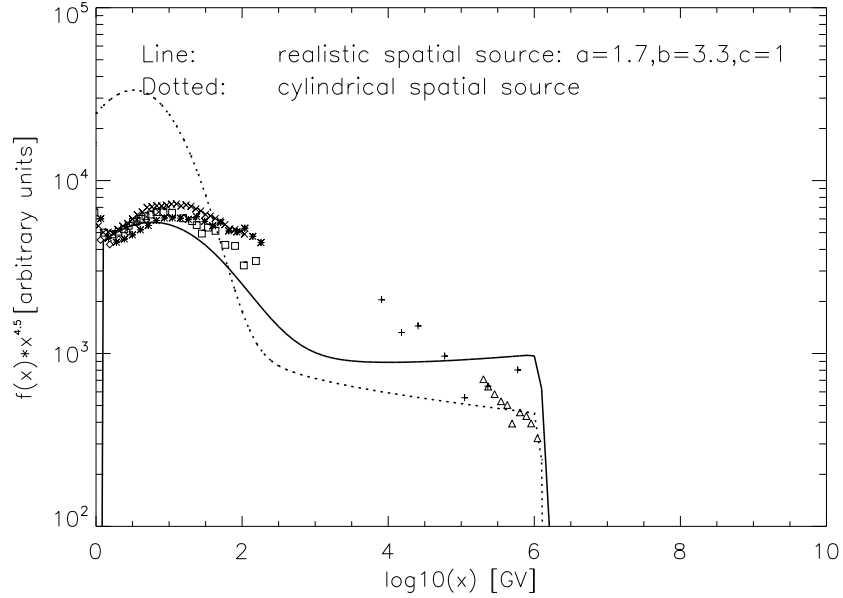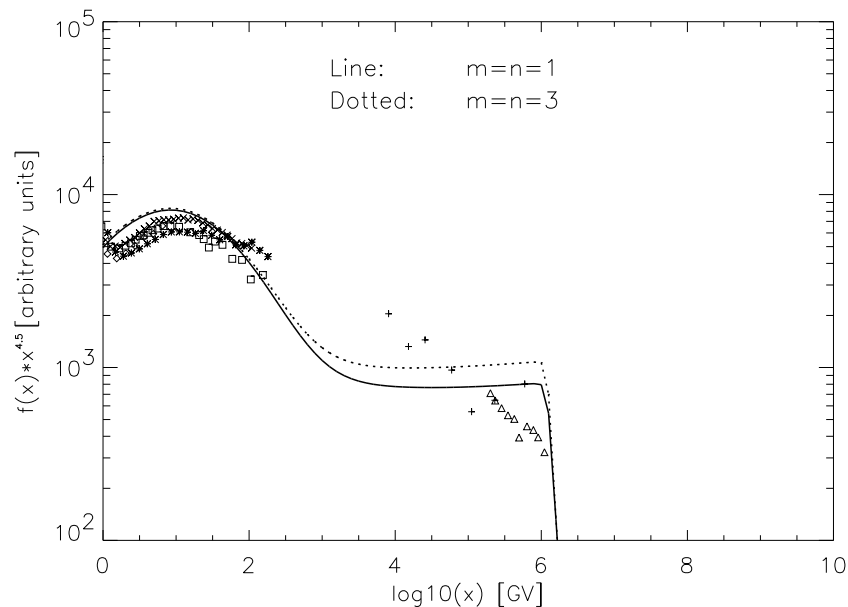
Figure 7.7: Calculated spectra for a power law momentum source function and different m_{max}, n_{max} in comparison with data. The parameters used are: $\beta = 2.35$, $q = 1.9$, $x_{min} = 0.01$ GV, $x_{max} = 10^6$ GV, $\phi = 5$.

potential sources of galactic cosmic rays, improves the fit of the data considerably.

Calculating only one term of the eigenvalue expansion is often sufficient, because the deviations due to the other parameters like q and β are much larger. This first order approximation corresponds to the leaky box model.

The eigenvalues and, thus, the ratios of the momentum and the spatial time scale are very sensitive to the parameters used for the interstellar medium, which are not known exactly. Especially the influence of the spectral index q to the momentum turbulence is large, which we used here as a free parameter.

By considering the aspect of the knee feature in the energy spectrum of the hadronic cosmic rays, we can infer from the studies presented above, that for a mixture of slab Alfvén waves and fast magnetosonic waves the spectrum for protons breaks off relatively sharp at the maximum injection rigidity (here 10^6 GV) for larger turbulence spectral indices ($q \approx 1.9$), in contrast to smaller q, where we reach rididities several magnitudes higher than the maximum injection momentum (up to 10^9 GV for $q = 1.6$). For nuclei with higher Z, like iron ($Z = 56$), the energy that can be

achieved, is higher, because $E = Z R$. But for nuclei with $Z > 1$ we have to take into account catastrophic losses, which we do in the next chapter. The total cosmic ray spectrum is a superposition of all cosmic ray nuclei, which enter proportional to their abundance, i. e. respective the chemical composition. So, for larger momenta the heavy nuclei dominate the knee of the energy spectrum, but their fraction in comparison to hydrogen is smaller.

Chapter 8

The Confluent Hypergeometric Functions and the Associated Momentum Integral

The momentum solution of the transport equation for nuclei including catastrophic losses consists of integrals over the confluent hypergeometric functions M and U instead of the modified Bessel functions, which we dealt with in the preceeding chapters. To treat the integrals we first describe some properties and some representations of the M and U functions, which can be used for a computer calculation.

The reason why for this case the numerical calculations of the exact momentum integrals fail if inserting a momentum injection power law function are discussed subsequently.

An attempt to simplify the analytical and numerical situation by interchanging the integrals in the momentum double integral for a momentum power law does not succeed, and in order to make progress we have to approximate the integrals. In the last section the approximations are derived in the same way as in the I-K-case for a power law injection function.

From Chapter 4 we repeat for survey the momentum solution with catastrophic losses

$$f_{mn}(x) = T_f \alpha^\chi \int_0^\infty dx_0 x_0^2 q(x_0) G_{mn}(x, x_0) \tag{8.1}$$

with the Green's function

$$G_{mn}(x, x_0) = \frac{\left(2\sqrt{\phi_{mn}}\right)^{\frac{3}{\chi}-1}}{\chi^{\frac{3}{\chi}}} \frac{\Gamma\left[\frac{3}{2\chi} + \frac{\psi}{2\chi\sqrt{\phi_{mn}}}\right]}{\Gamma\left[\frac{3}{\chi}\right]} \exp\left[-\frac{\sqrt{\phi_{mn}}(x^\chi + x_0^\chi)}{\chi}\right] \times$$

$$\times \begin{cases} M\left(\frac{3}{2\chi} + \frac{\psi}{2\chi\sqrt{\phi_{mn}}}, \frac{3}{\chi}, \frac{2\sqrt{\phi_{mn}}x^\chi}{\chi}\right) U\left(\frac{3}{2\chi} + \frac{\psi}{2\chi\sqrt{\phi_{mn}}}, \frac{3}{\chi}, \frac{2\sqrt{\phi_{mn}}x_0^\chi}{\chi}\right) & ; \ 0 \le x \le x_0 \\ U\left(\frac{3}{2\chi} + \frac{\psi}{2\chi\sqrt{\phi_{mn}}}, \frac{3}{\chi}, \frac{2\sqrt{\phi_{mn}}x^\chi}{\chi}\right) M\left(\frac{3}{2\chi} + \frac{\psi}{2\chi\sqrt{\phi_{mn}}}, \frac{3}{\chi}, \frac{2\sqrt{\phi_{mn}}x_0^\chi}{\chi}\right) & ; \ x_0 \le x < \infty \end{cases} \tag{8.2}$$

Some properties of the Gamma function Γ can be found in Appendix G.

8.1 Representations for M and U

In this section we list the different representations for the functions M and U: the integral representations, a series for M, a formula for U using M and the confluent hypergeometric functions expressed in terms of the Whittaker functions.

In the literature the M-function is sometimes also denoted by $_1F_1$.

$M(a, b, x)$ and $U(a, b, x)$ are independent solutions of Kummer's differential equation:

$$x\frac{d^2 f(x)}{dx^2} + (b - x)\frac{df(x)}{dx} - af(x) = 0 \tag{8.3}$$

In general, the variable x can be complex.

8.1.1 Integral Representations

The integral representations are defined for the parameters $b > a > 0$
(see [Abramowitz & Stegun 1984] (12.2.1) and (12.2.5)):

$$M(a, b, x) = \frac{\Gamma(b)}{\Gamma(b - a)\Gamma(a)} \int_0^1 dt \, e^{xt} t^{a-1} (1 - t)^{b-a-1} \tag{8.4}$$

$$U(a, b, x) = \frac{1}{\Gamma(a)} \int_0^\infty dt \, e^{-xt} t^{a-1} (1 + t)^{b-a-1} \ . \tag{8.5}$$

8.1.2 A Series for M

A series for M is found e. g. in [Abramowitz & Stegun 1984] (13.1.2)

$$M(a, b, x) = \sum_{n=0}^{\infty} \frac{(a)_n x^n}{(b)_n n!} \tag{8.6}$$

where Pochhammer's symbol (see Eq. G.7) is defined as

$$(a)_n = a(a+1)(a+2)...(a+n-1), \ (a)_0 = 1 \ . \tag{8.7}$$

We have to pay attention to negative integer values of b: if one factor $(b+m)$ in the denominator of a term of the sum is 0, that is for $b = -m$, $m \in \{0, 1, ..., n-1\}$, then there emerges a pole in the series.

8.1.3 Another Formula for U Including M

U can be determined if M is known by using the expression
(cf. [Abramowitz & Stegun 1984] (13.1.3))

$$U(a, b, x) = \frac{\pi}{\sin(\pi b)} \left[\frac{M(a, b, x)}{\Gamma(1 + a - b)\Gamma(b)} - x^{1-b} \frac{M(1 + a - b, 2 - b, x)}{\Gamma(a)\Gamma(2 - b)} \right] \tag{8.8}$$

or, equivalently, in another form (see [Gradshteyn & Ryzhik 1994] (9.210).2):

$$U(a, b, x) = \frac{\Gamma(1 - b)}{\Gamma(a - b + 1)} M(a, b, x) + \frac{\Gamma(b - 1)}{\Gamma(a)} x^{1-b} M(1 + a - b, 2 - b, x) \ . \tag{8.9}$$

To transform both formulas into each other the following two relations must hold:

$$\frac{\pi}{\sin(\pi b)} \frac{1}{\Gamma(b)} = \Gamma(1 - b) \tag{8.10}$$

and

$$-\frac{\pi}{\sin(\pi b)} \frac{1}{\Gamma(2 - b)} = \Gamma(b - 1) \ . \tag{8.11}$$

With (G.5) for the Gamma function we confirm the correctness of the first equation

$$\Gamma(b)\Gamma(1 - b) = \pi \csc(\pi b) = \frac{\pi}{\sin(\pi b)} \tag{8.12}$$

and using additionally the recurrence relation (G.4) the second equation also is fulfilled:

$$\Gamma(b - 1) = -\frac{1}{\Gamma(2 - b)} \Gamma(b)\Gamma(1 - b) \tag{8.13}$$

$$-\Gamma(b-1) = \frac{1}{(1-b)\Gamma(1-b)}(b-1)\Gamma(b-1)\Gamma(1-b) \ . \tag{8.14}$$

One has to be careful, because poles of the Gamma function in the formula for U occur for $(1-b) \in \{0, -1, -2, ...\}$ and $(b-1) \in \{0, -1, -2, ...\}$, that means for $b \in \mathbb{Z}$.

Poles of the second M-function in the formula for U arise for the condition $(2 - b + m) = 0$ for $m \in \mathbb{N}$, in other words for $b \in \{-2, -3, ...\}$.

For any given parameter set the combination of the diverging terms in U has to be investigated in detail.

8.1.4 Representations With Whittaker Functions

The relations between the Whittaker functions $M\mu,\nu$ and $W\mu,\nu$ and the confluent hypergeometric functions M and U, respectively, read (see [Abramowitz & Stegun 1984] (13.1.32) and (13.1.33)):

$$M_{\mu,\nu}(x) = e^{-\frac{1}{2}x}x^{\frac{1}{2}+\nu}M\left(\frac{1}{2}+\nu-\mu, 1+2\nu, x\right) \tag{8.15}$$

$$W_{\mu,\nu}(x) = e^{-\frac{1}{2}x}x^{\frac{1}{2}+\nu}U\left(\frac{1}{2}+\nu-\mu, 1+2\nu, x\right) \ . \tag{8.16}$$

For the inverse transformation we get

$$M(a,b,x) = x^{-\frac{b}{2}}e^{\frac{1}{2}x}M_{\frac{b}{2}-a,\frac{b-1}{2}}(x) \tag{8.17}$$

and analogously

$$U(a,b,x) = x^{-\frac{b}{2}}e^{\frac{1}{2}x}W_{\frac{b}{2}-a,\frac{b-1}{2}}(x) \ . \tag{8.18}$$

8.2 On Calculating the Confluent Hypergeometric Functions and the Associated Momentum Integral

8.2.1 The Functions M and U for Some Parameter Sets

Figs. 8.1 and 8.2 show the M-function for different parameter sets, chosen such that the graphs can be drawn properly and avoiding singularities in the formulas for calculating the confluent hypergeometric functions. (For realistic parameter sets

the functions M and U are far too steep or too flat, so that one cannot investigate the characteristic properties by the respective graphs.)

Figure 8.1: The $M(a, b, x)$-function for the parameter a=1.1.
Black: M(1.1,1.5,x),
blue: M(1.1,2.5,x),
green: M(1.1,3.5,x),
red: M(1.1,4.5,x).

Figure 8.2: The $M(a, b, x)$-function for the parameter b=1.5.
Black: M(1.1,1.5,x),
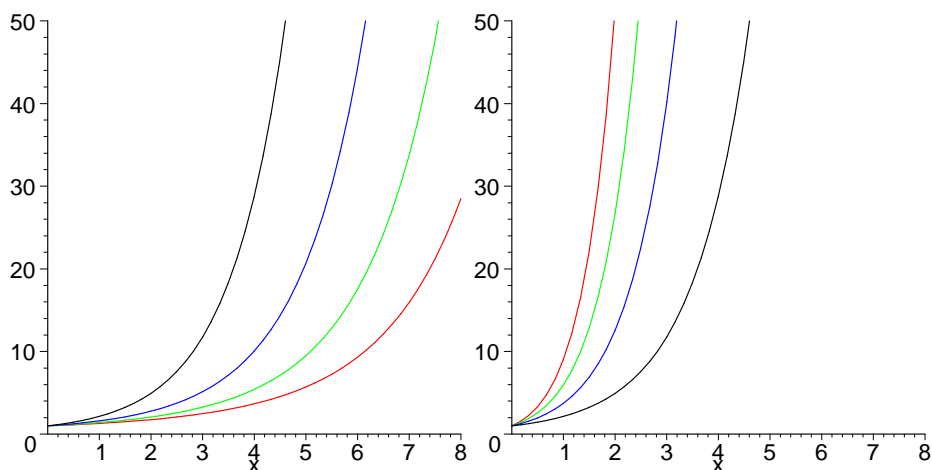blue: M(2.1,1.5,x),
green: M(3.1,1.5,x),
red: M(4.1,1.5,x).
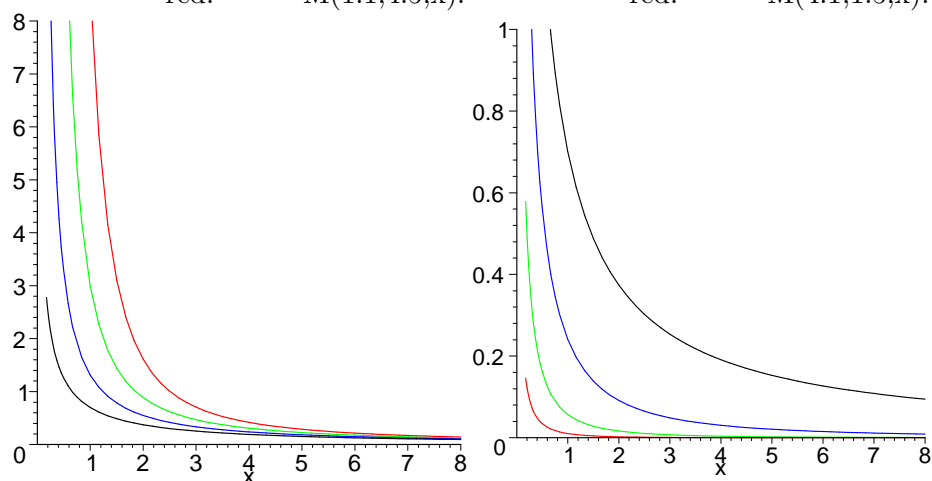
Figure 8.3: The $U(a, b, x)$-function for the parameter a=1.1.
Black: U(1.1,1.5,x),
blue: U(1.1,2.5,x),
green: U(1.1,3.5,x),
red: U(1.1,4.5,x).

Figure 8.4: The $U(a, b, x)$-function for the parameter b=1.5.
Black: U(1.1,1.5,x),
blue: U(2.1,1.5,x),
green: U(3.1,1.5,x),
red: U(4.1,1.5,x).

In the first figure the first parameter a of $M(a, b, x)$ is fixed and b varies, in the second figure b is fixed. For the same parameter sets the U-function is plotted in Figs. 8.3 and 8.4 where a is fixed and b changes as parameters of $U(a, b, x)$ and vice versa, respectively.

For $x \rightarrow \infty$ the M-functions approach infinity and the U-functions converge to zero.

8.2.2   Numerical Consistency Checks and Problems

Calculation With the Integral Representations

To verify the correctness of the numerical calculations of the M- and U-functions by their integral representations (8.4) and (8.5), they are compared with the values provided by the asymptotic formulas (F.10) and (F.11) for M and U, respectively. The results agree sufficiently and also consistency checks between the Maple and FORTRAN code integral calculations are satisfactory with numerical differences smaller than 10^{-6}.

So, the integrals calculated individually seem to be correct, but if implementing them in the Maple programm code for the whole momentum integral, the computer is not able to provide a result. For some required parameter sets numerical problems occur also with the FORTRAN integration routines.

Calculations With the M-series and the U-formula

Using the M-series (8.6) we have to take into account about 150 terms for a sufficient approximation (better then 10^{-6}; for about 100 terms the approximation is too bad), but we get problems in Maple with such large sums.

Applying the formula (8.8) for U, if we take care of the singularities, like it is mentioned in Section 8.1.3, a very high numerical accuracy is needed to yield correct results, because for parameter sets for our problems the formula (8.8) is a difference of two very large numbers which has to result in a very small number. These difficulties explain also the totally different numerical results in Maple for U if using different methods for its determination, like the integral representation (8.5), the formula (8.8) for U and the expressions with the Whittaker functions (8.18). An increase of the accuracy in Maple is possible but results in a very large computing time. And still the problem with the M-series remains.

We have to emphasize, that the these problems are of purely numerical nature

and there exist no mathematical reasons why the integrals and series should not converge. They behave smoothly in the considered parameter ranges.

8.2.3 Interchanging the Integrations for a Power Law Momentum Injection Function

In this subsection we try to simplify the integrations by interchanging the integration of the integral representations of the M and the U functions and the momentum integration for the special case of a power law momentum injection function. Our aim is to treat the integrations partially analytical and to cast them into a form, which can be handled better by the computer code:

$$
\begin{aligned}
f_{mn}(x) \quad \sim \quad & \int_0^x dx_0 x_0^2 q(x_0) \exp\left[-\frac{\sqrt{\phi_{mn}}(x^\chi + x_0^\chi)}{\chi}\right] \\
& U\left(\frac{3}{2\chi} + \frac{\psi}{2\chi\sqrt{\phi_{mn}}}, \frac{3}{\chi}, \frac{2\sqrt{\phi_{mn}}x^\chi}{\chi}\right) M\left(\frac{3}{2\chi} + \frac{\psi}{2\chi\sqrt{\phi_{mn}}}, \frac{3}{\chi}, \frac{2\sqrt{\phi_{mn}}x_0^\chi}{\chi}\right) \\
& + \int_x^\infty dx_0 \dots \\
\sim \quad & U\left(\frac{3}{2\chi} + \frac{\psi}{2\chi\sqrt{\phi_{mn}}}, \frac{3}{\chi}, \frac{2\sqrt{\phi_{mn}}x^\chi}{\chi}\right) \exp\left(-\frac{\sqrt{\phi_{mn}}}{\chi}x^\chi\right) \\
& \int_0^x dx_0 x_0^{-\beta} \exp\left(-\frac{\sqrt{\phi_{mn}}}{\chi}x_0^\chi\right) M\left(a, b, \frac{2\sqrt{\phi_{mn}}x_0^\chi}{\chi}\right) \\
& + M(\dots, \dots x^\chi) \exp(\dots x^\chi) \int_x^\infty dx_0 x_0^{-\beta} \exp(\dots x_0^\chi) U(\dots, \dots x_0^\chi) \\
\sim \quad & U(\dots, x^\chi) \exp(\dots x^\chi) \\
& \int_0^x dx_0 x_0^{-\beta} \exp\left(-\frac{\sqrt{\phi_{mn}}}{\chi}x_0^\chi\right) \int_0^1 dt \ \exp\left(\frac{2\sqrt{\phi_{mn}}x_0^\chi}{\chi}t\right) t^{a-1}(1-t)^{b-a-1} \\
& + M(\dots, \dots x^\chi) \exp(\dots x^\chi) \int_x^\infty dx_0 \dots \\
\sim \quad & U(\dots, x^\chi) \exp(\dots x^\chi) \\
& \int_0^1 dt \left[\int_0^x dx_0 x_0^{-\beta} \exp\left(x_0^\chi \frac{\sqrt{\phi_{mn}}}{\chi}(2t - 1)\right)\right] t^{a-1}(1-t)^{b-a-1} \\
& + M(\dots, \dots x^\chi) \exp(\dots x^\chi) \int_x^\infty dx_0 \dots \ .
\end{aligned}
$$

The integral to be solved is of the form

$$
I := \int_0^x dx_0 x_0^{-\beta} \exp\left(\delta x_0^\chi\right) . \tag{8.19}
$$

with

$$\delta := \frac{\sqrt{\phi_{mn}}}{\chi}(2t - 1) \tag{8.20}$$

The substitution

$$y = \delta x_0^\chi \Leftrightarrow x_0 = \left(\frac{y}{\delta}\right)^{\frac{1}{\chi}}, \ dx_0 = \frac{dy}{\delta \chi x_0^{\chi-1}} \tag{8.21}$$

leads to

$$
\begin{aligned}
I &= \frac{1}{\delta \chi} \int dy \left(\frac{y}{\delta}\right)^{\frac{1-\chi-\beta}{\chi}} \exp(y) \\
&= \frac{1}{\chi \delta^{\frac{1-\beta}{\chi}}} \int_0^{\delta x^\chi} dy\, y^{\frac{1-\chi-\beta}{\chi}} \exp(y) \ .
\end{aligned}
\tag{8.22}
$$

According to [Gradshteyn & Ryzhik 1994] (3.381).1

$$\int_0^u dx\, x^{\nu-1} \exp(-\mu x) = \mu^{-\nu} \gamma(\nu, \mu u) \text{ with } \operatorname{Re} \nu > 0 \tag{8.23}$$

we try to apply the definition [Gradshteyn & Ryzhik 1994](8.350).1 of the incomplete Gamma function (cf. Section G.1)

$$\gamma(\alpha, x) = \int_0^x dt\, t^{\alpha-1} \exp(-t) \ , \tag{8.24}$$

here with $\mu = -1$ and $\nu = \frac{1-\chi-\beta}{\chi} + 1 = \frac{1-\beta}{\chi}$. But with our typical values for β (cf. Chapter 7) and χ ($\chi = q - 2, q < 2$) we get $\nu < 0$, so we cannot use the incomplete Gamma function.

The numerical calculations with the computer for the case of interchanged integrations fail again, too.

Now another way is to calculate analytical approximations for special momentum injection functions, which we will do in the following.

8.2.4 Approximations of the Momentum Solution With Catastrophic Losses for a Power Law Injection Function

The momentum integral for catastrophic losses can be analytically approximated for the different momentum regimes if we insert a power law momentum source function (see Appendix F):

$$f_{mn}(x) \simeq \frac{q_0 T_f \alpha^\chi}{\beta - 1} \frac{(2\sqrt{\phi_{mn}})^{\frac{3}{\chi} - 1}}{\chi^{\frac{3}{\chi}} \left(\frac{3}{\chi} - 1\right)} x_{min}^{1-\beta} \left(\frac{x}{x_c}\right)^{\chi - 3} \qquad (8.25)$$

for $x \ll x_c$ (case 1 (Eq. F.22) and 2 (Eq. F.35)) and

$$f_{mn}(x) \simeq \frac{4 q_0 T_f \alpha^\chi (2\sqrt{\phi_{mn}})^{\frac{3}{\chi} - 1}}{\chi^{\frac{3}{\chi} + 1}} x_c^{\chi + 3} x^{-(\beta + 2 + \chi)} \qquad (8.26)$$

for $x \gg x_c$ (case 3 (Eq. F.44) and 4 (Eq. F.47)) containing the characteristic momentum

$$x_c := \left(\frac{\chi}{2\sqrt{\phi_{mn}}}\right)^{\frac{1}{\chi}} . \qquad (8.27)$$

Comparing with the respective approximations (5.7), (5.8) and (5.9) in Chapter 5 for the momentum integral omitting catastrophic losses we discover the same behaviour. The characteristic parameter ψ for the catastrophic losses does not emerge in the final terms any more. The approximation is too crude.

Again, above the maximum injection momentum x_{max} all spectra cut off exponentially, independent of the source index β (see Appendix F.50):

$$f_{mn}(x) \sim e^{-\frac{1}{2}\left(\frac{x}{x_c}\right)^\chi} x^{-\frac{3}{2} + \frac{\psi}{2\sqrt{\phi_{mn}}}} . \qquad (8.28)$$

Chapter 9

Summary and Discussion

In this work we investigated the analytical solutions of the stationary transport equation for galactic cosmic rays. The focus is laid on the influence of the spatial diffusion and the stochastic reacceleration by plasma waves existing in the interstellar medium.

The solution of the transport equation can be formulated as an infinite double sum of spatial and momentum eigenfunctions, where spatial and momentum source functions enter in the respective integrals. We assume initial power law momentum source spectra, which could result from shock acceleration of nuclei in supernova remnants. The Green's function for the case of no catastrophic losses contains the I- and K-Bessel functions, and the Green's function with consideration of spallation contains the confluent hypergeometric functions M and U.

To test the solution itself and our newly developed computer code for the final integrals, we made some theoretical and numerical consistency checks. Analytical approximations for the momentum integral for small and large momenta for the case of a power law source spectrum were provided and compared to the numerically calculated complete momentum solutions. For small momenta p the isotropic phase space distribution function f is proportional to p^{-q-1}, and for large momenta the initial power law spectrum $p^{-\beta-2}$ is steepened by an exponent $2 - q$, where q is the spectral index of the turbulence. It was shown that for larger indices q the stochastic momentum diffusion can accelerate particles to higher momenta, exceeding the upper momentum injection limit by several orders of magnitude. Besides, there is a competition between the spatial and momentum diffusion process: for a smaller momentum diffusion time scale more high energetic particles are produced, as we expected. The steepness of the initial source spectrum is reflected in the resulting momentum spectra. If we assume a perhaps more realistic source spectrum with a dispersive index, as a consequence of a sample of supernova remnants with different

power law indices, the calculations show a slightly flatter spectrum for large momenta. This is only a secondary effect so that the assumption of a simple power law spectrum is sufficient for the subsequent calculations.

In the spatial part of the solution we inserted a realistic spatial supernova remnant distribution and calculated the integrals partially analytical. For a good approximation it is sufficient to take only the first 9 terms of the infinite double sum ($m_{max} = n_{max} = 3$).

Then we made an assumption for the galactic turbulence by inserting diffusion coefficients for a mixture of slab Alfvén waves and fast magnetosonic waves and calculated some typical eigenvalues. The eigenvalues vary depending on the different astrophysical parameters, like the halo dimensions, the background magnetic field, the Alfvén velocity, the minimum turbulence wave number or the spectral index of the wave spectrum. The influence of the latter turned out to be very strong.

After having taken into account solar modulation, the proton spectra with no catastrophic losses were calculated for different parameter sets and compared to recent data from balloon and airshower array experiments. Again, a very strong dependence on the turbulence spectral index q could be stated because it emerges in the eigenvalues ϕ_{mn} as a consequence of our specific assumption of the diffusion coefficients. We could filter out this effect by adjusting the ratio of the momentum diffusion time to the spatial diffusion time to be equal at 1 GeV. Filtered or not, the value $q = 1.9$ gives the best fit, while for smaller values of q we have some orders of magnitude differences to the data. The discrepancy at higher energies is unfortunately growing, in contrast to the low energy regime, where the spectrum is bent by the solar wind. The best-fit values for the supernova power law source spectral index are $\beta = 2.35 - 2.4$, which is in good agreement with other models taking into account stochastic reacceleration (cf. [Drury et al. 2001]). If the eigenvalue $\phi_{11} =: \phi$ itself is taken as a free parameter, the ratio of the momentum and the spatial diffusion time scale, ϕ has to be at least larger than approximately 30 for $q = 1.6$ and $\phi \approx 5$ for $q = 1.9$. The fit for the Kolmogorov-like spectral index $q = 1.6$ provides a spectral index of the processed spectrum of -2.75 above 100 GV, as it can be found in the literature. But again, the fit for small momenta is not convincing. In that region a better fit is provided with $q = 1.9$. We could also show that a realistic spatial source function better explains the data. All in all, the eigenvalues and, thus, the ratios of the momentum and the spatial time scales are very sensitive to the parameters used for the interstellar medium, which, however, are not known exactly.

One important aspect that could explain the fact that the fit does not apply to the whole energy range is the missing fill up of the primary proton spectra by secondary

protons in our model. The secondary protons emerge in the spallation processes of heavier nuclei with the interstellar medium. This could, in principle, be taken into account by respective transport equations with catastrophic loss terms, consequently we discussed the treatment of the solution of these type of equations. The confluent hypergeometric functions enter into the Green's function of this solution. These functions and the corresponding momentum integrals are very difficult to handle for the required values of the physical parameters so that we encounter invincible purely numerical problems. Again, for a power law momentum source function, the analytical asymptotic cases were presented, but the functions turn out to be similar to the cases without catastrophic losses. This first-order approximation seems to be too crude, because the characteristic catastrophic loss time scale T_c does not occur in the resulting formulas any more. A second-order approximation, however, is very difficult to calculate.

For a complete description of all measured cosmic ray spectra, in principle, one has to solve a system of cascading transport equations, where the spallation products of nuclei with atomic number A enter as additional source terms in the transport equations for nuclei with lower A. Moreover, radioactive losses have to be taken into account. For a detailed calculation of the spallation term an explicit spatial gas distribution is required, with a density that is different in the galactic disk and in the halo.

Some other explanations for the discrepancy between theory and data in some energy regimes may be the neglect of spatial and momentum convection terms and of continuous losses. By taking into account these terms, the advantage of an analytical treatment of the transport equation then probably has to be dropped, and it remains only the possibility of a direct numerical solution of the differential equation, like it has been done by [Heinbach & Simon 1995],[Simon et al. 1986], [Seo & Ptuskin 1994], [Strong & Moskalenko 1998],[Moskalenko et al. 1998], [Jones et al. 2001] and [Maurin et al. 2002], who have also considered stochastic reacceleration.

For some special cases three-dimensional analytical calculations are possible for a non-stationary transport equation, like it is shown in [Büsching 2004], but in the work cited stochastic acceleration had to be neglected. Instead, the approximation of a homogeneous source distribution has been replaced by discrete sources and a purely numerical solution of the transport equation was necessary.

Because of the lack of in situ measurements it remains unclear, which modes of plasma waves are dominating in the interstellar medium. In the recent publication of [Shalchi et al. 2003], also a different behaviour of the diffusion coefficients at small energies has been stated. In [Lerche & Schlickeiser 2001] a modification of the

momentum diffusion coefficient is calculated for strongly anisotropic magnetohydrodynamic turbulence. [Schlickeiser 2004] discussed a spatial diffusion coefficient of the form

$$\kappa \sim \begin{cases} p^0 & , p \leq p_c \\ p^2 & , p > p_c \end{cases} \tag{9.1}$$

instead of $\kappa \sim p^{2-q}$ as done in the present work, and a momentum diffusion coefficient of the form

$$A_2 \sim \begin{cases} p^2 & , p \leq p_c \\ p^0 & , p > p_c \end{cases} \tag{9.2}$$

instead of $A_2 \sim p^q$, for a critical momentum $p_c \approx 4 \cdot Z \cdot 10^{15}$ eV/c. Then for $p \leq p_c$ we obtain the solution of the transport equation for the case $q = 2$, as presented in Appendix D, and the case $p > p_c$ results in

$$f \sim \exp\left(-\frac{p}{p_1}\right)^2 U\left(\frac{3}{4} + 4, \frac{3}{2}, 2\left(\frac{p}{p_1}\right)^2\right) . \tag{9.3}$$

Here again U is a confluent hypergeometric function and $p_1 = \text{const.}$

The condition of the turbulence spectrum being a power law across the whole wave number region has also to be confirmed more convincingly. We are not able to measure the plasma turbulence directly, therefore the connection between the detected electron densities and the wave number distribution needs further investigations.

Finally, a detection of TeV photon spectra of supernova remnants by existing and future experiments, which can only be explained by high energetic primary nuclei, gives the chance to fix the nowadays not exactly known form of the initial momentum source spectra.

In conclusion, in the present work we establish for the first time fits of cosmic ray proton data by calculating the integrals of the analytical eigenfunction sum solution of the transport equation, including reacceleration by interstellar plasma waves, realistic spatial source distributions and solar modulation. Different fit parameters, like the spectral index of the supernova remnants, the spectral index of the plasma turbulence and the ratio of the momentum diffusion time scale and the spatial diffusion time scale are obtained by taking into account 9 terms of the eigenfunction sum, which could be shown to be a sufficient approximation. Additionally, we provide analytical approximations of the momentum integrals for power law momentum injection functions, which are good momentum distribution approximations for the assumed primary sources of galactic cosmic rays, the supernova remnants.

Appendix A

Calculating the Solution of the Transport Equation Without Catastrophic Losses

In this chapter we calculate the solution of the transport equation, in our case (see Eq. (3.54))

$$L_{\vec{x}} f(\vec{x}, p) + L_p f(\vec{x}, p) = -Q_1(\vec{x}) \frac{Q_2(p)}{\kappa(p)} \tag{A.1}$$

by applying the "scattering time method" (see [Wang & Schlickeiser 1987]).

A.1   The Scattering Time Method

For separating the equation in two differential equations we introduce two new functions T and F and a new variable u by $f(x, \vec{p}) = \int_0^\infty du\, F(p, u) T(\vec{x}, u)$:

$$\int_0^\infty du\, F(p, u) L_{\vec{x}} T(\vec{x}, u) + \int_0^\infty du\, T(\vec{x}, u) L_p F(p, u) = -Q_1(\vec{x}) \frac{Q_2(p)}{\kappa(p)} \ . \tag{A.2}$$

Now we claim that $L_{\vec{x}}T$ and $L_p F$ have to be partial derivatives of T and F respectively; thus one gets two new differential equations with the variables $\vec{x}$ and u resp. p and u. The solution is provided subsequently with an exponential ansatz.

$$\boxed{\frac{\partial T(\vec{x}, u)}{\partial u} = L_{\vec{x}} T(\vec{x}, u)} \tag{A.3}$$

$$\boxed{\frac{\partial F(p,u)}{\partial u} = L_p F(p,u)} \tag{A.4}$$

After inserting into Eq. (A.2) the integrals cancel by applying partial integration to the first term of the left hand side

$$[FT]_0^\infty \underbrace{- \int du \, \frac{\partial F}{\partial u} T + \int du \, T \frac{\partial F}{\partial u}}_{=0} = -Q_1(\vec{x}) \frac{Q_2(p)}{\kappa(p)} \, , \tag{A.5}$$

and one gets the boundary conditions for F and T:

$$F(p, u \to \infty) \, T(\vec{x}, u \to \infty) - F(p, u = 0) \, T(\vec{x}, u = 0) = -Q_1(\vec{x}) \frac{Q_2(p)}{\kappa(p)} \, . \tag{A.6}$$

After fixing $F(p, u \to \infty) \, T(\vec{x}, u \to \infty) = 0$ it remains

$$\boxed{F(p, u = 0) = +\frac{Q_2(p)}{\kappa(p)}} \tag{A.7}$$

and

$$\boxed{T(\vec{x}, u = 0) = +Q_1(\vec{x})} \, . \tag{A.8}$$

[Lerche & Schlickeiser 1988] point out, that the scattering time method can be applied also to a more general form of the source term, like a sum

$$S(\vec{x}, p) = \sum_i Q_{1,i}(\vec{x}) Q_{2,i}(p) \tag{A.9}$$

or even a continuous formulation

$$S(\vec{x}, p) = \int du Q_1(u, \vec{x}) Q_2(u, p) \, . \tag{A.10}$$

A.2 The Spatial Problem

We have to solve Eq. (A.3):

$$\boxed{\frac{\partial T(\vec{x}, u)}{\partial u} = L_{\vec{x}} T(\vec{x}, u)} \, . \tag{A.11}$$

For the confinement region of the galactic cosmic rays, the halo, we assume a cylindrical disk with radius L and half-height H. At its edge the particles can escape ("free-escape boundary conditions") and outside the phase space distribution function therefore is zero:

$$\boxed{f(r \geq L, z, p) = f(r, z \geq H, p) = f(r, z \leq -H, p) = 0} \quad . \tag{A.12}$$

These properties are transferred subsequently to the spatial function T. From this later also follow the homogeneous boundary conditions for the solution of the spatial differential equation.

After introducing cylindrical coordinates (in the following we use ∂_x instead of $\frac{\partial}{\partial x}$)

$$\vec{\nabla}^2 = \left(\frac{1}{r} \partial_r r \partial_r + \frac{1}{r^2} \partial_\phi^2 + \partial_z^2 \right) \tag{A.13}$$

we assume additionally no ϕ dependence, that means a cylindrical symmetry of the galaxy:

$$L_{\vec{x}} = L_{z,r} = \kappa_0 \left(\frac{1}{r} \partial_r r \partial_r + \partial_z^2 \right) . \tag{A.14}$$

We can solve the differential equation

$$\frac{\partial T(r, z, u)}{\partial u} = L_{r,z} T(r, z, u) \tag{A.15}$$

with a combination of a separation and a series ansatz:

$$\boxed{T(r, z, u) = \sum_{m=1}^{\infty} \sum_{n=1}^{\infty} c_{mn} t_{mn}(r, z) e^{-\lambda_{mn}^2 u}} \quad . \tag{A.16}$$

From the scattering time method stems the constraint (cf. Eq. (A.8))

$$T(r, z, u = 0) = +Q_1(r, z) , \tag{A.17}$$

which will be used later to fix the coefficients c_{mn}.

Eq. (A.16) inserted in the differential equation gives

$$-\lambda_{mn}^2 T(r, z, u) = L_{r,z} T(r, z, u) \tag{A.18}$$

$$\Leftrightarrow \sum_{m=1}^{\infty} \sum_{n=1}^{\infty} c_{mn} e^{-\lambda_{mn}^2 u} \left[L_{r,z} + \lambda_{mn}^2 \right] t_{mn}(r, z) = 0 . \tag{A.19}$$

Shall the sum be zero for all possible values of r and z, after dividing by κ_0 and with the definition of the eigenvalues $\alpha_{mn}^2 := \frac{\lambda_{mn}^2}{\kappa_0}$ it follows an infinite set of differential equations for the functions $t_{mn}(r, z)$ indexed with m and n:

$$\left[\frac{1}{r}\partial_r r \partial_r + \partial_z^2 + \alpha_{mn}^2\right] t_{mn}(r, z) = 0\,. \tag{A.20}$$

This equation can be separated in terms depending on z and r:

$$\left[\left(\frac{1}{r}\partial_r r \partial_r + \alpha_n^2\right) t_n(r)\right] t_m(z) + \left[\left(\partial_z^2 + \alpha_m^2\right) t_m(z)\right] t_n(r) = 0 \tag{A.21}$$

with the product ansatz

$$t_{mn}(r, z) := t_m(z) t_n(r) \tag{A.22}$$

and

$$\alpha_{mn}^2 := \alpha_m^2 + \alpha_n^2\,, \tag{A.23}$$

and t_n and t_m obey the two independent differential equations

$$\boxed{\left[\partial_r r \partial_r + \alpha_n^2 r\right] t_n(r) = 0} \tag{A.24}$$

as well as

$$\boxed{\left[\partial_z^2 + \alpha_m^2\right] t_m(z) = 0}\,. \tag{A.25}$$

A.2.1 Solution of the Radial Part

The first Eq. (A.24) is an ordinary differential equation of second order with variable coefficients:

$$\left[\partial_r r \partial_r + \alpha_n^2 r\right] t_n(r) = 0 \tag{A.26}$$

$$\Longleftrightarrow \left[r\partial_r^2 + \partial_r + \alpha_n^2 r\right] t_n(r) = 0 \tag{A.27}$$

$$\Longleftrightarrow \left[\partial_r^2 + \frac{1}{r}\partial_r + \alpha_n^2\right] t_n(r) = 0\,. \tag{A.28}$$

In general one gets as a solution of a differential equation of the form

$$w''(z) - \frac{2\nu - 1}{z} w'(z) + \lambda^2 w(z) = 0 \tag{A.29}$$

according to [Abramowitz & Stegun 1984] (9.1.51) the functions $w(z) = z^\nu C_\nu(\lambda z)$ with $C_\nu \in \{J_\nu, Y_\nu, H_\nu^{(1)}, H_\nu^{(2)}\}$, whereas J_ν and Y_ν are Bessel functions of the 1. and 2. kind, respectively, and H_ν are Hankel functions, each of order ν.

For $\nu = 0$ the solution functions read:

$$w(z) = z^0 C_0(\lambda z) \,. \tag{A.30}$$

With the boundary condition $C_0(\alpha_n r)|_{r=L} = 0$ (from Eq. (A.12)) here it follows:

$$t_n(r) = A_n J_0(\alpha_n r) \tag{A.31}$$

with

$$\boxed{\alpha_n = \frac{y_n}{L}} \,, \tag{A.32}$$

wherein y_n are the zeros of the Bessel function J_0.

Determination of the Normalization Constants

The orthonormalization condition is applied to Eq. (A.31) to fix the constants A_n:

$$A_n A_{n'} \int_0^L dr\, r\, J_0(\alpha_n r) J_0(\alpha_{n'} r) \overset{!}{=} \delta_{nn'} \,. \tag{A.33}$$

$\alpha_n = y_n/L$ and the substitution $r' = r/L$ provides an integral from 0 to 1:

$$n = n' : \qquad A_n^2 L^2 \int_0^1 dr' r' J_0^2(y_n r') \overset{!}{=} 1 \,. \tag{A.34}$$

According to [Abramowitz & Stegun 1984] (11.4.5) (with $b = 0$) holds generally

$$\int_0^1 dt\, t\, J_\nu(\alpha_n t) J_\nu(\alpha_{n'} t) = \begin{cases} 0 & ; \ n \neq n', \ \nu > -1 \\ \frac{1}{2}[J_\nu'(\alpha_n)]^2 & ; \ n = n', \ \nu > -1 \end{cases} \,. \tag{A.35}$$

Here we have $\nu = 0$ and, therefore, according to [Abramowitz & Stegun 1984] (9.1.28): $J_0'(z) = -J_1(z)$, thus

$$\frac{1}{2} A_n^2 L^2 J_1^2(y_n) \overset{!}{=} 1 \tag{A.36}$$

$$\boxed{A_n = \frac{\sqrt{2}}{L J_1(y_n)}} \,. \tag{A.37}$$

A.2.2 Solution of the z-part

Eq. (A.25) is a linear ordinary differential equation namely the oscillator equation:

$$\left[\partial_z^2 + \alpha_m^2\right] t_m(z) = 0 \,. \tag{A.38}$$

By the requirement of the z-symmetry follows immediately

$$t_m(z) = A_m \cos(\alpha_m z) \,. \tag{A.39}$$

The eigenvalues are yielded again from the boundary conditions, which here read $t_m(z = H) = t_m(z = -H) = 0$:

$$\boxed{\alpha_m = \frac{(2m - 1)\pi/2}{H}} \,. \tag{A.40}$$

Determination of the Normalization Constants

As for the radial part we claim for the amplitudes:

$$A_m A_{m'} \int_{-H}^{H} dz \, \cos\left(\alpha_m z\right) \cos\left(\alpha_{m'} z\right) \overset{!}{=} \delta_{mm'} \,. \tag{A.41}$$

$$
\begin{aligned}
m = m' : \quad & A_m^2 \int_{-H}^{H} dz \, \cos^2\left(\alpha_m z\right) \\
= \quad & A_m^2 \left[\frac{1}{2}z + \frac{1}{4\alpha_m} \sin\left(\frac{(2m - 1)\pi}{H} z\right)\right]_{-H}^{H} \\
= \quad & A_m^2 H \\
\overset{!}{=} \quad & 1
\end{aligned} \tag{A.42}
$$

In the second step we have used [Bronstein & Semendjajew 1989].

So

$$\boxed{A_m = \frac{1}{\sqrt{H}}} \,. \tag{A.43}$$

A.2.3   The Complete Spatial Solution

With the results of the previous section we obtain for the solutions of the spatial equations

$$t_{mn}(r,z) = \frac{\sqrt{2}}{\sqrt{H}LJ_1(y_n)} \cos\left(\frac{(2m-1)\pi}{2H}z\right) J_0\left(\frac{y_n}{L}r\right) . \qquad (A.44)$$

and the eigenvalues provided by Eqs. (A.32) und (A.40)

$$\lambda_{mn}^2 \;:=\; \kappa_0\,\alpha_{mn}^2 \qquad (A.45)$$

$$=\; \kappa_0\left(\alpha_n^2 + \alpha_m^2\right) \qquad (A.46)$$

$$=\; \kappa_0\left(\frac{y_n^2}{L^2} + \frac{(2m-1)^2\pi^2}{4H^2}\right) . \qquad (A.47)$$

The coefficients in

$$T(r,z,u) = \sum_{m=1}^{\infty}\sum_{n=1}^{\infty} c_{mn}t_{mn}(r,z)e^{-\lambda_{mn}^2 u} \qquad (A.48)$$

can be determined by the side condition (A.8) of the scattering time method:

$$T(r,z,u=0) = Q_1(r,z) \qquad (A.49)$$

$$\sum_{m=1}^{\infty}\sum_{n=1}^{\infty} c_{mn}t_{mn}(r,z) = Q_1(r,z) . \qquad (A.50)$$

Because the t_{mn} form an orthonormal eigenfunction system we obtain the c_{mn} by projection:

$$\sum_{m=1}^{\infty}\sum_{n=1}^{\infty} c_{mn} \underbrace{\langle t_{mn}(r,z)|t_{m'n'}(r,z)\rangle}_{\delta_{mnm'n'}} = \langle Q_1(r,z)|t_{m'n'}(r,z)\rangle . \qquad (A.51)$$

Explicitely that means (after renaming m' and n' to m and n):

$$c_{mn} = \int_0^L dr\, r \int_{-H}^{H} dz\, Q_1(r,z)t_{mn}(r,z) . \qquad (A.52)$$

In the convolution enter the boundary values L and H and the spatial source distribution, which has to be put in an explicit form for a given problem.

A.3   The Momentum Problem

If the differential equation in the momentum space (A.4)

$$\boxed{\frac{\partial F(p, u)}{\partial u} = L_p F(p, u)}$$

(A.53)

is multiplied with T and if the resulting equation is integrated over u

$$\int_0^\infty du\, T(r, z, u) L_p F(p, u) = \int_0^\infty du\, T(r, z, u) \frac{\partial F(p, u)}{\partial u}$$

(A.54)

and if the ansatz (A.16) is inserted, then follows:

$$\sum_{m=1}^\infty \sum_{n=1}^\infty c_{mn} t_{mn}(r, z) \left[L_p \int_0^\infty du\, e^{-\lambda_{mn}^2 u} F(p, u) \right]$$

(A.55)

$$= \sum_{m=1}^\infty \sum_{n=1}^\infty c_{mn} t_{mn}(r, z) \int_0^\infty du\, \frac{\partial F(p, u)}{\partial u} e^{-\lambda_{mn}^2 u}$$

(A.56)

$$\overset{\text{part. int.}}{=} \sum_{m=1}^\infty \sum_{n=1}^\infty c_{mn} t_{mn}(r, z) \left\{ \left[F(p, u) e^{-\lambda_{mn}^2 u} \right]_{u=0}^{u=\infty} + \lambda_{mn}^2 \int_0^\infty du\, F(p, u) e^{-\lambda_{mn}^2 u} \right\}.$$

(A.57)

With the boundary condition (A.7) of the scattering time method we get

$$\left[F(p, u) e^{-\lambda_{mn}^2 u} \right]_0^\infty = -F(p, 0) = -\frac{Q_2(p)}{\kappa(p)}\,;$$

(A.58)

if we introduce in addition the function

$$N_{mn}(p) := \int_0^\infty du\, e^{-\lambda_{mn}^2 u} F(p, u)$$

(A.59)

the equation can be rewritten as

$$\sum_{m=1}^\infty \sum_{n=1}^\infty c_{mn} t_{mn} [L_p N_{mn}(p)] = \sum_{m=1}^\infty \sum_{n=1}^\infty c_{mn} t_{mn} \left[-\frac{Q_2(p)}{\kappa(p)} + \lambda_{mn}^2 N_{mn}(p) \right]$$

(A.60)

$$\Longleftrightarrow \sum_{m=1}^\infty \sum_{n=1}^\infty c_{mn} t_{mn} \left[(L_p - \lambda_{mn}^2) N_{mn}(p) + \frac{Q_2(p)}{\kappa(p)} \right] = 0\,.$$

(A.61)

The resulting differential equations for the N_{mn} are:

$$\left(L_p - \lambda_{mn}^2 \right) N_{mn}(p) = -\frac{Q_2(p)}{\kappa(p)} \; . \tag{A.62}$$

With the new functions N_{mn} the phase space distribution function can be written as:

$$
\begin{aligned}
f(r,z,p) &= \int_0^\infty du\, T(r,z,u)\, F(p,u) \\
&= \int_0^\infty du \left(\sum_{m=1}^\infty \sum_{n=1}^\infty c_{mn} t_{mn}(r,z) e^{-\lambda_{mn}^2 u} \right) F(p,u) \\
&= \sum_{m=1}^\infty \sum_{n=1}^\infty c_{mn} t_{mn}(r,z) \underbrace{\int_0^\infty du\, e^{-\lambda_{mn}^2 u} F(p,u)}_{=N_{mn}(p)}
\end{aligned}
\tag{A.63}
$$

$$f(r,z,p) = \sum_{m=1}^\infty \sum_{n=1}^\infty c_{mn} t_{mn}(r,z) N_{mn}(p) \; . \tag{A.64}$$

A.3.1 Momentum Solution Without Catastrophic Losses

Explicitly the self-adjoint momentum differential equations in the dimensionless momentum variable x read for $\psi = 0$ (see Chapter 4) for the assumed diffusion coefficients:

$$\left[\frac{d}{dx} \left(x^{4-\chi} \frac{d}{dx} \right) - \phi_{mn} x^{2+\chi} \right] f_{mn}(x) = -T_f \alpha^\chi x^2 q(x) \; . \tag{A.65}$$

The following way to the solution is according to [Mause 1993].

Solution for the Homogeneous Equation

Search for a function g_{mn}, which fulfils the homogeneous differential equation

$$\left[\partial_x (x^{4-\chi} \partial_x) - \phi_{mn} x^{\chi+2} \right] g_{mn}(x) = 0 \; . \tag{A.66}$$

(In the following we set $\partial_x := \frac{\partial}{\partial x} = \frac{d}{dx}$).

The complete solution for g_{mn} we get subsequently as a superposition of two linear independent solutions H_1 and H_2:

$$g_{mn}(x) = c_1 H_1(x) + c_2 H_2(x)\,, \tag{A.67}$$

wherein the momentum boundary conditions $H_1(x=0)=0$ and $H_2(x\to\infty)=0$ are fulfilled and from which the Green's function can be constructed directly (see [Arfken 1970]):

$$G_{mn}(x, x_0) = -\frac{1}{D} \begin{cases} H_1(x)H_2(x_0) & ;\ 0 \le x \le x_0 < \infty \\ H_1(x_0)H_2(x) & ;\ 0 < x_0 \le x < \infty \end{cases} \tag{A.68}$$

with

$$D = p_0(x)(H_1 H_2' - H_1' H_2)\Big|_{x=x_0} \quad,\text{ where }\quad p_0(x) = x^{4-\chi}\,. \tag{A.69}$$

At first we perform a transformation of the homogeneous solution with

$$\boxed{g_{mn}(x) = x^k h_{mn}(x)}\,, \tag{A.70}$$

where we introduce a new free parameter k.

$$\begin{aligned}
\partial_x(x^k h_{mn}) &= kx^{k-1}h_{mn} + x^k h_{mn}' \tag{A.71}\\
x^{4-\chi}\partial_x(x^k h_{mn}) &= kx^{3-\chi+k}h_{mn} + x^{4-\chi+k}h_{mn}' \tag{A.72}\\
\partial_x\left[x^{4-\chi}\partial_x(x^k h_{mn})\right] &= k(3-\chi+k)x^{2-\chi+k}h_{mn} + kx^{3-\chi+k}h_{mn}'\\
&\quad + (4-\chi+k)x^{3-\chi+k}h_{mn}' + x^{4-\chi+k}h_{mn}''\\
&= x^{2-\chi+k}[x^2\partial_x^2 + \underbrace{(k+4-\chi+k)}_{2k+4-\chi}x\partial_x\\
&\quad + k(3-\chi+k)]h_{mn} \tag{A.73}
\end{aligned}$$

Thus:

$$x^{2-\chi+k}\left[x^2\partial_x^2 + (2k+4-\chi)x\partial_x + k(3-\chi+k) - \phi_{mn}x^{2\chi}\right]h_{mn}(x) = 0\,. \tag{A.74}$$

Now we apply a second transformation, this time with the variable x, where another free parameter is used:

$$\boxed{x = t^\beta} \tag{A.75}$$

$$\Longrightarrow t = x^{\frac{1}{\beta}}\,. \tag{A.76}$$

The derivatives read:

$$\begin{aligned}
\frac{\partial}{\partial x} &= \frac{\partial t}{\partial x}\frac{\partial}{\partial t} \\
&= \frac{1}{\beta}x^{\frac{1}{\beta}-1}\frac{\partial}{\partial t} \\
&= \frac{1}{\beta}t^{1-\beta}\partial_t
\end{aligned} \tag{A.77}$$

$$\begin{aligned}
\frac{\partial}{\partial x}\frac{\partial}{\partial x} &= \frac{\partial}{\partial x}\left[\frac{1}{\beta}x^{\frac{1}{\beta}-1}\partial_t\right] \\
&= \frac{1}{\beta}\left[(\frac{1}{\beta}-1)x^{\frac{1}{\beta}-2}\partial_t + x^{\frac{1}{\beta}-1}\partial_x\partial_t\right] \\
&= \frac{1}{\beta}\left[\frac{1-\beta}{\beta}t^{1-2\beta}\partial_t + \frac{1}{\beta}t^{2-2\beta}\partial_t^2\right].
\end{aligned} \tag{A.78}$$

For the differential equation we get:

$$t^{\beta(2-\chi+k)}\left[t^{2\beta}\left(\frac{1-\beta}{\beta^2}t^{1-2\beta}\partial_t + \frac{1}{\beta^2}t^{2-2\beta}\partial_t^2\right)\right.$$
$$\left.+(2k+4-\chi)t^\beta\frac{1}{\beta}t^{1-\beta}\partial_t + k(3-\chi+k) - \phi_{mn}t^{2\beta\chi}\right]h_{mn}(x) = 0. \tag{A.79}$$

Cancelling out $t^{\beta(2-\chi+k)}$ and multiplying with β^2 gives:

$$\left[t^2\partial_t^2 + ((1-\beta)t + (2k+4-\chi)\beta t)\,\partial_t + \beta^2 k(3-\chi+k) - \beta^2\phi_{mn}t^{2\beta\chi}\right]h_{mn}(x) = 0. \tag{A.80}$$

Because of $(1-\beta) + \beta(2k+4-\chi) = 1 + \beta(2k+3-\chi)$, it follows:

$$\left[t^2\partial_t^2 + (1+\beta(2k+3-\chi))\,t\partial_t + \beta^2\left(k(3-\chi+k) - \phi_{mn}t^{2\beta\chi}\right)\right]h_{mn}(x) = 0. \tag{A.81}$$

Now β and k are fixed such that

$$2k+3-\chi = 0 \Longleftrightarrow k = \frac{\chi-3}{2} \tag{A.82}$$

and

$$2\beta\chi = 2 \Longleftrightarrow \beta = \frac{1}{\chi}. \tag{A.83}$$

With

$$
\begin{aligned}
\beta^2 k(3 - \chi + k) &= \frac{1}{\chi^2}\frac{\chi - 3}{2}\left(3 - \chi + \frac{\chi - 3}{2}\right) \\
&= \frac{1}{\chi^2}\left(\frac{\chi - 3}{2}\right)\left(\frac{3 - \chi}{2}\right) \\
&= -\left(\frac{\chi - 3}{2\chi}\right)^2
\end{aligned}
\tag{A.84}
$$

we get finally

$$
\left[t^2\partial_t^2 + t\partial_t - \left(\frac{\chi - 3}{2\chi}\right)^2 - \frac{\phi_{mn}}{\chi^2}t^2\right]h_{mn}(x) = 0\,.
\tag{A.85}
$$

Define

$$
\nu := \frac{3 - \chi}{2\chi}
\tag{A.86}
$$

and

$$
y := \frac{\sqrt{\phi_{mn}}}{\chi}t = \frac{\sqrt{\phi_{mn}}}{\chi}x^{\frac{1}{\beta}} = \frac{\sqrt{\phi_{mn}}}{\chi}x^\chi\,.
\tag{A.87}
$$

The differential equation now only contains terms with derivatives of the form $y^n\partial_y^n$, which are form-invariant if scaling with constant factors:

$$
\boxed{\left[y^2\partial_y^2 + y\partial_y - (\nu^2 + y^2)\right]h_{mn}(y) = 0}\,.
\tag{A.88}
$$

The solutions of these differential equations consist of modified Bessel functions of the order ν (see [Abramowitz & Stegun 1984] (9.6.1) and Appendix H):

$$
h_{mn}(y) = c_1 I_\nu(y) + c_2 K_\nu(y)\,.
\tag{A.89}
$$

The back transformations

$$
g_{mn}(x) = x^k h_{mn}(y(x)) \quad \text{mit} \quad k = \frac{\chi - 3}{2} \quad \text{und} \quad y(x) = \frac{\sqrt{\phi_{mn}}}{\chi}x^\chi
\tag{A.90}
$$

result in

$$
g_{mn}(x) = c_1\underbrace{x^{\frac{\chi-3}{2}}I_{\frac{3-\chi}{2\chi}}\left(\frac{\sqrt{\phi_{mn}}}{\chi}x^\chi\right)}_{=:H_1(x)} + c_2\underbrace{x^{\frac{\chi-3}{2}}K_{\frac{3-\chi}{2\chi}}\left(\frac{\sqrt{\phi_{mn}}}{\chi}x^\chi\right)}_{=:H_2(x)}\,.
\tag{A.91}
$$

The Green's Function

From that we gain G_{mn} (cf. Eq. (A.68)):

$$G_{mn}(x, x_0) = -\frac{1}{D} \begin{cases} H_1(x)H_2(x_0) & ; \ 0 \le x \le x_0 < \infty \\ H_1(x_0)H_2(x) & ; \ 0 < x_0 \le x < \infty \end{cases} \tag{A.92}$$

with

$$D = p_0(x)(H_1 H_2' - H_1' H_2)\big|_{x=x_0} \quad , \text{ where } \quad p_0(x) = x^{4-\chi}. \tag{A.93}$$

Calculating the Wronski-determinant (where we introduce $z := \frac{\sqrt{\phi_{mn}}}{\chi} x^\chi$):

$$
\begin{aligned}
D &= x^{4-\chi} \left\{ x^{\frac{-3+\chi}{2}} I_\nu(z) \partial_x \left[x^{\frac{-3+\chi}{2}} K_\nu(z) \right] - \partial_x \left[x^{\frac{-3+\chi}{2}} I_\nu(z) \right] x^{\frac{-3+\chi}{2}} K_\nu(z) \right\}_{x=x_0} \\
&= x^{4-\chi} x^{\frac{-3+\chi}{2}} \left\{ I_\nu(z) \left[\frac{-3+\chi}{2} x^{\frac{-5+\chi}{2}} K_\nu(z) + x^{\frac{-3+\chi}{2}} \sqrt{\phi_{mn}} x^{\chi-1} K_\nu'(z) \right] \right. \\
&\quad \left. - K_\nu(z) \left[\frac{-3+\chi}{2} x^{\frac{-5+\chi}{2}} I_\nu(z) + x^{\frac{-3+\chi}{2}} \sqrt{\phi_{mn}} x^{\chi-1} I_\nu'(z) \right] \right\}_{x=x_0} \\
&= x^{4-\chi} x^{-3+\chi} \sqrt{\phi_{mn}} x^{\chi-1} \left\{ \underbrace{I_\nu(z) K_\nu' - I_\nu'(z) K_\nu(z)}_{\substack{=-W\{K_\nu(z), I_\nu(z)\} = -\frac{1}{z} \\ \text{cf. [Abramowitz \& Stegun 1984] (9.6.15)}}} \right\}_{x=x_0} \\
&= \left. -x^\chi \sqrt{\phi_{mn}} \frac{\chi}{\sqrt{\phi_{mn}}} x^{-\chi} \right|_{x=x_0} \\
&= -\chi .
\end{aligned}
\tag{A.94}
$$

In the end the resulting solution of the Green's function is:

$$G_{mn}(x, x_0) = \frac{1}{\chi} x^{\frac{\chi-3}{2}} x_0^{\frac{\chi-3}{2}} \begin{cases} I_{\frac{3-\chi}{2\chi}}\!\left(\frac{\sqrt{\phi_{mn}}}{\chi} x^\chi\right) K_{\frac{3-\chi}{2\chi}}\!\left(\frac{\sqrt{\phi_{mn}}}{\chi} x_0^\chi\right) & ; \ 0 \le x \le x_0 < \infty \\[2mm] I_{\frac{3-\chi}{2\chi}}\!\left(\frac{\sqrt{\phi_{mn}}}{\chi} x_0^\chi\right) K_{\frac{3-\chi}{2\chi}}\!\left(\frac{\sqrt{\phi_{mn}}}{\chi} x^\chi\right) & ; \ 0 < x_0 \le x < \infty \end{cases} \tag{A.95}$$

The Complete Solution f_{mn}

The phase space distribution function then is composed as

$$f_{mn}(x) = T_f \alpha^\chi \int_0^\infty dx_0 \, x_0^2 \, q(x_0) G_{mn}(x, x_0) \tag{A.96}$$

for a given momentum source function $q(x_0)$.

Appendix B

Inserting the Momentum Solution Into the Differential Equation

In this chapter we insert the momentum solution into the differential equation to prove its correctness.

The momentum differential equation for the Green's function for no catastrophic losses reads (cf. Eq. 4.28):

$$\frac{d}{dx}\left[x^{4-\chi}\frac{dG_{mn}(x,x_0)}{dx}\right] - \left[\phi_{mn}x^{2+\chi}\right]G_{mn}(x,x_0) = -\delta(x-x_0) \quad. \tag{B.1}$$

In the following we set as abbreviations $\phi := \phi_{mn}$ and $G := G_{mn}$.

Restricted to the region $0 \le x \le x_0$ we have obtained the following solution:

$$G(x,x_0) = \frac{1}{\chi}x^{\frac{\chi-3}{2}}x_0^{\frac{\chi-3}{2}}I_{\frac{3-\chi}{2\chi}}\left(\frac{\sqrt{\phi}x^{\chi}}{\chi}\right)K_{\frac{3-\chi}{2\chi}}\left(\frac{\sqrt{\phi}x_0^{\chi}}{\chi}\right) \quad. \tag{B.2}$$

For checking the correctness we insert the term subsequently into the differential equation. The calculations are fully analogous for the region $x_0 \le x < \infty$.

At first we transform the equation to the new variable z by

$$x = \left(\frac{\chi \cdot z}{\sqrt{\phi}}\right)^{\frac{1}{\chi}} \quad, \tag{B.3}$$

which emerges as argument in the Bessel functions.

Herewith G changes to:

$$G(z, x_0) = \frac{1}{\chi} x_0^{\frac{\chi-3}{2}} K_\nu \left(\frac{\sqrt{\phi} x_0^\chi}{\chi} \right) \left(\frac{\chi}{\sqrt{\phi}} \right)^{-\nu} z^{-\nu} I_\nu(z) \tag{B.4}$$

with the abbreviation

$$\nu := \frac{3 - \chi}{2\chi} \ . \tag{B.5}$$

The differential element transforms via

$$\frac{d}{dx} = \frac{dz}{dx} \frac{d}{dz} = \sqrt{\phi} x^{\chi-1} \frac{d}{dz} = \sqrt{\phi} \left(\frac{\chi z}{\sqrt{\phi}} \right)^{\frac{\chi-1}{\chi}} \frac{d}{dz} \ . \tag{B.6}$$

For the first term of the differential equation we obtain:

$$
\begin{aligned}
& \frac{d}{dx} \left[x^{4-\chi} \frac{dG(x, x_0)}{dx} \right] \\
&= \frac{1}{\chi} x_0^{\frac{\chi-3}{2}} K_\nu \left(\frac{\sqrt{\phi} x_0^\chi}{\chi} \right) \sqrt{\phi} \left(\frac{\chi z}{\sqrt{\phi}} \right)^{\frac{\chi-1}{\chi}} \\
& \qquad \frac{d}{dz} \left[\left(\frac{\chi z}{\sqrt{\phi}} \right)^{\frac{4-\chi}{\chi}} \sqrt{\phi} \left(\frac{\chi z}{\sqrt{\phi}} \right)^{\frac{\chi-1}{\chi}} \frac{d}{dz} \left(\left(\frac{\chi}{\sqrt{\phi}} \right)^{-\nu} z^{-\nu} I_\nu(z) \right) \right] \\
&= \frac{1}{\chi} x_0^{\frac{\chi-3}{2}} K_\nu \left(\frac{\sqrt{\phi} x_0^\chi}{\chi} \right) \phi \left(\frac{\chi}{\sqrt{\phi}} \right)^{\frac{3\chi+1}{2\chi}} z^{\frac{\chi-1}{\chi}} \frac{d}{dz} \left[z^{\frac{3}{\chi}} \frac{d}{dz} \left(z^{-\nu} I_\nu(z) \right) \right] \ . \tag{B.7}
\end{aligned}
$$

Now we consider only the z-dependent part.

For its evaluation we need the following two relations (taken from [Abramowitz & Stegun 1984] (9.6.28)) for the derivatives of the modified Bessel functions:

$$\left(\frac{1}{z} \frac{d}{dz} \right)^k [z^\nu I_\nu(z)] = z^{\nu-k} I_{\nu-k}(z) \tag{B.8}$$

$$\left(\frac{1}{z} \frac{d}{dz} \right)^k \left[z^{-\nu} I_\nu(z) \right] = z^{-\nu-k} I_{\nu+k}(z) \ . \tag{B.9}$$

Here each with $k = 1$:

$$z^{\frac{\chi-1}{\chi}} \frac{d}{dz} \left[z^{\frac{3}{\chi}} \frac{d}{dz} \left(z^{-\nu} I_\nu(z) \right) \right]$$

$$
\begin{aligned}
&= z^{\frac{\chi-1}{\chi}} \frac{d}{dz}\left[z^{\frac{3}{\chi}} z^{-\nu} I_{\nu+1}(z)\right] \\
&= z^{\frac{\chi-1}{\chi}} \frac{d}{dz}\left[z^{\nu+1} I_{\nu+1}(z)\right] \\
&= z^{\frac{\chi-1}{\chi}} z^{\nu+1} I_{\nu}(z) \\
&= z^{\frac{3\chi+1}{2\chi}} I_{\nu}(z) .
\end{aligned}
\tag{B.10}
$$

All together we get:

$$
\boxed{\text{1. term} = \phi\frac{1}{\chi} x_0^{\frac{\chi-3}{2}} K_\nu\left(\frac{\sqrt{\phi} x_0^\chi}{\chi}\right)\left(\frac{\chi}{\sqrt{\phi}}\right)^{\frac{3\chi+1}{2\chi}} z^{\frac{3\chi+1}{2\chi}} I_\nu(z)} .
\tag{B.11}
$$

The 2. term in the differential equation results in:

$$
\begin{aligned}
&-\phi x^{2+\chi} G(x, x_0) \\
&= -\phi\frac{1}{\chi} x_0^{\frac{\chi-3}{2}} K_\nu\left(\frac{\sqrt{\phi} x_0^\chi}{\chi}\right)\left(\frac{\chi z}{\sqrt{\phi}}\right)^{\frac{2+\chi}{\chi}}\left(\frac{\chi}{\sqrt{\phi}}\right)^{\frac{\chi-3}{2\chi}} z^{-\nu} I_\nu(z) \\
&= -\phi\frac{1}{\chi} x_0^{\frac{\chi-3}{2}} K_\nu\left(\frac{\sqrt{\phi} x_0^\chi}{\chi}\right)\left(\frac{\chi}{\sqrt{\phi}}\right)^{\frac{3\chi+1}{2\chi}} z^{\frac{3\chi+1}{2\chi}} I_\nu(z) .
\end{aligned}
\tag{B.12}
$$

This second term is identical with the first term except for the sign, and the sum of both yields zero, as it should be.

Appendix C

Transition From the Solution With to That Without Catastrophic Losses

In this chapter the transition of the M-U-solution with catastrophic losses to the I-K-solution without catastrophic losses is performed.

The momentum Green's function with catastrophic losses reads (see section 4.2):

$$G(x, x_0) = \frac{\left(2\sqrt{\phi}\right)^{\frac{3}{\chi}-1}}{\chi^{\frac{3}{\chi}}} \frac{\Gamma\left[\frac{3}{2\chi} + \frac{\psi}{2\chi\sqrt{\phi}}\right]}{\Gamma\left[\frac{3}{\chi}\right]} \exp\left[-\frac{\sqrt{\phi}(x^\chi + x_0^\chi)}{\chi}\right] \times$$

$$\times \begin{cases} M\left(\frac{3}{2\chi} + \frac{\psi}{2\chi\sqrt{\phi}}, \frac{3}{\chi}, \frac{2\sqrt{\phi}x^\chi}{\chi}\right) U\left(\frac{3}{2\chi} + \frac{\psi}{2\chi\sqrt{\phi}}, \frac{3}{\chi}, \frac{2\sqrt{\phi}x_0^\chi}{\chi}\right) & ; \ 0 \leq x \leq x_0 \\ U\left(\frac{3}{2\chi} + \frac{\psi}{2\chi\sqrt{\phi}}, \frac{3}{\chi}, \frac{2\sqrt{\phi}x^\chi}{\chi}\right) M\left(\frac{3}{2\chi} + \frac{\psi}{2\chi\sqrt{\phi}}, \frac{3}{\chi}, \frac{2\sqrt{\phi}x_0^\chi}{\chi}\right) & ; \ x_0 \leq x < \infty \end{cases} . \text{(C.1)}$$

U and M are confluent hypergeometric functions and $\phi := \phi_{mn}$ and $G := G_{mn}$.

The time scale for catastrophic losses T_c enters into

$$\psi \sim \frac{T_f}{T_c} \tag{C.2}$$

and if neglecting these, i.e. $T_c \to \infty$:

$$\boxed{\psi = 0} . \tag{C.3}$$

For this case the Green's function reduces to

$$
\begin{aligned}
G(x, x_0) \;=\; & \frac{\left(2\sqrt{\phi}\right)^{\frac{3}{\chi}-1} \Gamma\left[\frac{3}{2\chi}\right]}{\chi^{\frac{3}{\chi}} \Gamma\left[\frac{3}{\chi}\right]} \exp\left[-\frac{\sqrt{\phi}(x^\chi + x_0^\chi)}{\chi}\right] \\
& \begin{cases}
M\left(\frac{3}{2\chi}, \frac{3}{\chi}, \frac{2\sqrt{\phi}x^\chi}{\chi}\right) U\left(\frac{3}{2\chi}, \frac{3}{\chi}, \frac{2\sqrt{\phi}x_0^\chi}{\chi}\right) & ;\ 0 \leq x \leq x_0 \\
U\left(\frac{3}{2\chi}, \frac{3}{\chi}, \frac{2\sqrt{\phi}x^\chi}{\chi}\right) M\left(\frac{3}{2\chi}, \frac{3}{\chi}, \frac{2\sqrt{\phi}x_0^\chi}{\chi}\right) & ;\ x_0 \leq x < \infty
\end{cases}
\end{aligned}
\quad . \text{(C.4)}
$$

According to [Abramowitz & Stegun 1984] (13.6.3):

$$
M\left(\nu + \frac{1}{2}, 2\nu + 1, 2z\right) = \Gamma(1+\nu)e^z \left(\frac{1}{2}z\right)^{-\nu} I_\nu(z) \tag{C.5}
$$

and [Abramowitz & Stegun 1984] (13.6.21):

$$
U\left(\nu + \frac{1}{2}, 2\nu + 1, 2z\right) = \frac{1}{\sqrt{\pi}}e^z \left(2z\right)^{-\nu} K_\nu(z) \ . \tag{C.6}
$$

we get the modified Bessel functions I and K (cf. Appendix H).
For the functions we deal with here we identify

$$
\nu + \frac{1}{2} = \frac{3}{2\chi} \ \rightarrow\ 2\nu + 1 = \frac{3}{\chi} \ . \tag{C.7}
$$

Thus:

$$
\nu = \frac{1}{2}\left(\frac{3}{\chi} - 1\right) = \frac{3-\chi}{2\chi} \ . \tag{C.8}
$$

In addition:

$$
z = \frac{\sqrt{\phi}x_0^\chi}{\chi} \text{ resp. } \frac{\sqrt{\phi}x^\chi}{\chi} \ . \tag{C.9}
$$

C.1   Calculation for the Region $0 \leq x \leq x_0$

$$
M\left(\frac{3}{2\chi}, \frac{3}{\chi}, \frac{2\sqrt{\phi}x^\chi}{\chi}\right) = \Gamma\left[\frac{1}{2}\left(\frac{3}{\chi}+1\right)\right] e^{\frac{\sqrt{\phi}x^\chi}{\chi}} \left(\frac{1}{2}\frac{\sqrt{\phi}x^\chi}{\chi}\right)^{\frac{\chi-3}{2\chi}} I_{\frac{3-\chi}{2\chi}}\left(\frac{\sqrt{\phi}x^\chi}{\chi}\right) \tag{C.10}
$$

$$
U\left(\frac{3}{2\chi}, \frac{3}{\chi}, \frac{2\sqrt{\phi}x_0^\chi}{\chi}\right) = \frac{1}{\sqrt{\pi}}e^{\frac{\sqrt{\phi}x_0^\chi}{\chi}} \left(2\frac{\sqrt{\phi}x_0^\chi}{\chi}\right)^{\frac{\chi-3}{2\chi}} K_{\frac{3-\chi}{2\chi}}\left(\frac{\sqrt{\phi}x_0^\chi}{\chi}\right) \tag{C.11}
$$

We get:

$$
\begin{aligned}
G(x, x_0) \;=\; & \frac{\left(2\sqrt{\phi}\right)^{\frac{3}{\chi}-1}}{\chi^{\frac{3}{\chi}}} \frac{\Gamma\left[\frac{3}{2\chi}\right]}{\Gamma\left[\frac{3}{\chi}\right]} e^{-\frac{\sqrt{\phi}(x^\chi + x_0^\chi)}{\chi}} e^{\frac{\sqrt{\phi}x^\chi}{\chi}} e^{\frac{\sqrt{\phi}x_0^\chi}{\chi}} \frac{1}{\sqrt{\pi}} \\
& \Gamma\left[\frac{1}{2}\left(\frac{3}{\chi}+1\right)\right] 2^{-\frac{\chi-3}{2\chi}} 2^{\frac{\chi-3}{2\chi}} \left(\frac{\sqrt{\phi}}{\chi}\right)^{1-\frac{3}{\chi}} x^{\frac{\chi-3}{2}} x_0^{\frac{\chi-3}{2}} \\
& I_{\frac{3-\chi}{2\chi}}\left(\frac{\sqrt{\phi}x^\chi}{\chi}\right) K_{\frac{3-\chi}{2\chi}}\left(\frac{\sqrt{\phi}x_0^\chi}{\chi}\right) \\
=\; & \frac{2^{\frac{3}{\chi}-1}}{\chi} \frac{1}{\sqrt{\pi}} \frac{\Gamma\left[\frac{3}{2\chi}\right]}{\Gamma\left[\frac{3}{\chi}\right]} \Gamma\left[\frac{1}{2}\left(\frac{3}{\chi}+1\right)\right] x^{\frac{\chi-3}{2}} x_0^{\frac{\chi-3}{2}} \\
& I_{\frac{3-\chi}{2\chi}}\left(\frac{\sqrt{\phi}x^\chi}{\chi}\right) K_{\frac{3-\chi}{2\chi}}\left(\frac{\sqrt{\phi}x_0^\chi}{\chi}\right) .
\end{aligned}
\tag{C.12}
$$

According to [Abramowitz & Stegun 1984] (6.1.18) the relation

$$
\Gamma(2z) = \frac{1}{\sqrt{2\pi}} 2^{2z-\frac{1}{2}} \Gamma(z) \Gamma\left(z + \frac{1}{2}\right)
\tag{C.13}
$$

holds and therewith

$$
\frac{\Gamma(z)}{\Gamma(2z)} = \frac{\sqrt{2\pi}\, 2^{\frac{1}{2}-2z}}{\Gamma\left(z + \frac{1}{2}\right)}
\tag{C.14}
$$

where for the case in question $z = \frac{3}{2\chi}$, in particular

$$
\frac{\Gamma(\frac{3}{2\chi})}{\Gamma(\frac{3}{\chi})} = \frac{\sqrt{2\pi}\, 2^{\frac{1}{2}-\frac{3}{\chi}}}{\Gamma\left(\frac{1}{2}\left(\frac{3}{\chi}+1\right)\right)} .
\tag{C.15}
$$

Finally we get:

$$
\boxed{\, G(x, x_0) = \frac{1}{\chi} x^{\frac{\chi-3}{2}} x_0^{\frac{\chi-3}{2}} I_{\frac{3-\chi}{2\chi}}\left(\frac{\sqrt{\phi}x^\chi}{\chi}\right) K_{\frac{3-\chi}{2\chi}}\left(\frac{\sqrt{\phi}x_0^\chi}{\chi}\right) \,}
\tag{C.16}
$$

C.2   The Region $x_0 \le x < \infty$

Because of the symmetry of $G(x, x_0)$ in the variables x and x_0 an analogous calculation for the region $x_0 \le x < \infty$ can be performed.

Appendix D

The Special Case $q = 2$ for the Momentum Differential Equation

We calculate the solution for the momentum differential equation for the special case $q = 2$ of the spectral index.

Starting with the differential equation for the momentum Green's function (4.28)

$$\left[\frac{d}{dx} \left(x^{4-\chi} \frac{d}{dx} \right) - (\psi x^2 + \phi_{mn} x^{2+\chi}) \right] G_{mn}(x, x_0) = -\delta(x - x_0) \qquad \text{(D.1)}$$

the corresponding homogeneous equation with $\chi = 0$ is

$$\boxed{\frac{d}{dx} \left[x^4 \frac{dg_{mn}(x)}{dx} \right] - x^2 \left[\psi + \phi_{mn} \right] g_{mn}(x) = 0} \qquad . \qquad \text{(D.2)}$$

Set

$$a := \psi + \phi_{mn} \ . \qquad \text{(D.3)}$$

Performing the derivatives and cancelling x^2 yields:

$$\left[x^2 \frac{d^2}{dx^2} + 4x \frac{d}{dx} - a \right] g_{mn}(x) = 0 \ . \qquad \text{(D.4)}$$

The ansatz

$$g_{mn}(x) = x^\alpha \qquad \text{(D.5)}$$

provides

$$\alpha(\alpha - 1)x^2 x^{\alpha-2} + 4\alpha x x^{\alpha-1} - ax^\alpha = 0 \qquad \text{(D.6)}$$

and we obtain as a condition for α:

$$\alpha(\alpha - 1) + 4\alpha - a = \alpha^2 + 3\alpha - a = 0 \tag{D.7}$$

with the solutions

$$\alpha = -\frac{3}{2} \pm \sqrt{\frac{9}{4} + a} \ . \tag{D.8}$$

The complete solution for the homogeneous differential equation then reads:

$$H(x) = c_1 H_1(x) + c_2 H_2(x) \tag{D.9}$$

wherein c_1 and c_2 are constants and

$$H_{1,2}(x) = x^{-\frac{3}{2} \pm \sqrt{\frac{9}{4}+a}} \ . \tag{D.10}$$

The Green's function for the self-adjoint differential equation is generated by

$$G_{mn}(x, x_0) = -\frac{1}{D} \begin{cases} H_1(x)H_2(x_0) & ; \ 0 \le x \le x_0 < \infty \\ H_1(x_0)H_2(x) & ; \ 0 < x_0 \le x < \infty \end{cases} \tag{D.11}$$

where the Wronski determinant is

$$D = p_0(x)(H_1(x)H_2'(x) - H_1'(x)H_2(x))\big|_{x=x_0} \tag{D.12}$$

with

$$p_0(x) = x^4 \ . \tag{D.13}$$

The calculation of the determinant yields

$$
\begin{aligned}
D &= \left[\left(-\frac{3}{2} - \sqrt{\frac{9}{4} + a} \right) x^{-\frac{3}{2}+\sqrt{\frac{9}{4}+a}} x^{-\frac{5}{2}-\sqrt{\frac{9}{4}+a}} \right. \\
&\quad \left. - \left(-\frac{3}{2} + \sqrt{\frac{9}{4} + a} \right) x^{-\frac{3}{2}-\sqrt{\frac{9}{4}+a}} x^{-\frac{5}{2}+\sqrt{\frac{9}{4}+a}} \right] x^4 \\
&= -2\sqrt{\frac{9}{4} + a} \ .
\end{aligned} \tag{D.14}
$$

Finally, we obtain for the Green's function:

$$G_{mn}(x, x_0) = \frac{1}{2\sqrt{\frac{9}{4}+a}} \begin{cases} x^{-\frac{3}{2}+\sqrt{\frac{9}{4}+a}} x_0^{-\frac{3}{2}-\sqrt{\frac{9}{4}+a}} & ; \ 0 \le x \le x_0 < \infty \\ x^{-\frac{3}{2}-\sqrt{\frac{9}{4}+a}} x_0^{-\frac{3}{2}+\sqrt{\frac{9}{4}+a}} & ; \ 0 < x_0 \le x < \infty \end{cases} \tag{D.15}$$

$$G_{mn}(x, x_0) = \frac{(xx_0)^{-\frac{3}{2}}}{2\sqrt{\frac{9}{4} + \psi + \phi_{mn}}} \begin{cases} (x/x_0)^{\sqrt{\frac{9}{4} + \psi + \phi_{mn}}} & ; \ 0 \leq x \leq x_0 < \infty \\ (x/x_0)^{-\sqrt{\frac{9}{4} + \psi + \phi_{mn}}} & ; \ 0 < x_0 \leq x \leq \infty \end{cases} .$$

(D.16)

132

Appendix E

Power Law Approximations of the Momentum Solution Without Catastrophic Losses

We calculate the approximations of the momentum solution of the phase space distribution function if inserting a power law momentum injection function for different momentum regions in the case of no catastrophic losses, that means $\psi = 0$.

E.1 Momentum Function for a Power Law Source

With the momentum source function

$$\boxed{q(x_0) = q_0 x_0^{-\beta-2}} \tag{E.1}$$

for the region $x_{min} < x_0 < x_{max}$ follows

$$
\begin{aligned}
f_{mn}(x) &= q_0\, T_f\, \alpha^\chi \int_{x_{min}}^{x_{max}} dx_0\, x_0^2 x_0^{-\beta-2} G_{mn}(x, x_0) \\
&= q_0\, T_f\, \alpha^\chi \frac{1}{\chi}\, x^{\frac{\chi-3}{2}} \left\{ K_\nu \left[\left(\frac{x}{x_c}\right)^\chi \right] \int_{x_{min}}^{x} dx_0\, x_0^{-\beta+\frac{\chi-3}{2}} I_\nu \left[\left(\frac{x_0}{x_c}\right)^\chi \right] \right. \\
&\quad \left. + I_\nu \left[\left(\frac{x}{x_c}\right)^\chi \right] \int_{x}^{x_{max}} dx_0\, x_0^{-\beta+\frac{\chi-3}{2}} K_\nu \left[\left(\frac{x_0}{x_c}\right)^\chi \right] \right\}
\end{aligned}
\tag{E.2}
$$

with the critical momentum

$$x_c := \left(\frac{\chi}{\sqrt{\phi_{mn}}}\right)^{\frac{1}{\chi}} \sim \left(\frac{T_{mn}}{T_f}\right)^{\frac{1}{2\chi}} \tag{E.3}$$

and

$$\nu := \frac{3-\chi}{2\chi} . \tag{E.4}$$

After the substitution

$$y = \left(\frac{x_0}{x}\right)^{\chi} \ \rightarrow \ x_0 = xy^{\frac{1}{\chi}} \ \rightarrow \ dx_0 = \frac{1}{\chi}xy^{\frac{1}{\chi}-1}dy \tag{E.5}$$

we get

$$
\begin{aligned}
f_{mn}(x) &= q_0\, T_f\, \alpha^{\chi}\, \frac{1}{\chi^2}\, x^{\frac{\chi-3}{2}} \left[K_\nu(B) \int_{\left(\frac{x_{min}}{x}\right)^{\chi}}^{1} dy\, x\, y^{\frac{1}{\chi}-1} \left(xy^{\frac{1}{\chi}}\right)^{-\beta+\frac{\chi-3}{2}} I_\nu(By) \right. \\
&\quad \left. + I_\nu(B) \int_{1}^{\left(\frac{x_{max}}{x}\right)^{\chi}} dy...K_\nu(By) \right] \\
&= q_0\, T_f\, \alpha^{\chi}\, \frac{1}{\chi^2}\, x^{\chi-\beta-2} \left[K_\nu(B) \int_{\left(\frac{x_{min}}{x}\right)^{\chi}}^{1} dy\, y^{-\frac{\chi+2\beta+1}{2\chi}} I_\nu(By) \right. \\
&\quad \left. + I_\nu(B) \int_{1}^{\left(\frac{x_{max}}{x}\right)^{\chi}} dy\, y^{-\frac{\chi+2\beta+1}{2\chi}} K_\nu(By) \right] \\
&=: q_0\, T_f\, \alpha^{\chi} \frac{1}{\chi^2}\, x^{\chi-\beta-2}(J_1 + J_2)
\end{aligned}
\tag{E.6}
$$

wherein we have defined

$$B := B(x) = \frac{\sqrt{\phi_{mn}}x^{\chi}}{\chi} = \left(\frac{x}{x_c}\right)^{\chi} \tag{E.7}$$

and in a side calculation we used

$$x^{1-\beta+\frac{\chi-3}{2}} x^{\frac{\chi-3}{2}} = x^{\chi-\beta-2} \tag{E.8}$$

and

$$y^{\frac{1}{\chi}-1-\frac{\beta}{\chi}+\frac{\chi-3}{2\chi}} = y^{\frac{2-2\chi-2\beta+\chi-3}{2\chi}} = y^{-\frac{\chi+2\beta+1}{2\chi}} . \tag{E.9}$$

E.2   Approximations for Different Regions

The asymptotic expansions of the modified Bessel function are required (see [Abramowitz & Stegun 1984] (9.6.7), (9.7.1), (9.6.9), (9.7.2)):

$$I_\nu(z) \simeq \begin{cases} \frac{\left(\frac{1}{2}z\right)^\nu}{\Gamma(\nu+1)} & ; \text{ for } |z| \ll 1 \\ \frac{e^z}{\sqrt{2\pi z}} & ; \text{ for } |z| \gg 1 \end{cases} \tag{E.10}$$

$$K_\nu(z) \simeq \begin{cases} \frac{1}{2}\Gamma(\nu)\left(\frac{1}{2}z\right)^{-\nu} & ; \text{ for } |z| \ll 1 \\ \sqrt{\frac{\pi}{2z}}e^{-z} & ; \text{ for } |z| \gg 1 \end{cases} . \tag{E.11}$$

E.2.1   The Case $x_{min} < x < x_{max} \ll x_c$

First, the integral

$$J_1 = K_\nu(B) \int_{\left(\frac{x_{min}}{x}\right)^\chi}^1 dy\, y^{-\frac{\chi+2\beta+1}{2\chi}} I_\nu(By) \tag{E.12}$$

is approximated.

Here we have

$$B \ll 1 \text{ and } By \in \left[\left(\frac{x_{min}}{x_c}\right)^\chi ; B\right] \ll 1 \tag{E.13}$$

and the approximations for I and K provide:

$$\begin{aligned} J_1 &\simeq \frac{1}{2}\Gamma(\nu)\left(\frac{1}{2}B\right)^{-\nu} \int_{\left(\frac{x_{min}}{x}\right)^\chi}^1 dy\, y^{-\frac{\chi+2\beta+1}{2\chi}} \frac{\left(\frac{1}{2}By\right)^\nu}{\Gamma(\nu+1)} \\ &= \frac{1}{2}\frac{\Gamma(\nu)}{\Gamma(\nu+1)} \int_{\left(\frac{x_{min}}{x}\right)^\chi}^1 dy\, y^{-\frac{\chi+2\beta+1-2\chi\nu}{2\chi}} . \end{aligned} \tag{E.14}$$

With a side calculation

$$-\frac{\chi+2\beta+1-2\chi\nu}{2\chi} = -\frac{\chi+2\beta+1-3+\chi}{2\chi} = -\frac{2\chi+2\beta-2}{2\chi} = \frac{1-\chi-\beta}{\chi} \tag{E.15}$$

and

$$\frac{1-\chi-\beta}{\chi} + 1 = \frac{1-\beta}{\chi} \tag{E.16}$$

and $\Gamma(\nu+1) = \nu\Gamma(\nu)$ follows:

$$
\begin{aligned}
J_1 &= \frac{1}{2\nu}\frac{\chi}{1-\beta}\left[y^{\frac{1-\beta}{\chi}}\right]_{\left(\frac{x_{min}}{x}\right)^{\chi}}^{1} \\
&= \frac{\chi^2}{(3-\chi)(1-\beta)}\left[1-\left(\frac{x_{min}}{x}\right)^{1-\beta}\right] .
\end{aligned}
\tag{E.17}
$$

Thus:

$$
\boxed{J_1 \simeq \frac{\chi^2}{(3-\chi)(\beta-1)}\left[\left(\frac{x}{x_{min}}\right)^{\beta-1}-1\right]} .
\tag{E.18}
$$

Here $\beta - 1 > 0$ for the physical values used in this work.

Analogously follows with

$$
By \in \left[B; \left(\frac{x_{max}}{x_c}\right)^{\chi}\right] \ll 1
\tag{E.19}
$$

for the second integral:

$$
\begin{aligned}
J_2 &\simeq \frac{\left(\frac{1}{2}B\right)^{\nu}}{\Gamma(\nu+1)}\int_1^{\left(\frac{x_{max}}{x}\right)^{\chi}} dy\, y^{-\frac{\chi+2\beta+1}{2\chi}}\frac{1}{2}\Gamma(\nu)\left(\frac{1}{2}By\right)^{-\nu} \\
&= \frac{1}{2\nu}\int_1^{\left(\frac{x_{max}}{x}\right)^{\chi}} dy\, y^{-\frac{\chi+2\beta+1+2\nu\chi}{2\chi}} \\
&= \frac{1}{2\nu}\frac{\chi}{\chi-\beta-2}\left[y^{\frac{\chi-\beta-2}{\chi}}\right]_1^{\left(\frac{x_{max}}{x}\right)^{\chi}} \\
&= \frac{\chi^2}{(3-\chi)}\frac{1}{\chi-\beta-2}\left[\left(\frac{x_{max}}{x}\right)^{\chi-\beta-2}-1\right]
\end{aligned}
\tag{E.20}
$$

with the side calculations

$$
-\frac{\chi+2\beta+1+3-\chi}{2\chi} = -\frac{2\beta+4}{2\chi} = -\frac{\beta+2}{\chi}
\tag{E.21}
$$

and

$$
-\frac{\beta+2}{\chi}+1 = \frac{\chi-\beta-2}{\chi} .
\tag{E.22}
$$

Thus:

$$J_2 \simeq \frac{\chi^2}{(3-\chi)(\beta+2-\chi)} \left[1 - \left(\frac{x}{x_{max}} \right)^{2+\beta-\chi} \right] \quad . \tag{E.23}$$

Here $2 + \beta - \chi > 0$ with the physical values used in this work.

With these results we get:

$$
\begin{aligned}
f_{mn}(x) &\simeq q_0 T_f \alpha^\chi x^{\chi-\beta-2} \frac{1}{3-\chi} \left\{ \frac{1}{\beta-1} \left[\left(\frac{x}{x_{min}} \right)^{\beta-1} - 1 \right] \right. \\
&\quad \left. + \frac{1}{\beta+2-\chi} \left[1 - \left(\frac{x}{x_{max}} \right)^{2+\beta-\chi} \right] \right\} \\
&= \frac{q_0 T_f \alpha^\chi}{(3-\chi)(\beta-1)} x^{\chi-\beta-2} \left\{ \left(\frac{x}{x_{min}} \right)^{\beta-1} - 1 + \frac{\beta-1}{\beta+2-\chi} \left[1 - \left(\frac{x}{x_{max}} \right)^{2+\beta-\chi} \right] \right\} \\
&= \frac{q_0 T_f \alpha^\chi}{(3-\chi)(\beta-1)} x^{\chi-\beta-2} \left(\frac{x}{x_{min}} \right)^{\beta-1} \\
&\quad \left\{ 1 - \left(\frac{x_{min}}{x} \right)^{\beta-1} + \frac{\beta-1}{\beta+2-\chi} \left(\frac{x_{min}}{x} \right)^{\beta-1} - \frac{\beta-1}{\beta+2-\chi} \frac{x^{3-\chi} x_{min}^{\beta-1}}{x_{max}^{2+\beta-\chi}} \right\} \\
&= \frac{q_0 T_f \alpha^\chi}{(3-\chi)(\beta-1)} x^{\chi-\beta-2} \left(\frac{x}{x_{min}} \right)^{\beta-1} \\
&\quad \left\{ 1 - \frac{3-\chi}{\beta+2-\chi} \left(\frac{x_{min}}{x} \right)^{\beta-1} - \frac{\beta-1}{\beta+2-\chi} \frac{x^{3-\chi} x_{min}^{\beta-1}}{x_{max}^{2+\beta-\chi}} \right\} \quad . \tag{E.24}
\end{aligned}
$$

(Here we have $\beta-1$, $3-\chi$ and $\beta+2-\chi > 0$ with the physical values used in this work.)

The last two terms can be neglected in comparison to 1 and it remains:

$$f_{mn}(x) \simeq \frac{q_0 T_f \alpha^\chi}{\beta-1} \frac{1}{3-\chi} x_{min}^{1-\beta} x^{\chi-3} \quad . \tag{E.25}$$

The obtained spectrum is independent of index β of the injection spectrum, i.e. the momentum diffusion is the dominating effect.

We compare the result with the approximations involving the M and U functions (cf. Eq. (F.22)):

$$f_{mn}(x) = \frac{q_0 T_f \alpha^\chi}{\beta-1} \frac{\left(2\sqrt{\phi_{mn}} \right)^{\frac{3}{\chi}-1}}{\chi^{\frac{3}{\chi}} \left(\frac{3}{\chi} - 1 \right)} x_{min}^{1-\beta} \left(\frac{x}{x_c} \right)^{\chi-3} \quad . \tag{E.26}$$

With $x_c = \left(\frac{\chi}{2\sqrt{\phi_{mn}}}\right)^{\frac{1}{\chi}}$ follows:

$$
\begin{aligned}
f_{mn}(x) &= \frac{q_0 T_f \alpha^\chi}{\beta - 1} x_{min}^{1-\beta} x^{\chi-3} \frac{\left(2\sqrt{\phi_{mn}}\right)^{\frac{3}{\chi}-1}}{\chi^{\frac{3}{\chi}}\left(\frac{3}{\chi}-1\right)} \left(\frac{\chi}{2\sqrt{\phi_{mn}}}\right)^{\frac{3}{\chi}-1} \\
&= \frac{q_0 T_f \alpha^\chi}{\beta - 1} x_{min}^{1-\beta} x^{\chi-3} \frac{1}{\chi\left(\frac{3}{\chi}-1\right)} \\
&= \frac{q_0 T_f \alpha^\chi}{\beta - 1} \frac{1}{3-\chi} x_{min}^{1-\beta} x^{\chi-3} .
\end{aligned}
\tag{E.27}
$$

E.2.2 The Case $x_{min} < x \ll x_c \ll x_{max}$

The integral J_1 is calculated like in the previous section because here also $B \ll 1$ and $By \ll 1$ in the considered region.

The second integral is split into two parts:

$$
J_2 = \int_1^{\left(\frac{x_c}{x}\right)^\chi} dy... + \int_{\left(\frac{x_c}{x}\right)^\chi}^{\left(\frac{x_{max}}{x}\right)^\chi} dy...
\tag{E.28}
$$

where the approximations for the first term $(=: T_1)$ are executed analogously as for J_2 in the previous section

$$
\boxed{T_1 \simeq \frac{\chi^2}{(3-\chi)(\beta+2-\chi)}\left[1 - \left(\frac{x}{x_c}\right)^{2+\beta-\chi}\right]} .
\tag{E.29}
$$

In the second term $(=: T_2)$ the I function is approximated for small B and the K function for large arguments, because By lies in the interval $\left[1; \left(\frac{x_{max}}{x_c}\right)^\chi\right]$.

$$
\begin{aligned}
T_2 &\simeq \frac{\left(\frac{1}{2}B\right)^\nu}{\Gamma(\nu+1)} \int_{\left(\frac{x_c}{x}\right)^\chi}^{\left(\frac{x_{max}}{x}\right)^\chi} dy\, y^{-\frac{\chi+2\beta+1}{2\chi}} \sqrt{\frac{\pi}{2By}} e^{-By} \\
&= \frac{\sqrt{\pi}}{\Gamma(\nu+1)} \left(\frac{1}{2}\right)^{\nu+\frac{1}{2}} B^{\nu-\frac{1}{2}} \int_{\left(\frac{x_c}{x}\right)^\chi}^{\left(\frac{x_{max}}{x}\right)^\chi} dy\, y^{-\frac{2\chi+2\beta+1}{2\chi}} e^{-By} .
\end{aligned}
\tag{E.30}
$$

The substitution

$$
t = By \iff y = \frac{t}{B}
\tag{E.31}
$$

yields:

$$
\begin{aligned}
T_2 & \simeq \frac{\sqrt{\pi}}{\Gamma(\nu+1)} \left(\frac{1}{2}\right)^{\nu+\frac{1}{2}} B^{\nu-\frac{1}{2}-1+\frac{2\chi+2\beta+1}{2\chi}} \int_1^{\left(\frac{x_{max}}{x_c}\right)^\chi} dt \, t^{-\frac{2\chi+2\beta+1}{2\chi}} e^{-t} \\
& = \frac{\sqrt{\pi}}{\Gamma(\nu+1)} \left(\frac{1}{2}\right)^{\nu+\frac{1}{2}} B^{\frac{3-\chi-\chi-2\chi+2\chi+2\beta+1}{2\chi}} \int_1^{\left(\frac{x_{max}}{x_c}\right)^\chi} dt \, ... \\
& = \frac{\sqrt{\pi}}{\Gamma(\nu+1)} \left(\frac{1}{2}\right)^{\nu+\frac{1}{2}} B^{\frac{\beta-\chi+2}{\chi}} \int_1^{\left(\frac{x_{max}}{x_c}\right)^\chi} dt \, ... \, . \quad \text{(E.32)}
\end{aligned}
$$

The remaining integral is of incomplete Gamma function type
(cf. [Abramowitz & Stegun 1984] (6.5.3) and Appendix G.1):

$$
\Gamma(r, x) = \int_x^\infty dt \, e^{-t} t^{r-1} = \Gamma(r) - \int_0^x dt \, e^{-t} t^{r-1} \, . \quad \text{(E.33)}
$$

For two arbitrary boundaries x_1 and x_2 follows:

$$
\begin{aligned}
\int_{x_1}^{x_2} dt \, e^{-t} t^{r-1} & = \int_0^{x_2} dt \, e^{-t} t^{r-1} - \int_0^{x_1} dt \, e^{-t} t^{r-1} \\
& = \Gamma(r) - \Gamma(r, x_2) - \Gamma(r) + \Gamma(r, x_1) \\
& = \Gamma(r, x_1) - \Gamma(r, x_2) \, . \quad \text{(E.34)}
\end{aligned}
$$

Here

$$
r := 1 + \frac{-2\chi - 2\beta - 1}{2\chi} = -\frac{2\beta + 1}{2\chi} = -\frac{\beta + \frac{1}{2}}{\chi} =: -\delta \, . \quad \text{(E.35)}
$$

Marginal note: this δ corresponds to the δ of the approximation of the M and U functions for $\psi = 0$ (cf. Eq. (F.28)), as it should be.

Therewith:

$$
\boxed{T_2 \simeq \frac{\sqrt{\pi}}{\Gamma(\nu+1)} \left(\frac{1}{2}\right)^{\nu+\frac{1}{2}} B^{\frac{\beta-\chi+2}{\chi}} \left[\Gamma\left(-\delta, \left(\frac{x_{max}}{x_c}\right)^\chi\right) - \Gamma(-\delta, 1) \right]} \, . \quad \text{(E.36)}
$$

For large arguments x the incomplete Gamma function changes to (cf. Section G.1):

$$
\Gamma(r, x) \simeq x^{r-1} e^{-x} \quad \text{(E.37)}
$$

Here $\left(\frac{x_{max}}{x_c}\right)^\chi \gg 1$ and the Gamma function is small.

Because $B \ll 1$, the term T_2 can be neglected in comparison to term T_1. With $x \ll x_c$ it remains like in the first case:

$$f_{mn}(x) \simeq \frac{q_0 T_f \alpha^\chi}{\beta - 1} \frac{1}{3 - \chi} \, x_{min}^{1-\beta} x^{\chi-3} \quad . \tag{E.38}$$

E.2.3 The Case $x_{min} \ll x_c \ll x < x_{max}$

First we consider J_2:

$$J_2 = I_\nu(B) \int_1^{\left(\frac{x_{max}}{x}\right)^\chi} dy \, y^{-\frac{\chi+2\beta+1}{2\chi}} K_\nu(By) \, . \tag{E.39}$$

Here $B \gg 1$ and $By \in \left[B; \left(\frac{x_{max}}{x_c}\right)^\chi\right] \gg 1$, so:

$$
\begin{aligned}
J_2 &\simeq \frac{e^B}{\sqrt{2\pi B}} \int_1^{\left(\frac{x_{max}}{x}\right)^\chi} dy \, y^{-\frac{\chi+2\beta+1}{2\chi}} \sqrt{\frac{\pi}{2By}} e^{-By} \\
&= \frac{1}{2} \frac{e^B}{B} \int_1^{\left(\frac{x_{max}}{x}\right)^\chi} dy \, y^{-\frac{\chi+2\beta+1}{2\chi}-\frac{1}{2}} e^{-By} \\
&= \frac{1}{2B} e^B \int_1^{\left(\frac{x_{max}}{x}\right)^\chi} dy \, y^{-\frac{2\chi+2\beta+1}{2\chi}} e^{-By} \\
&= \frac{1}{2B} j_3
\end{aligned}
\tag{E.40}
$$

with

$$
\begin{aligned}
j_3 &:= e^B \int_1^{\left(\frac{x_{max}}{x}\right)^\chi} dy \, y^{-\frac{2\chi+2\beta+1}{2\chi}} e^{-By} \\
&= e^B \int_0^{\left(\frac{x_{max}}{x}\right)^\chi - 1} dt (t+1)^{-\frac{2\chi+2\beta+1}{2\chi}} e^{-Bt} e^{-B}
\end{aligned}
\tag{E.41}
$$

where we have substituted $t = y - 1$. The upper integration limit remains positive.

The main contributions of the integral j_3 stem from values, for which the arguments of the exponential function $Bt \ll 1$, so for $t \leq \frac{1}{B} \ll 1$. t can be neglected in comparison to 1 and it remains an integral up to the upper limit $\frac{1}{B}$:

$$
\begin{aligned}
j_3 &\simeq \int_0^{\frac{1}{B}} dt \, e^{-Bt} \\
&= -\frac{1}{B} \left[e^{-1} - 1 \right] \\
&\simeq \frac{1}{B} \, .
\end{aligned}
\tag{E.42}
$$

Thus:

$$\boxed{J_2 \simeq \frac{1}{2}\frac{1}{B^2}} . \tag{E.43}$$

J_1 is splitted into two intervals. Here $B \gg 1$ and $By < 1$ for the first integral and $By > 1$ for the second integral:

$$
\begin{aligned}
J_1 &= K_\nu(B) \int_{\left(\frac{x_{min}}{x}\right)^\chi}^1 dy\, y^{-\frac{\chi+2\beta+1}{2\chi}} I_\nu(By) \\
&= K_\nu(B) \left\{ \int_{\left(\frac{x_{min}}{x}\right)^\chi}^{\left(\frac{x_c}{x}\right)^\chi} dy... + \int_{\left(\frac{x_c}{x}\right)^\chi}^1 dy... \right\} \\
&\simeq \sqrt{\frac{\pi}{2B}} e^{-B} \left\{ \int_{\left(\frac{x_{min}}{x}\right)^\chi}^{1/B} dy\, y^{-\frac{\chi+2\beta+1}{2\chi}} \frac{\left(\frac{1}{2}By\right)^\nu}{\Gamma(\nu+1)} + \int_{1/B}^1 dy\, y^{-\frac{\chi+2\beta+1}{2\chi}} \frac{e^{By}}{\sqrt{2\pi By}} \right\} \\
&= \sqrt{\frac{\pi}{2B}} e^{-B} \left\{ \frac{\left(\frac{1}{2}B\right)^\nu}{\Gamma(\nu+1)} \frac{\chi}{1-\beta} \left[y^{\frac{1-\beta}{\chi}} \right]_{\left(\frac{x_{min}}{x}\right)^\chi}^{\left(\frac{x_c}{x}\right)^\chi} + \frac{1}{\sqrt{2\pi B}} \int_{1/B}^1 dy\, y^{-\frac{2\chi+2\beta+1}{2\chi}} e^{By} \right\} \\
&= \sqrt{\frac{\pi}{2B}} e^{-B} \left\{ \frac{\left(\frac{1}{2}B\right)^\nu}{\Gamma(\nu+1)} \frac{\chi}{1-\beta} \left[\left(\frac{x_c}{x}\right)^{1-\beta} - \left(\frac{x_{min}}{x}\right)^{1-\beta} \right] \right. \\
&\quad + \left. \frac{e^B}{\sqrt{2\pi B}} \int_0^{1-1/B} dt\, (1-t)^{-\frac{2\chi+2\beta+1}{2\chi}} e^{-Bt} \right\} \tag{E.44}
\end{aligned}
$$

where in the last step first the integration limits were changed and then $t = 1 - y$ was replaced. With the second integral we proceed as above with j_3.

Then we get:

$$J_1 = \sqrt{\frac{\pi}{2B}} e^{-B} \left\{ \frac{\left(\frac{1}{2}B\right)^\nu}{\Gamma(\nu+1)} \frac{\chi}{\beta-1} \left(\frac{x_{min}}{x}\right)^{1-\beta} \left[1 - \left(\frac{x_{min}}{x_c}\right)^{\beta-1} \right] + \frac{e^B}{\sqrt{2\pi B}} \frac{1}{B} \right\} . \tag{E.45}$$

Because of $e^B \gg 1$ it remains in first order only the last term and it follows:

$$\boxed{J_1 \simeq \frac{1}{2}\frac{1}{B^2} \simeq J_2} . \tag{E.46}$$

Thus:

$$f_{mn}(x) \simeq q_0 T_f \alpha^\chi \frac{1}{\chi^2} x^{\chi - \beta - 2} \frac{1}{B^2} \tag{E.47}$$

and with $B = \frac{\sqrt{\phi_{mn} x^\chi}}{\chi}$:

$$\boxed{f_{mn}(x) \simeq q_0 T_f \alpha^\chi \frac{1}{\phi_{mn}} x^{-\chi - \beta - 2}} \ . \tag{E.48}$$

This spectrum is steepened by χ in comparison to the injection spectrum. In this case the acceleration does not play much a role because typically $\chi < 1$.

Comparison with the results for the calculations with the approximations of the M and U functions (cf. Eq. (F.44)) gives:

$$
\begin{aligned}
f_{mn}(x) \quad &\simeq \quad q_0 T_f \alpha^\chi \frac{4 \left(2\sqrt{\phi_{mn}} \right)^{\frac{3}{\chi} - 1}}{\chi^{\frac{3}{\chi} + 1}} x_c^{\chi + 3} x^{-(\beta + 2 + \chi)} \\
&= \quad q_0 T_f \alpha^\chi \frac{4 \left(2\sqrt{\phi_{mn}} \right)^{\frac{3}{\chi} - 1}}{\chi^{\frac{3}{\chi} + 1}} \frac{\chi^{1 + \frac{3}{\chi}}}{\left(2\sqrt{\phi_{mn}} \right)^{\frac{3}{\chi} + 1}} x^{-(\beta + 2 + \chi)} \\
&= \quad q_0 T_f \alpha^\chi \frac{2^{\frac{3}{\chi} + 1} \left(\sqrt{\phi_{mn}} \right)^{-2}}{2^{\frac{3}{\chi} + 1}} x^{-(\beta + 2 + \chi)} \\
&= \quad q_0 T_f \alpha^\chi \frac{1}{\phi_{mn}} x^{-(\beta + 2 + \chi)} \ . \tag{E.49}
\end{aligned}
$$

E.2.4 The Case $x_c \ll x_{min} < x < x_{max}$

In this case $By \gg 1$ and $B \gg 1$ in both integrals and for J_2 one obtains the same result as in the section above.

For J_1 we get:

$$
\begin{aligned}
J_1 \quad &= \quad K_\nu(B) \int_{\left(\frac{x_{min}}{x} \right)^\chi}^1 dy \, y^{-\frac{\chi + 2\beta + 1}{2\chi}} I_\nu(By) \\
&\simeq \quad \sqrt{\frac{\pi}{2B}} e^{-B} \int_{\left(\frac{x_{min}}{x} \right)^\chi}^1 dy \, y^{-\frac{\chi + 2\beta + 1}{2\chi}} \frac{e^{By}}{\sqrt{2\pi By}} \\
&= \quad \frac{e^{-B}}{2B} \int_{\left(\frac{x_{min}}{x} \right)^\chi}^1 dy \, y^{-\frac{2\chi + 2\beta + 1}{2\chi}} e^{By} \ . \tag{E.50}
\end{aligned}
$$

Now again the integration limits are interchanged and the substitution $y = 1 - t$ is performed.

In the end we get like in the third case:

$$\boxed{J_1 \simeq \frac{1}{2}\frac{1}{B^2} \simeq J_2} \tag{E.51}$$

and

$$\boxed{f_{mn}(x) \simeq q_0 T_f \alpha^\chi \frac{1}{\phi_{mn}} x^{-\chi-\beta-2}} . \tag{E.52}$$

E.2.5 The Case $x_{max} < x$

In this case only one integral of the Green's function remains, which is not a function of x anymore:

$$\boxed{f_{mn}(x) = q_0 T_f \alpha^\chi \frac{1}{\chi} x^{\frac{\chi-3}{2}} K_\nu \left(\frac{x}{x_c}\right)^\chi \int_{x_{min}}^{x_{max}} dx_0\, x_0^{-\beta+\frac{\chi-3}{2}} I_\nu \left(\frac{x_0}{x_c}\right)^\chi} . \tag{E.53}$$

The shape of the curve depending on x is given by $x^{\frac{\chi-3}{2}} K_\nu \left(\frac{x}{x_c}\right)^\chi$.

For the case $x \gg x_c$ the approximation of K for large arguments reads:

$$f_{mn}(x) \sim x^{\frac{\chi-3}{2}} \frac{e^{-\left(\frac{x}{x_c}\right)^\chi}}{\left(\frac{x}{x_c}\right)^{\frac{\chi}{2}}} , \tag{E.54}$$

hence

$$\boxed{f_{mn}(x) \sim x^{-\frac{3}{2}} e^{-\left(\frac{x}{x_c}\right)^\chi}} . \tag{E.55}$$

Appendix F

Power Law Approximations of the Momentum Solution With Catastrophic Losses

Now we calculate the approximations of the momentum solution of the phase space distribution function if inserting a power law momentum injection function for different momentum regions including catastrophic losses.

F.1 Momentum Function for a Power Law Source

With the momentum source function

$$\boxed{q(x_0) = q_0 x_0^{-\beta-2}} \tag{F.1}$$

for the region $x_{min} < x < x_{max}$ follows

$$
\begin{aligned}
f_{mn}(x) &= q_0\, T_f\, \alpha^\chi \int_{x_{min}}^{x_{max}} dx_0\, x_0^2 x_0^{-\beta-2} G_{mn}(x, x_0) \\
&= q_0\, g_0\, T_f\, \alpha^\chi e^{-\frac{B}{2}} \left[U(a, b, B) \int_{x_{min}}^{x} dx_0 e^{-\frac{\sqrt{\phi_{mn}} x_0^\chi}{\chi}} x_0^{-\beta} M\left(a, b, \frac{2\sqrt{\phi_{mn}}}{\chi} x_0^\chi\right) \right. \\
&\quad \left. + M(a, b, B) \int_{x}^{x_{max}} dx_0 e^{-\frac{\sqrt{\phi_{mn}} x_0^\chi}{\chi}} x_0^{-\beta} U\left(a, b, \frac{2\sqrt{\phi_{mn}}}{\chi} x_0^\chi\right) \right] \tag{F.2}
\end{aligned}
$$

with

145

$$g_0 := \frac{(2\sqrt{\phi_{mn}})^{\frac{3}{\chi}-1}}{\chi^{\frac{3}{\chi}}} \frac{\Gamma(a)}{\Gamma(b)} \tag{F.3}$$

$$a := \frac{3}{2\chi} + \frac{\psi}{2\chi\sqrt{\phi_{mn}}} \tag{F.4}$$

$$b := \frac{3}{\chi} \tag{F.5}$$

$$B := B(x) = \frac{2\sqrt{\phi_{mn}}x^\chi}{\chi} = \left(\frac{x}{x_c}\right)^\chi \tag{F.6}$$

$$\boxed{x_c := \left(\frac{\chi}{2\sqrt{\phi_{mn}}}\right)^{\frac{1}{\chi}}} . \tag{F.7}$$

After the substitution

$$y = \left(\frac{x_0}{x}\right)^\chi \ \rightarrow \ x_0 = xy^{\frac{1}{\chi}} \ \rightarrow \ dx_0 = \frac{1}{\chi}xy^{\frac{1}{\chi}-1}dy \tag{F.8}$$

we get

$$
\begin{aligned}
f_{mn}(x) &= q_0\, g_0\, T_f\, \alpha^\chi\, \frac{1}{\chi}e^{-\frac{B}{2}}\Bigg[U(a,b,B)\int_{\left(\frac{x_{min}}{x}\right)^\chi}^1 dy\, xy^{\frac{1}{\chi}-1}x^{-\beta}y^{-\frac{\beta}{\chi}}e^{-\frac{By}{2}}M(a,b,By) \\
&\quad + M(a,b,B)\int_1^{\left(\frac{x_{max}}{x}\right)^\chi} dy...U(a,b,By)\Bigg] \\
&= q_0\, g_0\, T_f\, \alpha^\chi\, \frac{1}{\chi}x^{1-\beta}e^{-\frac{B}{2}}\Bigg[U(a,b,B)\int_{\left(\frac{x_{min}}{x}\right)^\chi}^1 dy\, y^{\frac{1-\beta-\chi}{\chi}}e^{-\frac{By}{2}}M(a,b,By) \\
&\quad + M(a,b,B)\int_1^{\left(\frac{x_{max}}{x}\right)^\chi} dy\, y^{\frac{1-\beta-\chi}{\chi}}e^{-\frac{By}{2}}U(a,b,By)\Bigg] \\
&=: q_0\, g_0\, T_f\, \alpha^\chi\, \frac{1}{\chi}x^{1-\beta}e^{-\frac{B}{2}}(J_1+J_2) .
\end{aligned}
\tag{F.9}
$$

F.2   Approximations for Different Regions

The asymptotic expansions of the confluent hypergeometric functions are required (see [Abramowitz & Stegun 1984] (13.5.1), (13.5.2), (13.5.5), (13.5.6)):

$$M(a,b,z) \simeq \left\{ \begin{array}{ll} 1 & ; \text{ for } |z| \ll 1 \\ \frac{\Gamma(b)}{\Gamma(a)}z^{a-b}e^z & ; \text{ for } |z| \gg 1 \end{array} \right. \tag{F.10}$$

$$U(a,b,z) \simeq \begin{cases} \frac{\Gamma(b-1)}{\Gamma(a)}z^{1-b} & ; \text{ for}|z| \ll 1 \\ z^{-a} & ; \text{ for}|z| \gg 1 \end{cases}.$$ (F.11)

F.2.1   The Case $x_{min} < x < x_{max} \ll x_c$

First the integral

$$J_1 = U(a,b,B) \int_{\left(\frac{x_{min}}{x}\right)^\chi}^1 dy\, y^{\frac{1-\beta-\chi}{\chi}} e^{-\frac{By}{2}} M(a,b,By)$$ (F.12)

is approximated.

Here we have

$$B \ll 1 \text{ and } By \in \left[\left(\frac{x_{min}}{x_c}\right)^\chi; B\right] \ll 1$$ (F.13)

and the approximations for M and U as well as $e^{-\frac{By}{2}} \approx 1$ provide:

$$\begin{aligned} J_1 &\simeq \frac{\Gamma(b-1)}{\Gamma(a)}B^{1-b} \int_{\left(\frac{x_{min}}{x}\right)^\chi}^1 dy\, y^{\frac{1-\beta-\chi}{\chi}} \\ &= \frac{\Gamma(b-1)}{\Gamma(a)}B^{1-b} \left[\frac{\chi}{1-\beta}y^{\frac{1-\beta-\chi}{\chi}+1}\right]_{\left(\frac{x_{min}}{x}\right)^\chi}^1 \\ &= \frac{\Gamma(b-1)}{\Gamma(a)}B^{1-b}\frac{\chi}{1-\beta}\left[1 - \left(\frac{x_{min}}{x}\right)^{1-\beta}\right]. \end{aligned}$$ (F.14)

Thus:

$$\boxed{J_1 = \frac{\chi}{\beta-1}\frac{\Gamma(b-1)}{\Gamma(a)}\left(\frac{x}{x_c}\right)^{\chi-3}\left[\left(\frac{x}{x_{min}}\right)^{\beta-1} - 1\right]}.$$ (F.15)

Here $\beta - 1 > 0$ for the physical values used in this work.

Analogously follows with

$$By \in \left[B; \left(\frac{x_{max}}{x_c}\right)^\chi\right] \ll 1$$ (F.16)

and again $e^{-\frac{By}{2}} \approx 1$ for the second integral:

$$
\begin{aligned}
J_2 &= M(a,b,B) \int_1^{\left(\frac{x_{max}}{x}\right)^\chi} dy\, y^{\frac{1-\beta-\chi}{\chi}} e^{-\frac{By}{2}} U(a,b,By) \\
&\simeq \frac{\Gamma(b-1)}{\Gamma(a)} \int_1^{\left(\frac{x_{max}}{x}\right)^\chi} dy\, y^{\frac{1-\beta-\chi}{\chi}} (By)^{1-b} \\
&= \frac{\Gamma(b-1)}{\Gamma(a)} B^{1-b} \int_1^{\left(\frac{x_{max}}{x}\right)^\chi} dy\, y^{\frac{1-\beta-\chi+\chi-b\chi}{\chi}} \\
&= \frac{\Gamma(b-1)}{\Gamma(a)} B^{1-b} \int_1^{\left(\frac{x_{max}}{x}\right)^\chi} dy\, y^{-\frac{\beta+2}{\chi}} \\
&= \frac{\Gamma(b-1)}{\Gamma(a)} \left(\frac{x}{x_c}\right)^{\chi-3} \left[\frac{\chi}{\chi-\beta-2} y^{\frac{\chi-\beta-2}{\chi}}\right]_1^{\left(\frac{x_{max}}{x}\right)^\chi}
\end{aligned} \tag{F.17}
$$

$$
\boxed{J_2 = \frac{\chi}{\beta+2-\chi} \frac{\Gamma(b-1)}{\Gamma(a)} \left(\frac{x}{x_c}\right)^{\chi-3} \left[1 - \left(\frac{x}{x_{max}}\right)^{\beta+2-\chi}\right]} \ . \tag{F.18}
$$

Here $\beta + 2 - \chi > 0$ for the physical values used in this work.

With these results we get (here also with $e^{-\frac{B}{2}} \approx 1$):

$$
\begin{aligned}
f_{mn}(x) &\simeq \frac{q_0 T_f \alpha^\chi}{\chi} \frac{(2\sqrt{\phi_{mn}})^{\frac{3}{\chi}-1}}{\chi^{\frac{3}{\chi}}} \frac{\Gamma(a)}{\Gamma(b)} x^{1-\beta} \frac{\Gamma(b-1)}{\Gamma(a)} \left(\frac{x}{x_c}\right)^{\chi-3} \frac{\chi}{\beta-1} \\
&\quad \left[\left(\frac{x}{x_{min}}\right)^{\beta-1} - 1 + \frac{\beta-1}{\beta+2-\chi}\left(1 - \left(\frac{x}{x_{max}}\right)^{\beta+2-\chi}\right)\right] \ . \tag{F.19}
\end{aligned}
$$

With

$$
\frac{\Gamma(a)}{\Gamma(b)} \frac{\Gamma(b-1)}{\Gamma(a)} = \frac{1}{b-1} = \frac{1}{\frac{3}{\chi}-1} \tag{F.20}
$$

follows:

$$
\begin{aligned}
f_{mn}(x) &= \frac{q_0 T_f \alpha^\chi}{\beta-1} \frac{(2\sqrt{\phi_{mn}})^{\frac{3}{\chi}-1}}{\chi^{\frac{3}{\chi}}\left(\frac{3}{\chi}-1\right)} \left(\frac{x}{x_c}\right)^{\chi-3} x^{1-\beta} \left(\frac{x}{x_{min}}\right)^{\beta-1} \\
&\quad \left[1 - \left(\frac{x_{min}}{x}\right)^{\beta-1} + \frac{\beta-1}{\beta+2-\chi}\left(\frac{x_{min}}{x}\right)^{\beta-1} - \frac{\beta-1}{\beta+2-\chi} \frac{x^{3-\chi} x_{min}^{\beta-1}}{x_{max}^{\beta+2-\chi}}\right]
\end{aligned}
$$

$$
= \frac{q_0 T_f \alpha^\chi}{\beta - 1} \frac{(2\sqrt{\phi_{mn}})^{\frac{3}{\chi} - 1}}{\chi^{\frac{3}{\chi}} \left(\frac{3}{\chi} - 1 \right)} \left(\frac{x}{x_c} \right)^{\chi - 3} x_{min}^{1 - \beta}
$$

$$
\left[1 - \frac{3 - \chi}{\beta + 2 - \chi} \left(\frac{x_{min}}{x} \right)^{\beta - 1} - \frac{\beta - 1}{\beta + 2 - \chi} \frac{x^{3 - \chi} x_{min}^{\beta - 1}}{x_{max}^{\beta + 2 - \chi}} \right] . \tag{F.21}
$$

(Here we have $\beta - 1$, $3 - \chi$ and $\beta + 2 - \chi > 0$ for the physical parameters used in this work.)

The last two terms can be neglected in comparison to 1 and it remains:

$$
\boxed{ f_{mn}(x) \simeq \frac{q_0 T_f \alpha^\chi}{\beta - 1} \frac{(2\sqrt{\phi_{mn}})^{\frac{3}{\chi} - 1}}{\chi^{\frac{3}{\chi}} \left(\frac{3}{\chi} - 1 \right)} x_{min}^{1 - \beta} \left(\frac{x}{x_c} \right)^{\chi - 3} } . \tag{F.22}
$$

F.2.2 The Case $x_{min} < x \ll x_c \ll x_{max}$

The integral J_1 is calculated like in the previous section because here also $B \ll 1$ and $By \ll 1$ in the considered region.

The second integral is split into two parts:

$$
J_2 = \int_1^{\left(\frac{x_c}{x} \right)^\chi} dy... + \int_{\left(\frac{x_c}{x} \right)^\chi}^{\left(\frac{x_{max}}{x} \right)^\chi} dy... \tag{F.23}
$$

where the approximations for the first term $(=: T_1)$ are executed analogously as for J_2 in the previous section:

$$
T_1 \simeq \frac{\chi}{\beta + 2 - \chi} \frac{\Gamma(b - 1)}{\Gamma(a)} \left(\frac{x}{x_c} \right)^{\chi - 3} \left[1 - \left(\frac{x}{x_c} \right)^{\beta + 2 - \chi} \right] . \tag{F.24}
$$

In the second term $(=: T_2)$ the M function is approximated for small B and the U function for large arguments, because By lies in the interval $\left[1; \left(\frac{x_{max}}{x_c} \right)^\chi \right]$:

$$
T_2 \simeq B^{-a} \int_{\left(\frac{x_c}{x} \right)^\chi}^{\left(\frac{x_{max}}{x} \right)^\chi} dy \, y^{\frac{1 - \beta - \chi - a\chi}{\chi}} e^{-\frac{By}{2}} . \tag{F.25}
$$

The substitution

$$
t = \frac{By}{2} \iff y = \frac{2t}{B} \tag{F.26}
$$

yields:

$$
\begin{aligned}
T_2 &= 2B^{-a-1} \int_{\frac{1}{2}}^{\frac{1}{2}\left(\frac{x_{max}}{x_c}\right)^{\chi}} dt \left(\frac{2t}{B}\right)^{\frac{1-\beta-\chi-a\chi}{\chi}} e^{-t} \\
&= 2^{\frac{\chi+1-\beta-\chi-a\chi}{\chi}} B^{\frac{-a\chi-\chi-1+\beta+\chi+a\chi}{\chi}} \int_{\frac{1}{2}}^{\frac{1}{2}\left(\frac{x_{max}}{x_c}\right)^{\chi}} dt \, t^{\frac{1-\beta-\chi-a\chi}{\chi}} e^{-t} \\
&= 2^{\frac{1-\beta-a\chi}{\chi}} B^{\frac{\beta-1}{\chi}} \int dt... \\
&= 2^{-\delta} \left(\frac{x}{x_c}\right)^{\beta-1} \int dt...
\end{aligned}
\tag{F.27}
$$

with

$$
\delta := \frac{\beta + a\chi - 1}{\chi} = \frac{\beta + \frac{3}{2} + \frac{\psi}{2\sqrt{\phi_{mn}}} - 1}{\chi} = \frac{\beta + \frac{1}{2} + \frac{\psi}{2\sqrt{\phi_{mn}}}}{\chi} .
\tag{F.28}
$$

The remaining integral is of incomplete Gamma function type ([Abramowitz & Stegun 1984] (6.5.3) and Appendix G.1):

$$
\Gamma(r, x) = \int_x^{\infty} dt \, e^{-t} t^{r-1} = \Gamma(r) - \int_0^x dt \, e^{-t} t^{r-1} .
\tag{F.29}
$$

For two arbitrary boundaries x_1 and x_2 follows:

$$
\begin{aligned}
\int_{x_1}^{x_2} dt \, e^{-t} t^{r-1} &= \int_0^{x_2} dt \, e^{-t} t^{r-1} - \int_0^{x_1} dt \, e^{-t} t^{r-1} \\
&= \Gamma(r) - \Gamma(r, x_2) - \Gamma(r) + \Gamma(r, x_1) \\
&= \Gamma(r, x_1) - \Gamma(r, x_2) .
\end{aligned}
\tag{F.30}
$$

Here

$$
r - 1 := \frac{1 - \beta - \chi - a\chi}{\chi} \rightarrow r = -\delta .
\tag{F.31}
$$

Therewith:

$$
\boxed{T_2 = 2^{-\delta} \left(\frac{x}{x_c}\right)^{\beta-1} \left[\Gamma\left(-\delta, \frac{1}{2}\left(\frac{x_{max}}{x_c}\right)^{\chi}\right) - \Gamma\left(-\delta, \frac{1}{2}\right)\right]}
\tag{F.32}
$$

Altogether:

$$J_2 = \frac{\chi}{\beta + 2 - \chi} \frac{\Gamma(b-1)}{\Gamma(a)} \left(\frac{x}{x_c}\right)^{\chi-3} \left\{ 1 - \left(\frac{x}{x_c}\right)^{\beta+2-\chi} \right.$$

$$+ 2^{-\delta} \frac{\Gamma(a)}{\Gamma(b-1)} \frac{\beta + 2 - \chi}{\chi} \left(\frac{x}{x_c}\right)^{\beta+2-\chi}$$

$$\left. \left[\Gamma\left(-\delta, \frac{1}{2}\left(\frac{x_{max}}{x_c}\right)^{\chi}\right) - \Gamma\left(-\delta, \frac{1}{2}\right) \right] \right\} . \tag{F.33}$$

For large arguments x the incomplete Gamma function changes to (cf. Section G.1):

$$\Gamma(r, x) \simeq x^{r-1} e^{-x} . \tag{F.34}$$

Here $\left(\frac{x_{max}}{x_c}\right)^{\chi} \gg 1$ and the Gamma function is small. Because $\left(\frac{x}{x_c}\right) \ll 1$, we can neglect the last three terms in comparison to 1.

It remains like in the first case:

$$\boxed{f_{mn}(x) \simeq \frac{q_0 T_f \alpha^{\chi}}{\beta - 1} \frac{\left(2\sqrt{\phi_{mn}}\right)^{\frac{3}{\chi}-1}}{\chi^{\frac{3}{\chi}}\left(\frac{3}{\chi}-1\right)} x_{min}^{1-\beta} \left(\frac{x}{x_c}\right)^{\chi-3}} . \tag{F.35}$$

F.2.3 The Case $x_{min} \ll x_c \ll x < x_{max}$

First we consider J_2:

$$J_2 = M(a, b, B) \int_1^{\left(\frac{x_{max}}{x}\right)^{\chi}} dy \, y^{\frac{1-\beta-\chi}{\chi}} e^{-\frac{By}{2}} U(a, b, By) . \tag{F.36}$$

Here $B \gg 1$ and $By \in \left[B; \left(\frac{x_{max}}{x_c}\right)^{\chi}\right] \gg 1$, so:

$$J_2 \simeq \frac{\Gamma(b)}{\Gamma(a)} B^{a-b} e^B \int_1^{\left(\frac{x_{max}}{x}\right)^{\chi}} dy \, y^{\frac{1-\beta-\chi}{\chi}} e^{-\frac{By}{2}} (By)^{-a}$$

$$= \frac{\Gamma(b)}{\Gamma(a)} B^{-b} e^{\frac{B}{2}} j_3 \tag{F.37}$$

with

$$j_3 := e^{\frac{B}{2}} \int_1^{\left(\frac{x_{max}}{x}\right)^{\chi}} dy \, y^{\frac{1-\beta-\chi-a\chi}{\chi}} e^{-\frac{By}{2}}$$

$$= e^{\frac{B}{2}} \int_0^{\left(\frac{x_{max}}{x}\right)^{\chi}-1} dt \, (t+1)^{\frac{1-\beta-\chi-a\chi}{\chi}} e^{-\frac{Bt}{2}} e^{-\frac{B}{2}} \tag{F.38}$$

where we have substituted $t = y - 1$. The upper integration limit remains positive.

The main contributions of the integral j_3 stem from values, for which the arguments of the exponential function $\frac{Bt}{2} \ll 1$, so for $t \le \frac{2}{B} \ll 1$. t can be neglected in comparison to 1 and it remains an integral up to the upper limit $\frac{2}{B}$:

$$
\begin{aligned}
j_3 &\simeq \int_0^{\frac{2}{B}} dt \, e^{-\frac{Bt}{2}} \\
&= -\frac{2}{B} \left[e^{-1} - 1 \right] \\
&\simeq \frac{2}{B} .
\end{aligned}
\tag{F.39}
$$

Thus:

$$
\boxed{J_2 = 2 \frac{\Gamma(b)}{\Gamma(a)} B^{-b-1} e^{\frac{B}{2}}} .
\tag{F.40}
$$

J_1 is splitted in two intervals. Here $B \gg 1$ and $By < 1$ for the first integral and $By > 1$ for the second integral:

$$
\begin{aligned}
J_1 &= U(a, b, B) \int_{\left(\frac{x_{min}}{x}\right)^\chi}^1 dy \, y^{\frac{1-\beta-\chi}{\chi}} e^{-\frac{By}{2}} M(a, b, By) \\
&\simeq B^{-a} \left\{ \int_{\left(\frac{x_{min}}{x}\right)^\chi}^{\left(\frac{x_c}{x}\right)^\chi} dy \, y^{\frac{1-\beta-\chi}{\chi}} \right. \\
&\quad \left. + \frac{\Gamma(b)}{\Gamma(a)} B^{a-b} \int_{\left(\frac{x_c}{x}\right)^\chi}^1 dy \, y^{\frac{1-\beta-\chi}{\chi}} e^{-\frac{By}{2}} e^{By} y^{a-b} \right\} \\
&= B^{-a} \left\{ \frac{\chi}{1-\beta} \left[\left(\frac{x_c}{x}\right)^{1-\beta} - \left(\frac{x_{min}}{x}\right)^{1-\beta} \right] \right. \\
&\quad \left. + \frac{\Gamma(b)}{\Gamma(a)} B^{a-b} \int_{\left(\frac{x_c}{x}\right)^\chi}^1 dy \, y^{\frac{1-\beta+(a-b-1)\chi}{\chi}} e^{\frac{By}{2}} \right\} \\
&= B^{-a} \left\{ \frac{\chi}{\beta-1} \left(\frac{x_{min}}{x}\right)^{1-\beta} \left[1 - \left(\frac{x_{min}}{x_c}\right)^{\beta-1} \right] \right. \\
&\quad \left. + \frac{\Gamma(b)}{\Gamma(a)} B^{a-b} e^{\frac{B}{2}} \int_0^{1-\left(\frac{x_c}{x}\right)^\chi} dt \, (1-t)^{\frac{1-\beta+(a-b-1)\chi}{\chi}} e^{-\frac{Bt}{2}} \right\}
\end{aligned}
\tag{F.41}
$$

where in the last step first the integration limits were changed and then $t = 1 - y$ was replaced. With the second integral we proceed as above with j_3.

Then we get:

$$
\begin{aligned}
J_1 \; \simeq \; & B^{-a}\left\{\frac{\chi}{\beta-1}\left(\frac{x_{min}}{x}\right)^{1-\beta}\left[1-\left(\frac{x_{min}}{x_c}\right)^{\beta-1}\right]\right. \\
& \left. + 2\frac{\Gamma(b)}{\Gamma(a)}B^{a-b-1}e^{\frac{B}{2}}\right\} \; .
\end{aligned}
\tag{F.42}
$$

Because of $e^{\frac{B}{2}} \gg 1$ it remains in first order only the last term and it follows:

$$
\boxed{J_1 \simeq 2\frac{\Gamma(b)}{\Gamma(a)}B^{-b-1}e^{\frac{B}{2}} \simeq J_2}\;.
\tag{F.43}
$$

Thus:

$$
\boxed{f_{mn}(x) \simeq \frac{4q_0 T_f \alpha^\chi (2\sqrt{\phi_{mn}})^{\frac{3}{\chi}-1}}{\chi^{\frac{3}{\chi}+1}}x_c^{\chi+3}x^{-(\beta+2+\chi)}}\;.
\tag{F.44}
$$

F.2.4 The Case $x_c \ll x_{min} < x < x_{max}$

In this case $By \gg 1$ and $B \gg 1$ in both integrals and for J_2 one obtains the same result as in the section above.

For J_1 we get:

$$
\begin{aligned}
J_1 \; \simeq \; & B^{-a}\frac{\Gamma(b)}{\Gamma(a)}\int_{\left(\frac{x_{min}}{x}\right)^\chi}^{1} dy\, y^{\frac{1-\beta-\chi}{\chi}}e^{-\frac{By}{2}}(By)^{a-b}e^{By} \\
= \; & \frac{\Gamma(b)}{\Gamma(a)}B^{-b}\int_{\left(\frac{x_{min}}{x}\right)^\chi}^{1} dy\, y^{\frac{1-\beta-\chi+(a-b)\chi}{\chi}}e^{\frac{By}{2}}\;.
\end{aligned}
\tag{F.45}
$$

Now again the integration limits are interchanged and the substitution $y = 1 - t$ is performed.

In the end we get like in the third case:

$$
\boxed{J_1 \simeq 2\frac{\Gamma(b)}{\Gamma(a)}B^{-b-1}e^{\frac{B}{2}} \simeq J_2}
\tag{F.46}
$$

and

$$f_{mn}(x) \simeq \frac{4q_0 T_f \alpha^\chi (2\sqrt{\phi_{mn}})^{\frac{3}{\chi}-1}}{\chi^{\frac{3}{\chi}+1}} x_c^{\chi+3} x^{-(\beta+2+\chi)}$$. (F.47)

F.2.5 The Case $x_{max} < x$

In this case only one integral of the Green's function remains, which is not a function of x anymore:

$$f_{mn}(x) = q_0 T_f g_0 \alpha^\chi e^{-\frac{B}{2}} U(a,b,B) \int_{x_{min}}^{x_{max}} dx_0 \; e^{-\frac{\sqrt{\phi_{mn}}x_0^\chi}{\chi}} x_0^{-\beta} M\left(a,b,\frac{2\sqrt{\phi_{mn}}}{\chi} x_0^\chi\right)$$.
(F.48)

The shape of the curve depending on x is given by $e^{-\frac{B}{2}} U(a,b,B)$.

For the case $x \gg x_c$ the approximation of U for large arguments reads:

$$f_{mn}(x) \sim e^{-\frac{B}{2}} B^{-a} ,$$ (F.49)

hence

$$f_{mn}(x) \sim e^{-\frac{1}{2}\left(\frac{x}{x_c}\right)^\chi} x^{-\frac{3}{2}+\frac{\psi}{2\sqrt{\phi_{mn}}}}$$. (F.50)

Appendix G

The Gamma Function

We recall the Gamma function and some of its properties.

The Gamma function for positive arguments can be defined by Euler's integral (see [Abramowitz & Stegun 1984] (6.1.1)):

$$\Gamma(x) = \int_0^\infty dt \, t^{z-1} e^{-t} \tag{G.1}$$
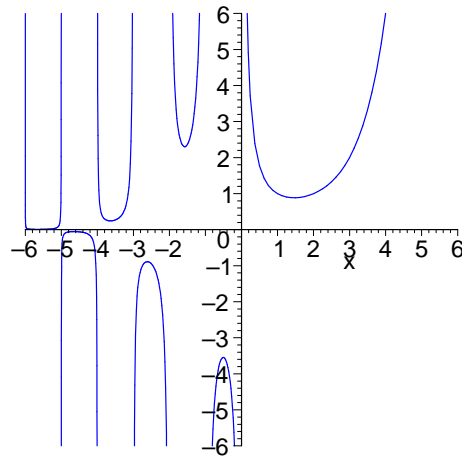
Figure G.1: Plot of the Gamma function.

Omitting the poles of the Gamma function for $x = 0, -1, -2, ...$ (cf. Fig. G.1), Euler's formula is also useful (see [Abramowitz & Stegun 1984] (6.1.2)):

$$\Gamma(x) = \lim_{n \to \infty} \frac{n! \, n^x}{x(x+1)...(x+n)} \tag{G.2}$$

Γ is a continuation of the faculty to real arguments, so for natural numbers the Gamma function is shortly

$$\Gamma(n+1) = n! \tag{G.3}$$

The following recurrence formula often is useful:

$$\Gamma(x+1) = x\Gamma(x) \tag{G.4}$$

and another formula holds:

$$\Gamma(x)\Gamma(1-x) = -x\Gamma(-x)\Gamma(x) = \pi\csc(\pi x) \tag{G.5}$$

An asymptotic expansion for $x \to \infty$ is represented by the famous Stirling's formula:

$$\Gamma(x) \approx e^{-x}x^{x-\frac{1}{2}}\sqrt{2\pi}\left(1 + \frac{1}{12x} + ...\right) \tag{G.6}$$

The Gamma function is connected to Pochhammer's symbol by

$$(x)_n = x(x+1)(x+2)...(x+n-1) = \frac{\Gamma(x+n)}{\Gamma(x)} \tag{G.7}$$

G.1   Incomplete Gamma Functions

The Gamma function is the sum of the two incomplete Gamma functions

$$\Gamma(\alpha) = \gamma(\alpha, x) + \Gamma(\alpha, x) \tag{G.8}$$

with

$$\gamma(\alpha, x) := \int_0^x dt\, t^{\alpha-1}\exp(-t)\,,\ \alpha > 0 \tag{G.9}$$

and

$$\Gamma(\alpha, x) := \int_x^\infty dt\, t^{\alpha-1}\exp(-t) \tag{G.10}$$

For large arguments we get an asymptotic expansion according to
[Abramowitz & Stegun 1984] (6.5.32):

$$\Gamma(\alpha, x) \approx x^{\alpha-1}e^{-x}\left(1 + \frac{\alpha-1}{x} + \frac{(\alpha-1)(\alpha-2)}{x^2} + ...\right) \tag{G.11}$$

Appendix H

The Modified Bessel Functions

We give formulas for the modified Bessel functions and draw some graphs to illustrate their behaviour.

The Bessel functions $I(z)$ and $K(z)$ are independent solutions of a differential equation of the form

$$z^2 \frac{d^2 f(z)}{dz^2} + z \frac{df(z)}{dz} - (z^2 + \nu^2) f(z) = 0 \qquad \text{(H.1)}$$

with z and ν in general being complex variables.

Series representations are (cf. [Abramowitz & Stegun 1984] (9.6.10) and (9.6.11))

$$I_\nu(z) = \left(\frac{1}{2} z \right)^\nu \sum_{k=0}^{\infty} \frac{\left(\frac{1}{4} z^2 \right)^k}{k! \, \Gamma(\nu + k + 1)} \qquad \text{(H.2)}$$

and

$$
\begin{aligned}
K_n(z) \;=\; & \frac{1}{2} \left(\frac{1}{2} z \right)^{-n} \sum_{k=0}^{n-1} \frac{(n-k-1)!}{k!} \left(-\frac{1}{4} z^2 \right)^k + (-1)^{n+1} \ln \left(\frac{1}{2} z \right) I_n(z) \\
& + (-1)^n \frac{1}{2} \left(\frac{1}{2} z \right)^n \sum_{k=0}^{\infty} \left(\psi(k+1) + \psi(n+k+1) \right) \frac{(\frac{1}{4} z^2)^k}{k!(n+k)!}
\end{aligned}
\qquad \text{(H.3)}
$$

only for integer numbers n. Here ψ is the Digamma function

$$\psi(z) := \Gamma'(z) / \Gamma(z) \qquad \text{(H.4)}$$

where we refer to the Gamma function in Appendix G.

Some integral representations can also be found in [Abramowitz & Stegun 1984] (9.6.18, 9.6.23):

$$I_\nu(z) \;=\; \frac{(\frac{1}{2}z)^\nu}{\sqrt{\pi}\,\Gamma(\nu + \frac{1}{2})} \int_0^\pi d\theta\, \exp(\pm z\cos\theta)\sin^{2\nu}\theta \tag{H.5}$$

$$=\; \frac{(\frac{1}{2}z)^\nu}{\sqrt{\pi}\,\Gamma(\nu + \frac{1}{2})} \int_{-1}^1 dt\,(1-t^2)^{\nu-\frac{1}{2}} \exp(\pm zt) \tag{H.6}$$

$$(Re(\nu) > -\frac{1}{2})$$

$$K_\nu(z) \;=\; \frac{\sqrt{\pi}(\frac{1}{2}z)^\nu}{\Gamma(\nu + \frac{1}{2})} \int_0^\infty dt\, \exp(-z\cosh t)\sinh^{2\nu} t \tag{H.7}$$

$$=\; \frac{\sqrt{\pi}(\frac{1}{2}z)^\nu}{\Gamma(\nu + \frac{1}{2})} \int_1^\infty dt\, \exp(-zt)(t^2-1)^{\nu-\frac{1}{2}} \tag{H.8}$$

$$(Re(\nu) > -\frac{1}{2},\, |\arg z| < \frac{1}{2}\pi)$$

The real I-functions approach infinity as $x \to \infty$, and the real K-functions converge to zero for $x \to \infty$ and have poles at $x = 0$.
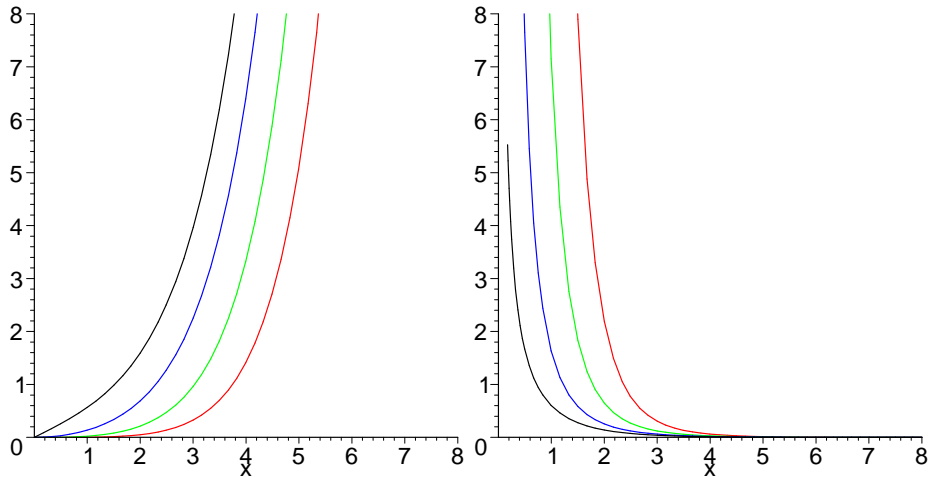
Figure H.1: The modified Bessel function I for different parameters. Black: $I_1(x)$, blue: $I_2(x)$, green: $I_3(x)$, red: $I_4(x)$.

Figure H.2: The modified Bessel function K for different parameters. Black: $K_1(x)$, blue: $K_2(x)$, green: $K_3(x)$, red: $K_4(x)$.

List of Figures

List of Tables

162

Index of Variables and Functions

Symbol	Explanation
a	$= \psi + \phi_{mn}$ (for the case $q = 2$)
a	$= \frac{3}{2\chi} + \frac{\psi}{2\chi\sqrt{\phi_{mn}}}$, parameter of the confluent hypergeometric functions M and U
a, b, c, z_k	parameters of the realistic spatial source function
$(a)_n$	Pochhammer's symbol
A	atomic number
$A_1, A_2 = A_2(p)$	momentum diffusion coefficients
A_n, A_m	normalization factors for $t_n(r)$ and $t_m(z)$, respectively
α	$= A/Z$
α	$= -\frac{3}{2} \pm \sqrt{\frac{9}{4} + a}$ (for the case $q = 2$)
α_{mn}^2	$= \alpha_m^2 + \alpha_n^2 = \frac{\lambda_{mn}^2}{\kappa_0}$
b	$= \frac{3}{\chi}$, parameter of the confluent hypergeometric functions M and U
$B(x)$	$= \left(\frac{x}{x_c}\right)^{\chi}$
$\vec{B}(t, \vec{x})$	magnetic field
$\delta\vec{B}(t, \vec{x}), \delta B$	magnetic turbulence
B_0	background magnetic field
β	spectral index of the momentum power law source spectrum
β	free parameter for determination of the momentum solution without catastrophic losses, $\beta = \frac{1}{\chi}$
c	velocity of light
c_{mn}	coefficients of the eigenfunction sum for f
χ	$\chi = 2 - q$
D	determinant
D	diffusion coefficient in wave number space

163

$D_{x_\sigma x_\nu}$	25 Fokker-Planck coefficients
$D(\tilde{p})$	$= A_2(p)/A^2$
D_1	$D(\tilde{p}) = D_1 \alpha^{q-2} \tilde{p}^q$
δ	$= -r$ (r: substitution variable)
$\delta_{mn}, \delta(x - x_0)$	discrete and continuous Delta function
e	electron charge number
E	energy
E_{max}	maximum energy of the particles in a supernova shockfront
$\vec{E}(t, \vec{x})$	electric field
$\delta\vec{E}(t, \vec{x})$	electric turbulence
ϵ	charge sign
$\eta(q)$	parameter in the spatial and momentum diffusion coefficients
$\tilde{f}$	phase space density
$f_j(t, \vec{x}, \vec{v})$	phase space distribution function for a particle j
$f_a(t, \vec{x}, \vec{v})$	phase space distribution function for particles of species a
$f_a(t, \vec{x}, \vec{p})$	relativistic phase space distribution function for a particle of species a
$f(t, \vec{x}, p)$	isotropic phase space distribution function
$f_{mn}(x)$	$= (m_p c)^3 F_{mn}(\tilde{p})$
$\delta f_a(t, \vec{x}, \vec{p})$	$f_a(t, \vec{x}, \vec{p}) - F_a(t, \vec{x}, \vec{p})$
$\vec{F}$	flux in wave number space
$F(p, u)$	momentum function separated by the scattering time method
$F_a(t, \vec{x}, \vec{p})$	$< f_a(t, \vec{x}, \vec{p}) >$
$\vec{F}$	force
$F_{mn}(\tilde{p})$	$= A^3 N_{mn}(p)$
g_σ	generalized force term
$g_{mn}(x)$	momentum solution with $q(x) = 0$
$G_{mn}(x, x_0)$	Green's function
γ	Lorentz factor
γ	spectral index
$\gamma(\alpha, x)$	$= \int_0^x dt\, t^{\alpha-1} \exp(-t)$, incomplete Gamma function
$Gamma_i$	damping or growing rate of the waves
$\Gamma(x)$	Gamma function
$\Gamma(\alpha, x)$	$= \int_x^\infty dt\, t^{\alpha-1} \exp(-t)$, incomplete Gamma function

$h_{mn}(x)$	$g_{mn}(x) = x^k h_{mn}(x)$; $h_{mn}(y) = c_1 I_\nu(y) + c_2 K_\nu(y)$
H	half-height of the galactic halo
$H(x), H_1(x), H_2(x)$	solutions of the homogeneous momentum differential equation
$H_\nu^{(1)}(x), H_\nu^{(2)}(x)$	Hankel functions
$I_\nu(x)$	modified Bessel function of order ν
j_3	integral: $J_2 \simeq J_2(j_3)$
$\vec{j}(t, \vec{x})$	current of particles
$\vec{J}(t, \vec{x})$	current density
J_1, J_2	integrals for the power law approximations of the momentum solution
$J_\nu(x)$	Bessel function of first kind
k	free parameter for determination of the momentum solution without catastrophic losses, $k = \frac{\chi - 3}{2}$
k_{min}	minimum wave number of turbulence
$K_\nu(x)$	modified Bessel function of order ν
K_1	$\kappa_0 \kappa(\tilde{p}) = K_1 (\alpha \tilde{p})^{2-q}$
$\kappa_{zz} = \kappa_0 \kappa(p), \kappa_{XX}, \kappa_{XY}, \kappa_{YY}, \kappa_{YX}$	spatial diffusion coefficients
L	radius of the galaxy halo
$L_{c.r.}$	luminosity of hadronic cosmic rays
$L_{c.r.,\odot}$	cosmic ray luminosity of the sun
$L_{\vec{x}}$	spatial operator
L_p	momentum operator
λ	path length of cosmic rays
λ_{mn}	eigenvalue of the eigenfunction sum for f
m	summation index
m_{max}	maximum summation index
m, m_0, m_p, m_e	mass, rest mass, proton mass, electron mass
M_g	galactic gas mass
M_G	mass of the galaxy
$M_\odot$	solar mass
$M(a, b, x)$	confluent hypergeometric function
$M_{\mu,\nu}(x)$	Whittaker function
μ	pitch angle
n	summation index
n_{max}	maximum summation index
n	particle density
n_e	electron density
$n(t, \vec{x})$	particle density

$N_{mn}(p)$	momentum functions of the eigenfunction sum for f
ν	$= \frac{3-\chi}{2\chi}$
Ω	gyrofrequency
ω_{mn}^2	$= \kappa_0 \alpha_{mn}^2$
$\dot{p}(p, \vec{x})$	momentum loss rate
$\vec{p}, p = |\vec{p}|$	momentum
p_{IM}, p_{TOA}	momentum of the galactic cosmic rays in the interstellar medium resp. at the top of the atmosphere
P_{esc}	escape probability
$P_\mu^{-\nu}(x)$	associated Legendre functions of the first kind
ϕ	azimuth angle of momentum
ϕ_{mn} or only ϕ	$= \frac{T_f}{T_{lm}} \alpha^{2(2-q)}$
ϕ_{SM}	solar modulation parameter
Φ_{IM}, Φ_{TOA}	flux of the galactic cosmic rays in the interstellar medium and at the top of the atmosphere, respectively
ψ	$= \frac{T_f}{T_c} \alpha^{2-q}$
q	electric charge
q	power law index of the wave number distribution of the turbulence spectrum
$q(x)$	$= (m_p c)^3 Q(\tilde{p})$; momentum source function
q_0	normalization factor for $q(x)$
$Q_1(\vec{x}), Q_2(p)$	source functions, separated in space and momentum: $S(\vec{x}, p) = Q_1(\vec{x}) Q_2(p)$
$Q_{1,0}$	normalization factor of the spatial source distribution
$Q(\tilde{p})$	$= A^3 Q_2(p)$
r	radial spatial coordinate
r	substitution variable $r = -\frac{\beta + \frac{1}{2}}{\chi}$ for the power law approximations of the momentum solution
r_0	radius of the spatial source distribution
r_g	gyroradius
r_s	radius of the position of the solar system in the realistic spatial source function
R	rigidity

$\vec{R}$	spatial vector of the guiding center of gyro-rotating particle with coordinates X, Y, Z
ρ	gas density
$\rho(t, \vec{x})$	charge density
$S(t, \vec{x}, \vec{p}), S_a(t, \vec{x}, \vec{p})$	source function (of species a)
$S_i(k)$	injection or sink term in wave number space
σ	dispersion parameter of the dispersive momentum source function
t	time
$t = t(x)$	momentum transformation variable: $t = x^{\frac{1}{\beta}}$
$t_{c.r.}$	lifetime of hadronic cosmic rays
t_e	lifetime of cosmic ray electrons
$t_{mn}(\vec{x}) = t_m(z)t_n(r)$	spatial functions of the eigenfunction sum for f
$T(\vec{x}, u)$	spatial function separated by the scattering time method
T_1, T_2	$J_2 = T_1 + T_2$
T_{esc}	escape time of the galactic cosmic rays from the galaxy
T_c	catastrophic loss time
T_f	momentum diffusion time scale
T_{mn}	spatial diffusion time scale
$\tau_s(k)$	spectral energy transfer time scale
θ	spherical angle of momentum
$U(a, b, x)$	confluent hypergeometric function
U_B	energy density of the magnetic field
$\vec{v}$	velocity vector
V	cosmic ray bulk speed
v_a	Alfvén velocity
$w_{c.r.}$	energy density of hadronic cosmic rays
w_e	energy density of cosmic ray electrons
$W_{c.r.}$	total energy of hadronic cosmic rays
W_e	total energy of cosmic ray electrons
$W_i(\vec{k})$	spectral density of wave mode i
$W_i(k)$	isotropic spectral density of wave mode i
$W_{\mu,\nu}(x)$	Whittaker function
x	dimensionless momentum variable $x = \tilde{p}/(m_p c)$
x_{min}, x_{max}	minimum and maximum momentum variable

x_c	characteristic momentum: $x_c = \left(\dfrac{\chi}{\sqrt{\phi_{mn}}}\right)^{\frac{1}{\chi}}$ for $\psi = 0$ and $x_c = \left(\dfrac{\chi}{2\sqrt{\phi_{mn}}}\right)^{\frac{1}{\chi}}$ for $\psi \neq 0$
x_σ	coordinates (p, μ, ϕ, X, Y, Z)
$\vec{x}$	space vector with coordinates x, y, z
ξ	fraction of energy
$y = y(x)$	$= \frac{\phi_{mn}}{\chi} x^\chi$
y_n	zeros of Bessel function J_0
$Y_\nu(x)$	Bessel function of second kind
z	z spatial coordinate
$z = z(x)$	$= \frac{\phi_{mn}}{\chi} x^\chi$
z_0	z-coordinate of the spatial source distribution
Z	charge number

Bibliography

[Abramowitz & Stegun 1984] **Abramowitz, M., Stegun, I. A.**, 1984,
Pocketbook of Mathematical Functions,
Verlag Harri Deutsch, Frankfurt/Main

[Aharonian et al. 1999a] **Aharonian, F. A., et al.**, 1999,
*The Time Averaged TeV Energy Spectrum of Mkn 501 of the Extraordinary
1997 Outburst as Measured With the Stereoscopic Cherenkov Telescope System
of HEGRA*,
Astron. & Astrophys., **349**, 11

[Aharonian et al. 1999b] **Aharonian, F. A., et al.**, 1999,
*The Temporal Characteristics of the TeV γ-emission From Mkn 501 in 1997.
II. Results From HEGRA CT1 and CT2*,
Astron. & Astrophys., **349**, 29

[Aharonian et al. 2005] **Aharonian, F. A., et al.**, 2005,
*A New Population of Very High Energy Gamma-Ray Sources in the Milky
Way*,
Science, **307**, 1938

[Allen et al. 1997] **Allen, G. E., et al.**, 1997,
*Evidence of X-Ray Synchrotron Emission From Electrons Accelerated to
40 TeV in the Supernova Remnant Cassiopeia A*,
Astrophys. J., **487**, L97

[Alves 2000] **Alves, D. R.**, 2000,
K-Band Calibration of the Red Clump Luminosity,
Astrophys. J., **539**, 732

[Amenomori et al. 2000] **Amenomori, M., et al.**, 2000,
*Primary Proton Spectrum Between 200 TeV and 1000 TeV Observed With the
Tibet Burst Detector and Air Shower Array*,
Phys. Rev. D, **62**, 112002

[Arbeiter 1999] **Arbeiter, C.**, 1999,
Nichtthermische Strahlungsprozesse in den Jets Aktiver Galaktischer Kerne,
Diploma Thesis, Ruhr-Universität Bochum

[Arfken 1970] **Arfken, G.**, 1970,
Mathematical Methods for Physicists,
Academic Press, New York

[Armstrong et al. 1995] **Armstrong, J. W., Rickett, B. J., Spangler, S. R.**,
1995,
Electron Density Power Spectrum in the Local Interstellar Medium,
Astrophys. J., **443**, 209

[Asakimori et al. 1998] **Asakimori, K., et al.**, 1998,
Cosmic-Ray Proton and Helium Spectra: Results From the JACEE Experiment,
Astrophys. J., **502**, 278

[Baring et al. 1999] **Baring, M. G., et al.**, 1999,
Radio to Gamma-Ray Emission From Shell-Type Supernova Remnants: Predictions From Nonlinear Shock Acceleration Models,
Astrophys. J., **513**, 311

[Berezhko 2001] **Berezhko, E. G.**, 2001,
Particle Acceleration in Supernova Remnants,
Proceedings 27th Int. Cosmic Ray Conf., **Invited, Rapporteur and Highlight Papers**, 226

[Berezhko et al. 2002] **Berezhko, E. G., Ksenofontov, L. T., Völk, H. J.**, 2002,
Emission of SN 1006 Produced by Accelerated Cosmic Rays,
Astron. & Astrophys., **395**, 943

[Berezinskii et al. 1990] **Berezinskii, V. S., et al.**, 1990,
Astrophysics of Cosmic Rays,
North-Holland, Amsterdam

[Berger 1992] **Berger, C.**, 1992,
Teilchenphysik,
Springer, Berlin

[Boezio et al. 1999] **Boezio, M., et al.**, 1999,
The Cosmic-Ray Proton and Helium Spectra Between 0.4 and 200 GV,
Astrophys. J., **518**, 457

[Bojahr 2002] **Bojahr, H.**, 2002,
Suche nach TeV-Blazaren mit dem HEGRA-System der abbildenden Cherenkov-Teleskope,
PhD Thesis, Universität Wuppertal

[Bronstein & Semendjajew 1989] **Bronstein, I. N., Semendjajew, K. A.**, 1989,
Taschenbuch der Mathematik,
Verlag Harri Deutsch, Frankfurt/Main

[Büsching et al. 2001] **Büsching, I., Pohl, M., Schlickeiser, R.**, 2001,
Excess GeV Radiation and Cosmic Ray Origin,
Astron. & Astrophys., **377**, 1056

[Büsching 2004] **Büsching, I.**, 2004,
On the Time-Dependent Propagation of Cosmic Rays,
PhD Thesis, Ruhr-Universität Bochum

[Büsching et al. 2005] **Büsching, I., et al.**, 2005,
Cosmic-Ray Propagation Properties for an Origin in Supernova Remnants,
Astrophys. J., **619**, 314

[Carroll & Ostlie 1996] **Carroll, B. W., Ostlie, D. A.**, 1996,
An Introduction to Modern Astrophysics,
Addison-Wesley Publishing Company, Boston

[Case & Bhattacharya 1996] **Case, G., Bhattacharya, D.**, 1996,
Revisiting the Galactic Supernova Remnant Distribution,
Astron. & Astrophys. Suppl. Ser., **120**, 437

[Case & Bhattacharya 1998] **Case, G., Bhattacharya, D.**, 1998,
A new Σ-D Relation and its Application to the Galactic Supernova Remnant Distribution,
Astrophys. J., **504**, 781

[Chen 1984] **Chen, F. F.**, 1984,
Introduction to Plasma Physics and Controlled Fusion; Volume 1: Plasma Physics,
Plenum Press, New York

[Drury et al. 1994] **Drury, L. O'C., Aharonian, F. A., Völk, H. J.**, 1994,
The Gamma-Ray Visibility of Supernova Remnants. A Test of Cosmic Ray Origin,
Astron. & Astrophys., **287**, 959

172

[Drury et al. 2001] **Drury, L. O'C., et al.**, 2001,
   Test of Galactic Cosmic Ray Source Models,
   Space Sci. Rev., **99**, 329

[Duric et al. 1995] **Duric, N., et al.**, 1995,
   The Relativistic ISM in M33: Role of the Supernova Remnants,
   Astrophys. J., **445**, 173

[Federmann 2003] **Federmann, G.**, 2003,
   Viktor Hess und die Entdeckung der Kosmischen Strahlung,
   Diploma Thesis, Institut für Radiumforschung und Kernphysik, Wien

[Fichtner 2000] **Fichtner, H.**, 2000,
   Anomalous Cosmic Rays: Messengers From the Outer Heliosphere,
   Habilitationsschrift, Universität Bonn

[Fließbach 1995] **Fließbach, T.**, 1995,
   Lehrbuch zur Theoretischen Physik IV: Statistische Physik,
   Spektrum Akademischer Verlag, Heidelberg

[Gaisser 1990] **Gaisser, T. K.**, 1990,
   Cosmic Rays and Particle Physics,
   Cambridge University Press, Cambridge

[Glassmeier & Scholer 1991] **Glassmeier, K.-H., Scholer, M.**, 1991,
   Plasmaphysik im Sonnensystem,
   BI-Wissenschaftsverlag, Mannheim

[Gleeson & Axford 1968] **Gleeson, L. J., Axford, W. I.**, 1968,
   Solar Modulation of Galactic Cosmic Rays ,
   Astrophys. J., **154**, 1011

[Gradshteyn & Ryzhik 1994] **Gradshteyn, I. S., Ryzhik, I. M.**, 1994,
   Table of Integrals, Series and Products,
   Academic Press, San Diego

[Green 2000] **Green, D. A.**, 2000,
   Galactic Supernova Remnants: An Overview of Their Radio Properties,
   Int. Symp. on High Energy Gamma-Ray Astrononmy, Heidelberg, AIP Conference Proceedings, **558**, 59

[Griffiths 1996] **Griffiths, D.**, 1996,
   Einführung in die Elementarteilchenphysik,
   Akademie Verlag, Berlin

[Grupen 1993] **Grupen, C.**, 1993,
Teilchendetektoren,
BI-Wissenschaftsverlag, Mannheim

[Harwit 1988] **Harwit, M.**, 1988,
Astrophysical Concepts,
Springer, New York

[Heinbach & Simon 1995] **Heinbach, U., Simon, M.**, 1995,
Propagation of Galactic Cosmic Rays Under Diffusive Reacceleration,
Astrophys. J., **441**, 209

[Hess 1912] **Hess, V. F.**, 1912,
Über Beobachtungen der durchdringenden Strahlung bei sieben Freiballon-fahrten,
Physikalische Zeitschrift, **13**, 1084

[Jones et al. 2001] **Jones, F. C., et al.**, 2001,
The Modified Weighted Slab Technique: Models and Results,
Astrophys. J., **547**, 264

[Kallenrode 1998] **Kallenrode, M.-B.**, 1998,
Space Physics,
Springer, Berlin

[Kampert 2001] **Kampert, K.-H.**, 2001,
Methods of Determination of the Energy and Mass of Primary Cosmic Ray Particles at Extensive Air Shower Energies,
J. Phys. G, Nucl. Part. Phys., **27**, 1663

[Kirk & Dendy 2001] **Kirk, J. G., Dendy, R. O.**, 2001,
Shock Acceleration of Cosmic Rays - a Critical Review,
J. Phys. G, Nucl. Part. Phys., **27**, 1589

[Klapdor & Grotz 1989] **Klapdor, H. V., Grotz, K.**, 1989,
Die schwache Wechselwirkung in Kern-, Teilchen- und Astrophysik,
Teubner Studienbücher, Stuttgart

[Klapdor-Kleingrothaus & Zuber 1997] **Klapdor-Kleingrothaus, H. V., Zuber, K.**, 1997,
Teilchenastrophysik,
Teubner Studienbücher, Stuttgart

174

[Lemoine & Sigl 2001] **Lemoine, M., Sigl., G.**, 2001,
Physics and Astrophysics of Ultra-High-Energy Cosmic Rays,
Springer, Berlin

[Lerche & Schlickeiser 1985] **Lerche, I., Schlickeiser, R.**, 1985,
An Explanation of the Secondary-to-Primary Ratio in Galactic Cosmic Radiation. No Contradiction With Continuous Fermi Acceleration,
Astron. & Astrophys., **151**, 408

[Lerche & Schlickeiser 1988] **Lerche, I., Schlickeiser, R.**, 1988,
On the Energy Spectrum of Galactic Primary Cosmic Rays: Results From the Transport Equation,
Astrophys. & Space Sci., **145**, 319

[Lerche & Schlickeiser 2001] **Lerche, I., Schlickeiser, R.**, 2001,
Cosmic Ray Transport in Anisotropic Magnetohydrodynamic Turbulence. I. Fast Magnetosonic Waves,
Astron. & Astrophys., **378**, 279

[Li et al. 1991] **Li, Z., et al.**, 1991,
A Statistical Study of the Correlation of Galactic Supernova Remnants and Spiral Arms,
Astrophys. J., **378**, 93

[Lockwood & Webber 1997] **Lockwood, J. A., Webber, W. R.**, 1997,
A Comparison of Cosmic Ray Intensities Near the Earth at the Sunspot Minima in 1976 and 1987 and During 1995 and 1996,
J. Geophys. Res., **102**, 24221

[Longair 1992] **Longair, M. S.**, 1992,
High Energy Astrophysics, Volume 1: Particles, Photons and Their Detection,
Cambridge University Press, Cambridge

[Longair 1994] **Longair, M. S.**, 1994,
High Energy Astrophysics, Volume 2: Stars, the Galaxy and the Interstellar Medium,
Cambridge University Press, Cambridge

[Lyne et al. 1985] **Lyne, A. G., Manchester, R. N., Taylor, J. H.**, 1985,
The Galactic Population of Pulsars,
MNRAS, **213**, 613

[Magnus et al. 1966] **Magnus, W., Oberhettinger, F., Soni, R. P.**, 1966,
Formulas and Theorems for the Special Functions of Mathematical Physics,
Springer, New York

[Mannheim 1997] **Mannheim, K.**, 1997,
AGN Models: High-Energy Emission,
CERN Preprint, astro-ph/9703184

[Mannheim & Schlickeiser 1994] **Mannheim, K., Schlickeiser, R.**, 1994,
Interactions of Cosmic Ray Nuclei,
Astron. & Astrophys., **286**, 1994

[Marsch & Tu 1990] **Marsch, E., Tu, C.-Y.**, 1990,
Spectral and Spatial Evolution of Compressible Turbulence in the Inner Solar Wind,
J. Geophys. Res., **95**, 11945

[Maurin et al. 2002] **Maurin, D., Taillet, R., Donato, F.**, 2002,
New Results on Source and Diffusion Spectral Features of Galactic Cosmic Rays: I B/C Ratio,
Astron. & Astrophys., **394**, 1039

[Mause 1993] **Mause, H.**, 1993,
Beschleunigung Kosmischer Strahlung in Galaxien,
Diploma Thesis, MPI für Radioastronomie Bonn

[Mause 1996] **Mause, H.**, 1996,
Theoretische Modellierung des Zeitverhaltens und der Breitbandspektren von Gamma-Blazaren,
PhD Thesis, Universität Bonn

[Menn et al. 2000] **Menn, W., et al.**, 2000,
The Absolute Flux of Protons and Helium at the Top of the Atmosphere Using IMAX,
Astrophys. J., **533**, 281

[Meyer et al. 1974] **Meyer, P., Ramaty, R., Webber, W. R.**, 1974,
Cosmic Rays - Astronomy With Energetic Particles,
Phys. Today, **27**

[Minter & Spangler 1997] **Minter, A. H., Spangler, S. R.**, 1997,
Heating of the Interstellar Diffuse Ionized Gas via the Dissipation of Turbulence,
Astrophys. J., **485**, 182

[Moskalenko et al. 1998] **Moskalenko, I. V., Strong, A. W., Reimer, O.**, 1998,
Diffuse Galactic Gamma-Rays, Cosmic-Ray Nucleons and Antiprotons,
Astron. & Astrophys., **338**, L75

176

[Nagano & Watson 2000] **Nagano, M., Watson, A. A.**, 2000,
Recent Observations and Implications of the Ultrahigh-Energy Cosmic Rays,
Rev. Mod. Phys., **72**, 689

[Nagano 2002] **Nagano, M.**, 2002,
Recent Observational Results on Ultrahigh-Energy Cosmic Rays,
Texas in Tuscany, XXI Symp. on Relativistic Astrophysics, Florence, 405

[Pohl & Esposito 1998] **Pohl, M., Esposito, J. A.**, 1998,
Electron Acceleration in Supernova Remnants and Diffuse Gamma Rays Above 1 GeV,
Astrophys. J., **507**, 327

[Pohl 2001] **Pohl, M.**, 2001,
Gamma-Ray Astronomy,
Proceedings 27th Int. Cosmic Ray Conf., **Invited, Rapporteur, and Highlight Papers**, 147

[Pohl 2002] **Pohl, M.**, 2002,
Einführung in die Hochenergieastrophysik,
Shaker Verlag, Aachen

[Prölss 2001] **Prölss, G. W.**, 2001,
Physik des erdnahen Weltraums,
Springer, Berlin

[Reimer & Pohl 2002] **Reimer, O., Pohl, M.**, 2002,
No Evidence yet for Hadronic TeV Gamma-Ray Emission From SNR RX J1713.7-3946,
Astron. & Astrophys., **390**, L43

[Ressell & Turner 1990] **Ressell, M. T., Turner, M. S.**, 1990,
The Grand Unified Photon Spectrum - A Coherent View of the Diffuse Extragalactic Background Radiation,
Comm. Astroph., **14**, 323

[Sanuki et al. 2000] **Sanuki, T., et al.**, 2000,
Precise Measurement of Cosmic-Ray Proton and Helium Spectra With the BESS Spectrometer,
Astrophys. J., **545**, 1135

[Schaeffer 1975] **Schaeffer, O. A.**, 1975,
Constancy of Galactic Cosmic Rays in Time and Space,
Proceedings 14th Int. Cosmic Ray Conf., **11**, 3508

[Scheffler & Elsässer 1992] **Scheffler, H., Elsässer, H.**, 1992,
Bau und Physik der Galaxis,
BI-Wissenschaftsverlag, Mannheim

[Scheffler 1997] **Scheffler, H.**, 1997,
Bergmann - Schaefer, Band 8: Sterne und Weltraum,
Walter de Gruyter, Berlin

[Scherer et al. 2000] **Scherer, K., Fichtner, H., Marsch, E.**, 2000,
The Outer Heliosphere: Beyond the Planets,
Copernicus Gesellschaft e. V., Katlenburg-Lindau

[Schlickeiser 1989] **Schlickeiser, R.**, 1989,
Cosmic-Ray Transport and Acceleration: I. Derivation of the Kinetic Equation and Application to Cosmic Rays in Static Cold Media,
Astrophys. J., **336**, 243

[Schlickeiser 2001] **Schlickeiser, R.**, 2001,
Cosmic Ray Astrophysics,
Springer, Berlin

[Schlickeiser 2004] **Schlickeiser, R.**, 2004,
Private communication

[Schönfelder 2001] **Schönfelder, V.**, 2001,
The Universe in Gamma Rays,
Springer, Berlin

[Seo & Ptuskin 1994] **Seo, E. S., Ptuskin, V. S.**, 1994,
Stochastic Reacceleration of Cosmic Rays in the Interstellar Medium,
Astrophys. J., **431**, 705

[Shalchi 2003] **Shalchi, A.**, 2003,
Transport kosmischer Strahlung in der anisotropen magnetohydrodynamischen Turbulenz,
PhD Thesis, Ruhr-Universität Bochum

[Shalchi et al. 2003] **Shalchi, A., Lerche, I., Schlickeiser, R.**, 2003,
Cosmic Ray Transport in Anisotropic Magnetohydrodynamic Turbulence. II. Shear Alfvén Waves,
Astron. & Astrophys., **397**, 777

178

[Shalchi & Schlickeiser 2004] **Shalchi, A., Schlickeiser, R.**, 2004,
Quasilinear Perpendicular Diffusion of Cosmic Rays in Weak Dynamical Turbulence,
Astron. & Astrophys., **420**, 821

[Simon et al. 1986] **Simon, M., Heinrich, W., Mathis, K. D.**, 1986,
Propagation of Injected Cosmic Rays Under Distributed Reacceleration,
Astrophys. J., **300**, 30

[Sokolsky 1989] **Sokolsky, P.**, 1989,
Introduction to Ultrahigh Energy Cosmic Ray Physics,
Addison-Wesley Publishing Company, Redwood City

[Spangler 1991] **Spangler, S. R.**, 1991,
The Dissipation of Magnetohydrodynamic Turbulence Responsible for Interstellar Scintillation and the Heating of the Interstellar Medium,
Astrophys. J., **376**, 540

[Spitzer 1978] **Spitzer, L.**, 1978,
Physical Processes in the Interstellar Medium,
John Wiley & Sons, New York

[Stawicki 2003] **Stawicki, O.**, 2003,
On Solar Wind Magnetic Fluctuations and Their Influence on the Transport of Charged Particles in the Heliosphere,
PhD Thesis, Ruhr-Universität Bochum

[Stecker & Jones 1977] **Stecker, F. W., Jones, F., C.**, 1977,
The Galactic Halo Question - New Size Constraints From Galactic Gamma-Ray Data,
Astrophys. J., **217**, 843

[Strong & Moskalenko 1998] **Strong, A., Moskalenko, I.**, 1998,
Propagation of Cosmic-Ray Nucleons in the Galaxy,
Astrophys. J., **509**, 212

[Unsöld & Baschek 1999] **Unsöld, A., Baschek, B.**, 1999,
Der neue Kosmos,
Springer, Berlin

[Voigt 1991] **Voigt, H. H.**, 1991,
Abriss der Astronomie,
BI-Wissenschaftsverlag, Mannheim

[Völk 2001] **Völk, H. J.**, 2001,
Gamma-Ray Astronomy of Cosmic Rays,
Proceedings 27th Int. Cosmic Ray Conf., **Invited, Rapporteur, and Highlight Papers**, 3

[Wang & Schlickeiser 1987] **Wang, Y.-M. and Schlickeiser, R.**, 1987,
Smearing of a Beaming Pattern by an Isotropic Cloud: An Analysis With Applications to Nonpulsing X-Ray Sources and Cosmic Rays,
Astrophys. J., **313**, 200

[Wang et al. 2001] **Wang, Q. D., et al.**, 2001,
Chandra Detection of a Hot Gaseous Corona Around the Edge-on Galaxy NGC 4631,
Astrophys. J., **555**, L99

[Wang et al. 2002] **Wang, J. Z., et al.**, 2002,
Measurement of Cosmic-Ray Hydrogen and Helium and Their Isotopic Composition With the BESS Experiment,
Astrophys. J., **564**, 244

[Webber et al. 1992] **Webber, W. R., Lee, M. A., Gupta, M.**, 1992,
Propagation of Cosmic-Ray Nuclei in a Diffusing Galaxy With Convective Halo and Thin Matter Disk,
Astrophys. J., **390**, 96

[Wiebel-Sooth 1998] **Wiebel-Sooth, B.**, 1998,
Measurement of the Allparticle Energy Spectrum and Chemical Composition of Cosmic Rays With the HEGRA Detector,
PhD Thesis, Universität Wuppertal

[Wiebel-Sooth et al. 1998] **Wiebel-Sooth, B., Biermann, P. L., Meyer, H.**, 1998,
Cosmic rays VII. Individual Element Spectra: Prediction and Data,
Astron. & Astrophys., **333**, 389

References of Figures

Here we list the references of figures taken from the World Wide Web. Other references are given directly below the respective figures.

Fig. 2.6: http://www.esa.int/esaSC/SEMHKP7O0MD_index_1.html

Fig. 2.7: http://www.sunspot.noao.edu/sunspot/esfwww/pics.html

Fig. 2.8: http://sohowww.nascom.nasa.gov/

Fig. 2.10: http://cossc.gsfc.nasa.gov/images/epo/gallery/solar/

Fig. 2.15: http://antwrp.gsfc.nasa.gov/apod/ap980208.html

Fig. 2.16: http://antwrp.gsfc.nasa.gov/apod/ap960623.html

Fig. 2.17: http://www.nrao.edu/ (left), http://chandra.harvard.edu (right)

Fig. 2.18: http://antwrp.gsfc.nasa.gov/apod/ap030118.html

Fig. 2.24: http://hegra1.mppmu.mpg.de/MAGICWeb/

Acknowledgements

This thesis would not have seen light without the help and support of the persons mentioned below.

I want to thank:

- Prof. Dr. Reinhard Schlickeiser for the motivation of this thesis and his supervision throughout the whole time, for sharing his knowledge, for helpful discussions, for the possibility to join national and international conferences and for inducing a very good working climate in the group of the institute.

- Prof. Dr. Martin Pohl for his continuous assistance and useful discussions.

- Priv.-Doz. Dr. Horst Fichtner for lots of interesting discussions about various physics themes, for the cooperative work in preparing and leading some student exercises in theoretical physics and for reading the main parts of the manuscript.

- Dr. Peter Brühne, Dipl.-Math., for reading carefully the whole manuscript.

- Dr. Andreas Kopp, Dipl.-Phys., for reading some parts of the manuscript.

- Dipl.-Phys. Carsten Arbeiter as my room fellow for the friendly atmosphere and for reading the Subsection "Extragalactic Gamma-Rays".

- Dr. Claudia Schuster, Dipl.-Phys., for helping me in some problems with Maple.

- Bernd Neubacher and Dr. Udo Arendt, Dipl.-Phys., for supporting me in all matters of the computer network.

- Angelika Schmitz for assistance in some bureaucratic things.

- All other colleagues at the Institut für Theoretische Physik IV for the kind and open atmosphere.